# Mathematical Modelling of a Low–Temperature Hydrogen Production Process with *In Situ* $CO_2$ Capture

Georgios Koumpouras

October 2007

A thesis submitted for the degree of Doctor of Philosophy of the University of London and for the Diploma of Membership of Imperial College London

Department of Chemical Engineering and Chemical Technology,
Imperial College London, United Kingdom

RIRL
LO

# Abstract

The development of alternative concepts for the production of hydrogen via steam methane reforming (SMR) has attracted a lot of attention due to the limitations associated with the performance of conventional catalytic reactors. Multifunctional reactors combine in a single unit chemical reaction, physical separation, and energy integration in order to enhance overall performance. The investigation of such hybrid configurations has been the subject of particular interest in industrial and academic research. The sorption-enhanced SMR process concept offers potential for process simplification as well as prospective energy conservation. In recent times, numerous theoretical and experimental studies on this concept have been published, investigating different process conditions and/or configurations. Most investigations cited in the literature focus on the use of a fixed bed packed with an admixture of reforming catalyst and adsorbent for the selective removal of $CO_2$.

In the present work, the flow of pneumatically conveyed $CO_2$ adsorbent particles within a stationary SMR structured catalyst is proposed, with adsorbent regeneration taking place in a separate unit. Hence, the reaction and regeneration stages are decoupled, resolving the problem of possible disparity between the adsorption and desorption kinetics. Furthermore, the pneumatic transport of a $CO_2$ acceptor enables a steady state (non-periodic) operation, characterised by additional flexibility towards optimisation, including potential for heat integration, *i.e.*, the use of regenerated adsorbent as an energy carrier into the monolithic adsorptive reactor.

This work summarises theoretical studies on this newly proposed process. Mathematical models for the adsorptive reactor and the regeneration unit are developed and a detailed

fundamental analysis of the process is presented. Important design and operating parameters necessary for process optimisation are identified. Systematic parametric studies are carried out to investigate the effect of the adsorbent characteristics on the overall process performance. Simulation and optimisation results reveal the feasibility of this process concept. The findings indicate a considerable degree of reaction enhancement through the use of a flowing adsorbent medium. The research output also identifies the scope and directions for further process development.

# Acknowledgements

I would like to start by thanking my supervisors, Esat Alpay for his invaluable guidance and advice, and Frantisek Stepanek for his sound support. Many thanks are due to Yulong Ding (University of Leeds) and Alexei Lapkin (University of Bath) for useful discussion on various important aspects of the research. I also wish to thank Evangelos Vaitsis for his help during my first steps into the Ph.D., and, most importantly Cleo Kontoravdi for her assistance in the preparation of this dissertation. Finally, the financial support of the Engineering and Physical Sciences Research Council through Chemistry Innovation (formerly known as Crystal Faraday) is gratefully acknowledged.

# Notation

| | |
|---|---|
| $A$ | cross-sectional area of the monolith channel, $m^2$ |
| $b_{CO_2}$ | Langmuir model constant, $Pa^{-1}$ |
| $c$ | molar concentration, mol $m^{-3}$ |
| $c_{p,ads}$ | adsorbent heat capacity, J kg–ads$^{-1}$ $K^{-1}$ |
| $c_{p,g}$ | gas heat capacity, J $mol^{-1}$ $K^{-1}$ |
| $d_p$ | adsorbent particle diameter, m |
| $D_e$ | effective diffusivity, $m^2$ $s^{-1}$ |
| $E$ | conversion enhancement factor, % |
| $F$ | steam flow rate through the desorber, $m^3$ $s^{-1}$ |
| $H_2$ | hydrogen purity, mol % |
| $H_{2,eq}$ | $H_2$–equivalent term, – |
| $\Delta H_{ads}$ | heat of adsorption, J $mol^{-1}$ |
| $\Delta H_{Rj}$ | heat of reaction $j$, J $mol^{-1}$ |
| $k_h$ | gas - coating heat transfer coefficient, J $m^{-2}$ $s^{-1}$ $K^{-1}$ |
| $k_{h,ads}$ | gas - adsorbent heat transfer coefficient, J $m^{-2}$ $s^{-1}$ $K^{-1}$ |
| $k_j$ | rate constant of reaction $j$; see Xu and Froment (1989a) for units |
| $k_{LDF}$ | LDF mass transfer coefficient, $s^{-1}$ |
| $k_m$ | mass transfer coefficient, m $s^{-1}$ |
| $K_i$ | adsorption constant for component $i$ (on catalyst surface): see Xu and Froment (1989a) for units |
| $K_j$ | equilibrium constant of reaction $j$; see Xu and Froment (1989a) for units |

| | |
|---|---|
| $L$ | reactor length, m |
| $LHV$ | lower heating values, kJ mol $^{-1}$ |
| $\dot{m}$ | adsorbent mass flux, kg–ads $s^{-1}$ |
| $m_{CO_2}$ | Langmuir model constant, mol kg–ads$^{-1}$ |
| $M$ | mass of adsorbent in the regeneration unit, kg |
| $M_i$ | molecular weight of component $i$, kg mol$^{-1}$ |
| $N_c$ | number of monolith channels, – |
| $Nu$ | Nusselt number, – |
| $\dot{n}$ | molar flow rate, mol $s^{-1}$ |
| $p_i$ | partial pressure of component $i$, Pa |
| $P$ | pressure $i$, Pa |
| $q$ | solid-phase concentration (average over an adsorbent particle), mol kg–ads$^{-1}$ |
| $Q_H$ | energy demand of the process, J $s^{-1}$ |
| $Q_r$ | energy input rate for the reactor, J $s^{-1}$ |
| $Q_{reg}$ | energy requirement for the regeneration unit, J $s^{-1}$ |
| $r$ | radial coordinate, m |
| $r_{ads}$ | rate of adsorption, mol kg–ads$^{-1}$ $s^{-1}$ |
| $r_{des}$ | rate of desorption, mol kg–ads$^{-1}$ $s^{-1}$ |
| $r_i$ | formation rate of component, $i$, mol kg–cat$^{-1}$ $s^{-1}$ |
| $R$ | recovery of $CO_2$, % |
| | (or universal gas constant, J mol$^{-1}$ K) |
| $R_c$ | monolith channel radius, m |
| $R_j$ | rate of reaction $j$, mol kg–cat$^{-1}$ $s^{-1}$ |
| $R_p$ | particle radius, m |
| $Sh$ | Sherwood number, – |
| $t$ | time coordinate, s |
| $T$ | temperature, K |
| $T_{in}$ | temperature of steam at the desorber inlet, K |

| | |
|---|---|
| $u$ | superficial velocity , m $s^{-1}$ |
| $X$ | conversion of $CH_4$, % |
| $Y_{H_2}$ | hydrogen yield, – |
| $z$ | axial coordinate, m |

*Greek letters*

| | |
|---|---|
| $\varepsilon$ | voidage, – |
| $\eta$ | catalyst effectiveness factor, – |
| $\vartheta$ | temperature difference $T_{ads} - T_f$, K |
| $\lambda$ | thermal conductivity, J $m^{-1}$ $s^{-1}$ $K^{-1}$ |
| $\mu$ | viscosity, Pa s |
| $\rho$ | density, kg $m^{-3}$ |
| $\sigma$ | parameters in Eqs. 3.45–3.46 (see Reid et al., 1987), Å |
| $\tau$ | residence time, s |
| $\Upsilon$ | adsorptive reactor efficiency, % |
| $\varphi$ | adsorbent loading, – |
| $\varphi_{i,j}$ | Chapman–Enskog parameter (Eq. 3.44), – |
| $\Omega$ | parameters in Eqs. 3.45–3.46 (see Reid et al., 1987), – |

*Subscripts and superscripts*

| | |
|---|---|
| $*$ | equilibrium |
| $ads$ | adsorbent (or adsorption) |
| $AD$ | presence of $CO_2$ adsorption |
| $c$ | wash coat (catalyst) |
| $des$ | desorption |
| $f$ | reactor feed |

| | |
|---|---|
| $g$ | gas |
| $i$ | component |
| $int$ | interstitial |
| $j$ | reaction |
| $NAD$ | absence of $CO_2$ adsorption |
| $s$ | saturation |

# Contents

**Abstract** i

**Acknowledgements** iii

**Notation** iv

**Contents** viii

**List of Figures** xi

**List of Tables** xv

**1 Introduction** 1

**2 Background and literature review** 9

2.1 Adsorption principles . . . . . 9

2.1.1 Adsorption phenomena and processes . . . . . 9

2.1.2 Adsorption within a solid particle . . . . . 19

2.1.3 Adsorbents . . . . . 22

2.1.4 Isotherms . . . . . 23

2.1.5 Mass transfer phenomena . . . . . 27

2.1.6 Heat transfer phenomena . . . . . 29

2.2 Sorption–Enhanced Reaction Process . . . . . 30

2.2.1 Sorption–enhanced SMR . . . . . 33
2.2.2 $CO_2$ adsorbents for SE–SMR . . . . . 39
2.3 Monolithic type reactors . . . . . 44
2.3.1 Modelling of monolith reactors . . . . . 46
2.4 Concluding remarks . . . . . 52

**3 Mathematical modelling** **54**
3.1 Process scheme . . . . . 54
3.2 Model assumptions . . . . . 54
3.3 Governing equations . . . . . 58
3.3.1 Component balance equations . . . . . 58
3.3.2 Energy balance equations . . . . . 59
3.3.3 Boundary conditions . . . . . 60
3.4 Reaction kinetics . . . . . 60
3.5 Adsorption equilibria and kinetics . . . . . 64
3.6 Regeneration unit . . . . . 65
3.7 Other process parameters . . . . . 67
3.8 Process performance indices . . . . . 70
3.9 Numerical discretisation and model solution . . . . . 72

**4 Simulation results** **78**
4.1 Process analysis . . . . . 78
4.1.1 Performance of the adsorptive reactor . . . . . 78
4.1.2 Overall process performance . . . . . 82
4.2 Effect of adsorbent characteristics . . . . . 88
4.2.1 Effect of adsorbent capacity . . . . . 89
4.2.2 Effect of sorption kinetics . . . . . 90

4.2.3 Effect of regeneration conditions . . . . . 92

4.3 Concluding remarks . . . . . 95

**5 Optimisation studies** **97**

5.1 Optimisation problem formulation . . . . . 98

5.2 Optimisation results . . . . . 100

5.3 Sensitivity analysis . . . . . 104

5.4 Concluding remarks . . . . . 106

**6 Concluding remarks and future directions** **107**

6.1 Summary of results . . . . . 107

6.2 Main conclusions . . . . . 109

6.3 Recommendations for future work . . . . . 110

**List of publications** **118**

**References** **120**

**Appendices** **135**

**A Mass balances derivations** **136**

A.1 Gas phase . . . . . 138

A.2 Catalyst phase . . . . . 139

A.3 Adsorbent phase . . . . . 140

**B Energy balances derivations** **141**

B.1 Gas phase . . . . . 141

B.2 Catalyst phase . . . . . 142

B.3 Adsorbent phase . . . . . 143

# List of Figures


1.1 Block diagram of the SMR process . . . . . 2

1.2 SMR equilibrium conversion (Joensen and Rostrup-Nielsen, 2002). . . . . 3

1.3 Schematic representation of a packed bed adsorptive reactor for hydrogen production through SE–SMR. . . . . 4

2.1 Operating steps in TSA processes. . . . . 11

2.2 Skarstrom pressure swing adsorption cycle. . . . . 15

2.3 Operating steps in RPSA processes. . . . . 18

2.4 Schematic representation of an adsorbent particle (Ruthven, 1984). . . . . 21

2.5 Types of adsorption isotherms. Type I: unimolecular adsorption characterised by a maximum limit in the amount adsorbed; Type II: multimolecular adsorption of BET type; Type III: multimolecular adsorption where the heat of adsorption of the first layer is less than that of succeeding layers; Type IV–V: hysteresis phenomena in multimolecular adsorption (see Seader and Henley, 2006, p. 559). . . . . 24

2.6 (a) The Langmuir isotherm (see Do, 1998, p.16) (b) Pure gas adsorption isotherms for $CH_4$ and $H_2$ on activated carbon (Waldron and Sircar, 2000). 26

2.7 Schematic diagram of Langmuir adsorption mechanism on a flat surface (see Do, 1998, p.14). . . . . 27

2.8 *In situ* separation functionalities integrated into the reactor (Krishna, 2002). 30

2.9 Diagram of the sequential SERP steps for the production of CO by the reverse water–gas shift reaction (Carvill et al., 1996). . . . . 32

2.10 Schematic of sorption–enhanced reactor with subsection–controlling strategy (Xiu et al., 2003b). . . . . 35

2.11 The conceptual scheme for the two–section model proposed by Wang and Rodrigues (2005). . . . . 36

2.12 Simplified schematic of the sorption–enhanced SMR process proposed by Johnsen et al. (2006a). . . . . 39

2.13 Structure of hydrotalcite–like compounds (Hutson et al., 2004). . . . . 40

2.14 Monolith, individual monolith channel, and cross–section of channel with catalytically active porous layer (Geus and van Giezen, 1999). . . . . 45

2.15 Sketch of a monolith channel indicating the relevant physical and chemical phenomena in the gas phase, washcoat, and substrate (Holder et al., 2006). 47

2.16 Idealised plot of reaction rate (or conversion) versus temperature exhibiting the possible rate–controlling regimes for monolithic reactors (Geus and van Giezen, 1999). . . . . 50

3.1 Schematic diagram of the proposed process. . . . . 55

3.2 Reaction and adsorption in an idealised monolith channel. . . . . 56

3.3 Schematic diagram of the well-mixed continuous flow desorber. . . . . 66

3.4 Equidistant finite difference grid. . . . . 73

4.1 Axial methane conversion profiles (Case 1: $\varphi = 0$; Case 2: $\varphi = 0.1$, $m_{CO_2} = 0$; Case 3: $\varphi = 0.1$, $m_{CO_2} = 0.65$ mol kg$^{-1}$). . . . . 79

4.2 Effect of the adsorbent inlet temperature on the conversion enhancement. . 80

4.3 $CO_2$ concentration profiles along the adsorptive reactor. . . . . 81

4.4 Temperature ($T_g, T_c, T_{ads}$) and adsorbent-phase $CO_2$ concentration ($q$) profiles along the adsorptive reactor. . . . . 82

4.5 Ratio of adsorbent temperature at the desorber outlet ($T$) over steam inlet temperature ($T_{in}$) as a function of steam flow rate ($F$) at different adsorbent loadings. . . . . 83

4.6 Relative amount of $CO_2$ desorbed ($1 - q/q_{in}$) as a function of steam flow rate ($F$) at different adsorbent loadings. . . . . 84

4.7 $CH_4$ conversion as function of steam flow rate ($F$) at different steam inlet temperatures ($T_{in}$) and 10% adsorbent loading. . . . . 85

4.8 Enhancement factor as function of steam flow rate ($F$) at different steam inlet temperatures ($T_{in}$) and 10% adsorbent loading. . . . . 86

4.9 $CO_2$ recovery as a function of steam flow rate ($F$) at different adsorbent loadings. . . . . 87

4.10 $CH_4$ conversion as a function of $CO_2$ molar fraction at different adsorbent loadings. . . . . 88

4.11 Conversion enhancement factor as function of adsorbent capacity $m_{CO_2}$ for several values of the linear driving force coefficient $k_{LDF}$. . . . . 90

4.12 $CO_2$ recovery as function of adsorbent capacity $m_{CO_2}$ for several values of the linear driving force coefficient $k_{LDF}$. . . . . 91

4.13 Langmuir isotherms and corresponding values of $q$ at the reactor exit. . . . 92

4.14 Conversion enhancement factor as function of linear driving force coefficient $k_{LDF}$ for several values of adsorbent capacity $m_{CO_2}$. . . . . 93

4.15 $CO_2$ recovery as function of linear driving force coefficient $k_{LDF}$ for several values of adsorbent capacity $m_{CO_2}$. . . . . 94

4.16 Conversion enhancement factor as function of the purge steam flowrate in the desorber. . . . . 95

4.17 $CO_2$ recovery as function of the purge steam flowrate in the desorber. . . . 96

6.1 Scale separation in a packed bed reactor with main scales and typical modelling tools: L and t are the corresponding length and time scales in m and s respectively. CAPE: computer-aided process engineering; CFD: computational fluid dynamics; DFT: density function theory; KMC: kinetic Monte Carlo; MD: molecular dynamics; TST: transition state theory. . . . . 112

A.1 Schematic representation of the computational domain. . . . . 137

# List of Tables


1.1 Thesis outline . . . . . 7

2.1 A typical 5–bed PSA process (Jiang et al., 2004) . . . . . 14

2.2 Equations for calculation of diffusivities . . . . . 22

2.3 Adsorption isotherm equations (general mathematical expressions) . . . . . 25

2.4 Properties of typical $CO_2$ adsorbents for SE–SMR . . . . . 41

2.5 Adsorption capacities (at 200°C and 107 kPa) for HTlc after heating to 200 and 400°C in vacuum (Hutson et al., 2004) . . . . . 43

2.6 Indicative correlations for Nu and Sh numbers . . . . . 51

3.1 Calculations in support of model assumptions . . . . . 57

3.2 Parameters for equations 3.16 and 3.17 . . . . . 62

3.3 Parameters (constants) used in the simulations . . . . . 77

4.1 Calculated asymptotic values of methane conversion ($X$), enhancement factor ($E$) and $CO_2$ recovery ($R$) at different values of steam temperature, $T_{in}$. 85

5.1 Summary of optimisation results . . . . . 103

5.2 Calculated values of E (%) for each optimisation scenario. . . . . 104

5.3 Sensitivity analysis results . . . . . 105

# Chapter 1

# Introduction

Hydrogen is a widely used feedstock in the chemical, petrochemical and petroleum refining industries. Areas in which hydrogen is employed include hydrogenation reactions (e.g. hydro-cracking and hydro-treating processes), synthesis gas applications (e.g. production of ammonia and methanol), Fischer-Tropsch synthesis, manufacture of chemicals with specific end uses, such as for pharmaceuticals and, of course, fuel cells. Above all, hydrogen is regarded as a future clean and renewable energy source. Obviously its key role in the world's economy has attracted a lot of interest.

Currently most of the large-scale hydrogen demand is met by steam methane reforming (SMR) (Armor, 1999). This process involves the incomplete endothermic transformation of methane and water to hydrogen, carbon monoxide and carbon dioxide. Due to equilibrium limitations this process must be carried out at high temperatures (up to 1100K) and is usually followed by a pressure swing adsorption (PSA) step to remove $CO_2$ and produce high purity $H_2$ (Scholz, 1993; Adris et al., 1996). This is a very energy– and capital–intensive process, although it should be noted that existing technologies approaches 90% of the maximum (thermodynamic) efficiency (Stitt, 2004).

A conventional methane reforming based hydrogen production process can be depicted by the block diagram in Fig. 1.1. Hot methane and steam are fed to the reformer where the following reversible reactions take place over supported nickel catalysts in tubular re-

actors (reformers):

$$CH_4 + H_2O \leftrightarrows CO + 3H_2 \quad (1)$$

$$CH_4 + 2H_2O \leftrightarrows CO_2 + 4H_2 \quad (2)$$

$$CO + H_2O \leftrightarrows CO_2 + H_2 \quad (3)$$

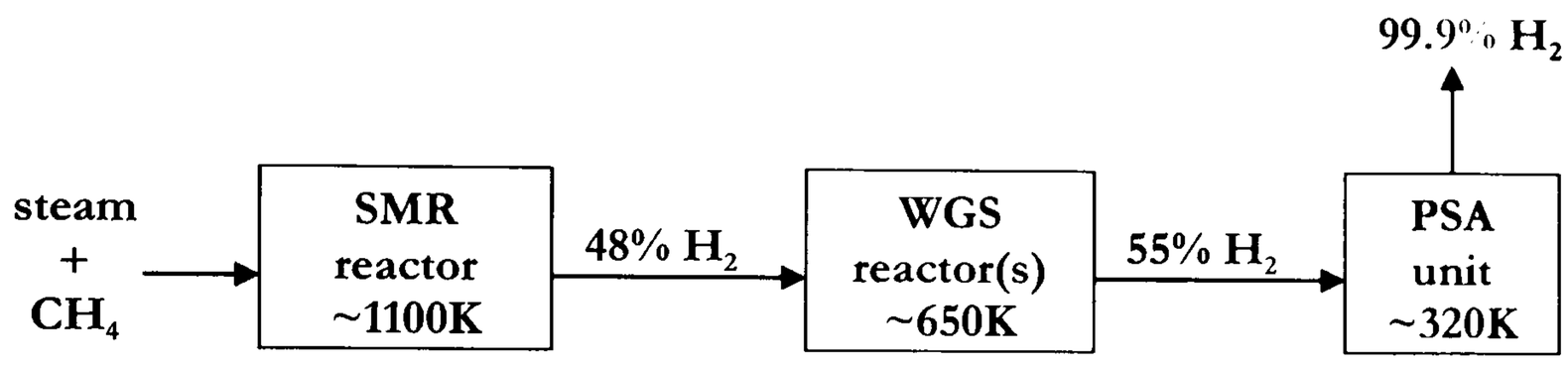



Figure 1.1: Block diagram of the SMR process

Reforming reactions (1) and (2) are strongly endothermic, so the forward reaction is favoured by high temperatures, while the water gas shift reaction (3) is moderately exothermic and is therefore favoured by low temperatures. The kinetics of these reactions on a $Ni/MgAl_2O_4$ catalyst have been studied by Xu and Froment (1989a,b). As shown in Fig. 1.2, the conversion of methane is favoured by high temperature, low pressure and high steam to carbon ratios (S/C). However, high temperatures promote carbon-producing reactions (*Methane cracking:* $CH_4 \leftrightarrows C + 2H_2$, *Boudouard reaction:* $2CO \leftrightarrows C + CO_2$, *CO reduction:* $CO + H_2 \leftrightarrows C + H_2O$) leading to catalyst deactivation. Carbon formation can be suppressed by the use of excess steam commonly with S/C in the region of 4 (minimum ~1.5, see Adris et al., 1996).

The overall SMR reactor operation requires heat to be provided to the reformer, and this is done through the combustion of methane and pressure swing adsorption (PSA) waste gas. Hydrogen is produced together with all the other species, and its generation is further increased in the water gas shift (WGS) reactor(s) where only the exothermic reaction

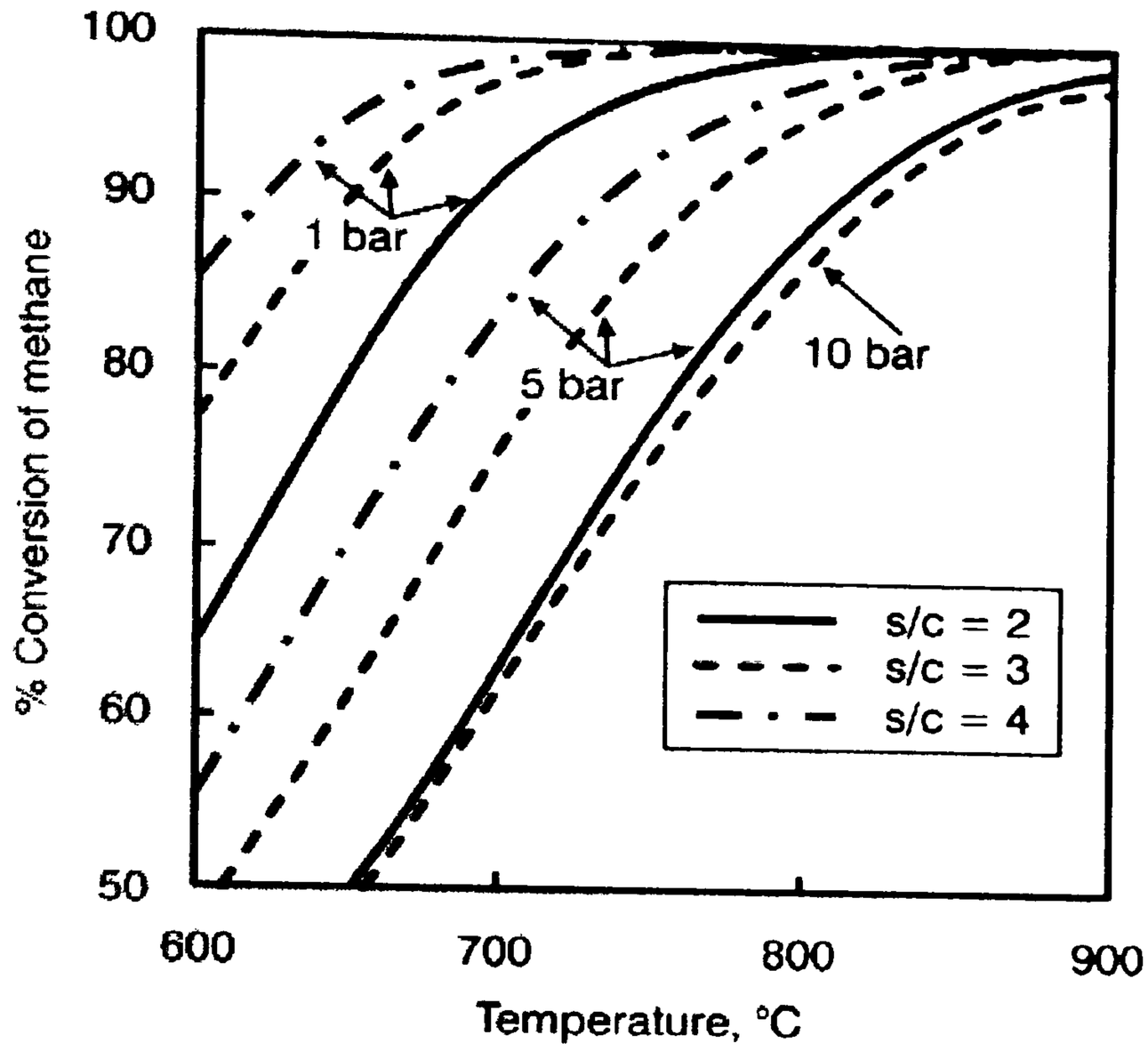



Figure 1.2: SMR equilibrium conversion (Joensen and Rostrup-Nielsen, 2002).

(2) is catalysed at temperatures lower than that of the reformer. Rase (1977) proposed a kinetic model for the low–temperature water gas shift reaction on a copper-zinc oxide catalyst for temperatures below 560K, while Keiski et al. (1996) studied the kinetics for the high-temperature water gas shift reaction on an $Fe_3O_4$–$Cr_2O_3$ catalyst for temperatures around 600K. Most of the water is separated by condensation as the gas stream is cooled to almost ambient temperatures before entering the PSA unit where hydrogen can be purified to 99.9+%. Species other than hydrogen are selectively adsorbed on a solid adsorbent at a relatively high pressure by contacting the gas with the solid in a packed column in order to produce a hydrogen enriched gas stream. The adsorbed species are then desorbed from the solid by lowering the pressure and purging with high-purity product hydrogen, and thus, the PSA waste gas is generated. Continuous flow of product is maintained by using multiple, properly synchronized adsorption beds. Combustion of the PSA waste gas and methane is used to provide heat for the reformer and also for the preheating of feeds and the generation of the export steam. Recovery of the waste heat from the still–hot gases leaving the reformer is also used to the same end. Optimisation

of the energy utilisation in this process can lead to cost reduction of hydrogen production, and therefore several studies addressing this issue have been reported (see Scholz, 1993; Rajesh et al., 2000; Posada and Manousiouthakis, 2005).

However, the main features of the conventional SMR process remain high energy consumption, considerable emissions of $CO_2$ as well as elevated capital and operating costs. The development of alternative concepts for production of hydrogen via SMR has therefore attracted considerable attention. In particular, the integration of SMR reaction systems with some form of *in situ* separation has been widely reported in the literature. The separation can be based either on selective permeation of $H_2$ through a membrane or adsorption of $CO_2$.

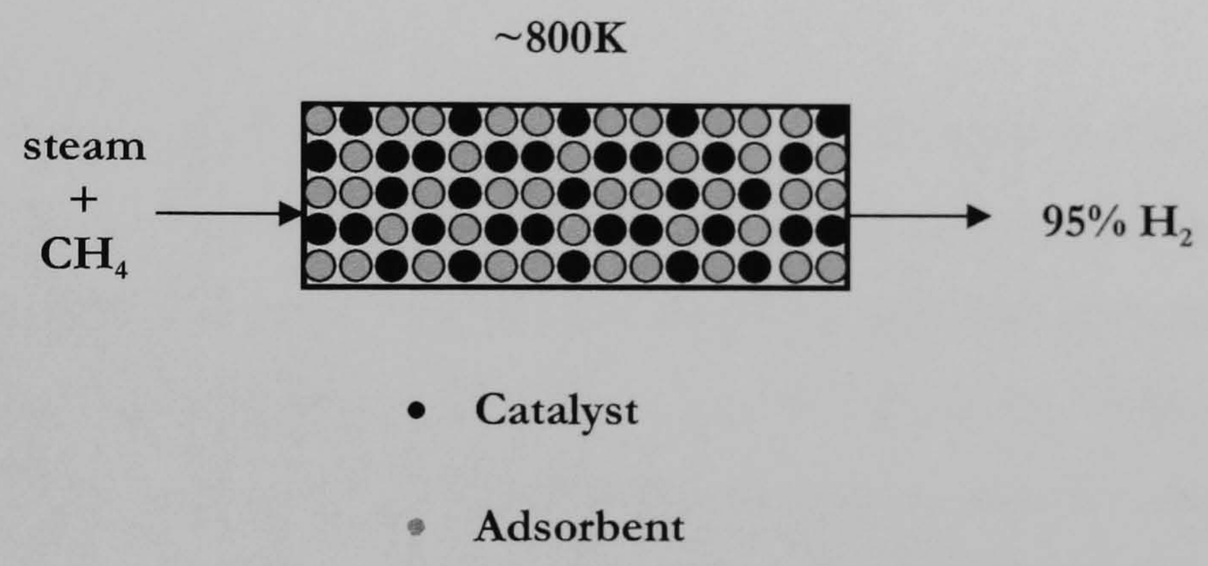



Figure 1.3: Schematic representation of a packed bed adsorptive reactor for hydrogen production through SE–SMR.

Notably, the sorption–enhanced reaction process (SERP), developed by Air Products and Chemicals Inc. (Carvill et al., 1996; Hufton et al., 1999), involves the addition of an adsorbent into the reaction system for the selective removal of $CO_2$, thereby shifting the equilibrium of the reversible reaction according to Le Chatelier's principle. The adsorptive reactor concept represents an important class of multifunctional reactors, which provide much potential for process intensification (Stankiewicz, 2003). By combining reaction and separation in a single unit operation, multifunctional reactors may substantially improve reactant conversion or product selectivity and, for reversible reactions, establish a more favourable reaction equilibrium than that achievable under conventional reactor operation

at identical conditions. Specifically, the SERP concept focuses on the hydrogen production via steam methane reforming in the presence of a $CO_2$ adsorbent by employing the well-established pressure and concentration swing adsorption principles for reaction enhancement; see also Vaporciyan and Kadlec (1989), Alpay et al. (1994a) and Chatsiriwech et al. (1994). Waldron et al. (2001) reported that this process concept can be used to directly produce high purity $H_2$ containing trace carbon oxides. Moreover the process allows high conversion of methane to hydrogen, while operating at a much lower reaction temperature (~750K) than that required by the conventional SMR reactor. Therefore, the SERP concept offers the potential for process simplification as well as prospective energy conservation, and numerous theoretical and experimental studies on this cyclic process have been recently published; see for example Ding and Alpay (2000b), Ortiz and Harrison (2001), Xiu et al. (2002a) and Wang and Rodrigues (2005).

Most of these studies suggest the utilisation of fixed beds packed with an admixture of reforming catalyst and $CO_2$ adsorbent; see Fig. 1.3. To enable continuous operation, such a configuration requires at least two parallel reactors operated alternatively and out of phase in reforming and adsorbent regeneration modes. Recently, Johnsen et al. (2006a) proposed a continuous sorption–enhanced SMR process based on parallel fluidised bed reactors. In any case, still both catalyst and adsorbent have to experience the desorption purging. Not only is the catalyst under-utilised in such an arrangement, but as Ding and Alpay (2000a) have shown, some adsorbents have much faster kinetics in the adsorption step than that during the desorption one, and therefore require different residence times in the reaction and regeneration stages.

In the present work, the flow of pneumatically conveyed adsorbent particles within a stationary SMR monolith is proposed, with adsorbent regeneration performed in a separate unit. Hence, the reaction and regeneration stages are decoupled, resolving the problem of possible disparity between the adsorption and desorption kinetics. Furthermore, using pneumatic transport of a $CO_2$ scavenger enables a steady state (non–periodic) operation, characterised by additional flexibility towards optimisation, including potential for heat integration, i.e. the use of regenerated adsorbent as energy carrier into the monolith reac-

tor. The idea of combining a stationary catalyst phase with a mobile adsorbent phase has also been proposed by Westerterp and Kuczynski (1987) in the case of methanol synthesis.

The choice of a monolithic–type reactor configuration instead of a packed bed is based on the findings of experimental studies on gas–solid two–phase mixtures through such arrangements (Ding et al., 2005), which indicate that the control of this type of flow through a packed bed system is extremely difficult. Moreover, the use of packed bed in the intended application is associated with an undesired high pressure drop due to static hold–up (i.e. particles trapped in the interstices of packed particles). In the process proposed in this work, three key elements are considered: pneumatic transport of adsorbent through the structured catalyst (Ding et al., 2005, 2006), $CO_2$ adsorbent performance (Ding and Alpay, 2000a; Yong et al., 2002; Abanades et al., 2004) and overall process optimisation.

This research encompasses the development of computational methods for rigorous modelling and simulation of the proposed process and their subsequent use for rational design and optimisation purposes. The theoretical studies are complementary to the experimental programmes carried out on reactor design aspects (University of Leeds) and novel adsorbents development (University of Bath). The overall project falls within a broader collaborative initiative of academia and industry (Chemistry Innovation, formerly known as Crystal Faraday) to promote sustainable chemical technology.

The **specific objectives** of this work are:

1. To develop mathematical models of the monolithic reactor and the adsorbent regeneration unit. Finding a good balance between a realistic (high–fidelity) and a computationally tractable model suitable for the conceptual design and optimisation of such a complex system is a focal point of this work.

2. To conduct parametric studies for the identification of important operating parameters of the adsorptive reactor and the fundamental analysis of the overall process performance, the results of which will be used to assess the feasibility of this novel concept.

3. To evaluate the effect of adsorbent properties on process performance. More specifically, this study will focus on the effects of $CO_2$ sorption capacity and absorption/desorption kinetics on the operation of the adsorptive reactor alone, as well as on that of the full integrated cycle of sorption–enhanced reaction and adsorbent regeneration.

4. To perform model–based optimisation studies in order to identify optimal values of the key design and operating parameters. Gauging the sensitivity of the optimal process performance on model parameters (or assumptions) will also be attempted.

5. To gain useful qualitative insights that will highlight the scope and reveal the directions for further process development (process schemes, designs and configurations).

Table 1.1: Thesis outline

| **Chapter** | **Contents** |
|---|---|
| **1 Introduction** | SMR process limitations; SERP concept; Research proposal & objectives; Thesis structure |
| **2 Literature Review** | Adsorption principles & processes; SE–SMR investigations; $CO_2$ adsorbents; Modelling of monoliths |
| **3 Mathematical modelling** | Reactor model: 1–D distinctly describing the catalyst, gaseous, and adsorbent phases; Desorber model: well–mixed fluidised–bed type of operation |
| **4 Simulation results** | Parametric studies; Adsorptive reactor performance; Fundamental process analysis; Effect of adsorbent characteristics |
| **5 Optimisation studies** | Optimisation approach & problem formulation: Results; Sensitivity analysis |
| **6 Conclusions, future directions** | Summary of results; Main concluding remarks; Recommendations for future work |

This thesis is organized into 6 chapters (see Table 1.1). In Chapter 2 a literature review covering essential features of the research is presented. Chapter 3 deals with the mathematical modelling work, whilst Chapter 4 presents simulation results in the form of systematic parametric studies. Their aim is to gain a useful insight into the parametric sensitivity of the novel process with respect to design and operating parameters. The outcome of this theoretical investigation guides the model–based optimisation of the process, presented in Chapter 5. Lastly, the final chapter outlines the conclusions of the research and suggests some possible future research directions.

# Chapter 2

# Background and literature review

This chapter contains a literature appraisal on the concepts and methodologies described in the introductory chapter. First of all, a comprehensive review of the adsorption principles and the periodic adsorption processes is given. This is followed by a review of studies on the adsorption–enhanced SMR for hydrogen production. Finally, aspects involved to the modelling of monolithic reactors are discussed in the last section of this chapter.

## 2.1 Adsorption principles

### 2.1.1 Adsorption phenomena and processes

The use of solids for removing substances from either gaseous or liquid solutions has been widely reported. This process, termed *adsorption*, involves the preferential partitioning of one or more substances from the fluid phase onto the surface of a solid substrate. The fluid that is adsorbed is referred to as the adsorbate and the underlying solid material as the adsorbent. Adsorption is favoured by low temperatures, high pressures, high enthalpies of adsorption and large adsorbent surface areas. The surface of an adsorbent represents a discontinuity of its structure with the forces acting at it being unsaturated. Therefore, when the adsorbent is exposed to a gas, the gas molecules will form bonds with it and become attached. When this bonding is characterised by relatively weak forces, mainly the van der Waals but also electrostatic forces, the adsorption is referred to as *physisorption*. On the other hand, when the bonding involves much stronger forces resulting

from electron transfer between the sorbate and the surface, the adsorption is referred to as *chemisorption*. As pointed out by Ruthven et al. (1994), physical adsorption is more useful for developing practical periodic adsorption processes as it is easier to reverse the adsorption, i.e. regenerate the original solid phase by manipulating the external operating conditions.

From the point of view of practical adsorptive process design, it is important to mention that an adsorbent has a finite capacity for a given adsorbate and the adsorption is ceased when the solid is saturated with the adsorbate. At this particular point, the solid must be cleaned or *regenerated* so that it can be re-utilised economically, and the recovery of the pure adsorbate is achieved. It is therefore crucial for the adsorption phenomena to be reversible. The two principal mechanisms used to regenerate the solid are:

- Thermal swing: the bed is heated by a hot gas purge. This is the so called *temperature swing adsorption* (TSA) process.
- Pressure swing: the system pressure is reduced at essentially constant temperature to desorb the adsorbate and then the bed is purged at low pressure. This is known as *pressure swing adsorption* (PSA) process.

Alternatively, the temperature or pressure levels in the bed can be manipulated by changing the composition of the fluid phase in order to control the direction of the adsorption. This type of operation, which is particularly useful when the fluid is a liquid, is termed *concentration swing adsorption* (CSA) process.

All these cyclic (semi–batch) processes can be collectively viewed as *periodic adsorption processes*. Particular implementations of these processes vary in their degree of complexity depending on the number of beds involved, the specific design parameters and the operating policy over each cycle. Recent works in this area are summarised in the following section.

### Temperature swing adsorption

In thermal swing adsorption processes (TSA) the bed is regenerated by heating, usually with a stream of hot gas, to a temperature at which the adsorbed species are desorbed and then removed from the bed in the gas stream. The simplest version of the TSA process operates with two beds, one adsorbing and the other desorbing, in order to enable continuous feed flow. Typically, a complete cycle of thermal swing adsorption comprises an adsorption step, a desorption step and possibly a cooling step. Gas flow in the desorption and cooling steps can be carried out either in the same or reverse axial direction as the adsorption step (see Fig. 2.1).

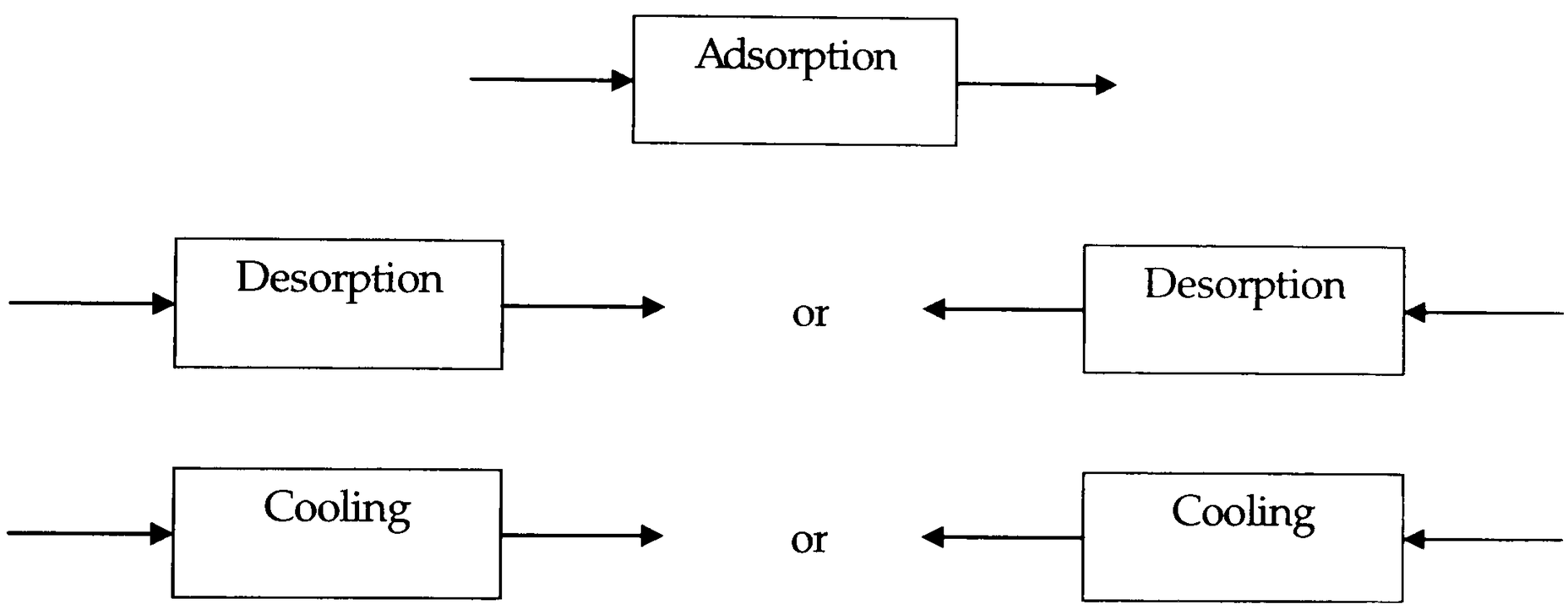



Figure 2.1: Operating steps in TSA processes.

Desorption in the reverse direction was found to be more energy efficient for a non-uniform initial distribution of adsorbate on the solid phase (Carter, 1975). The duration of desorption (or heating) step has an effect on the speed of convergence towards cyclic steady state operation. This is approached quickly with a long heating time, whereas steady state is achieved more slowly for a short heating time. For instance, if regeneration is carried out to completion, cyclic steady state would be achieved after one cycle, regardless of initial conditions of the bed. A cool-gas purge at the end of the desorption step can generally have an influence on the cycle efficiency, except under conditions where the thermal wave propagates faster than the concentration wave, such that the breakthrough is independent of the initial bed temperature (Davis and LeVan, 1987). As a rule, the

thermal wave lags the concentration wave. In their theoretical and experimental work, Davis and LeVan (1989) showed that a properly timed cooling step had a pronounce effect on the performance of the unit in terms of energy and purge gas utilisation, particularly for short regeneration times. The authors also proposed an optimal cycle for adsorbate recovery using hot purge gas. This cycle should involve a high-pressure heat-up step in order to create a high concentration level of adsorbate, followed by low-pressure purge.

In relation to the design of the desorber in this study (see §3.6), findings of experimental and theoretical studies of the TSA cycle are summarised below:

- Purge gas consumption decreases with increasing temperature (Kumar and Dissinger, 1986; Schork and Fair, 1988). The energy requirement is an increasing function of the regeneration temperature and the purge gas consumption, so there is an optimal purge gas temperature at which the energy requirement is at a minimum. The optimal temperature decreases as the effluent gas concentration decreases, hence, incomplete regeneration may be operationally favourable (Huang et al., 1993; Hwang et al., 1997).

- Martin and Swanton (1997) confirmed significant energy-saving implications for the thermal efficiency of the adsorption processes. Adsorbents degraded by coking, must be periodically regenerated, which is an energy-intensive process. Their work on coking and hydrothermal ageing improved understanding of how these relate to adsorbent structure and consequently allowed for operation of these processes under conditions that require less frequent regeneration, and in some cases enabled the elimination of an unnecessary thermal process step. Thus, considerable energy savings were enabled.

- The linear driving force mass transfer model – see §2.1.5 – provides an adequate fit to the experimental adsorption and regeneration data (Kumar and Dissinger, 1986; Schork and Fair, 1988; Hwang et al., 1997).

Within the scope of this work (well–mixed fluidised–bed type of operation see §3.6 in contrast to the fixed–bed configuration), an important concern is the attrition of the adsorbent particles. Important particle properties such as surface area, bulk density and size

distribution may change as a result of abrasion. In the context of SE SMR the literature on this issue is rather sparse, recently though Johnsen and Grace (2007) investigated the mechanical degradation of a dolomite and a limestone used in a SE-SMR fluidised bed environment. In addition to the loss of capacity due to chemical degradation for both adsorbents, the dolomite was reported to exhibit poorer resistance to attrition, although more stable chemically.

### Pressure swing adsorption

In pressure swing adsorption (PSA) systems, regeneration of the adsorbent during the desorption cycle is achieved simply by reducing the total pressure and purging the bed at low pressure with a small fraction of the product stream.

A typical PSA cycle involves three operating steps:

- Pressurisation step: the product end of the bed is closed and the bed is pressurised with the feed gas mixture. Normally, the duration of the step is relatively short. The strongly adsorbed components accumulate on the adsorbent, while the weakly adsorbed (and/or the non–adsorbed) components are enriched at the product end.
- Product release step: the gas mixture flows through the bed. The concentration of the strongly adsorbed component increases on the solid phase, while the weakly adsorbed components are withdrawn from the product end.
- Depressurisation (or blowdown) step: the product end in this step is closed. Gas flows in the reverse direction to that of the previous steps. As the bed pressure drops, the adsorbed components desorb from the adsorbent and elute from the feed end of the bed.

Additional steps, such as purge or backfill, may be introduced in order to improve the performance of the separation (see for example Table 2.1).

Early reports on pressure swing adsorption date from the 1930s, however, patents by Skarstrom (1960) and de Montgureuil and Domine (1964) are generally considered impor-

Table 2.1: A typical 5–bed PSA process (Jiang et al., 2004)

| | | |
|---|---|---|
| 1 | Feed product and repress gas | 140 s |
| 2 | First cocurrent depress | 30 s |
| 3 | Second cocurrent depress | 40 s |
| 4 | Provide purge | 70 s |
| 5 | Third cocurrent depress and blowdown | 30 s |
| 6 | Countercurrent blowdown | 40 s |
| 7 | Receive purge | 70 s |
| 8 | Third equalisation repress | 30 s |
| 9 | Second equalisation repress | 40 s |
| 10 | First equalisation repress | 30 s |
| 11 | Product repress | 110 s |

tant milestones in the PSA process development (see Fig. 2.2). Key applications include air separation, separation of normal and iso-alkanes, natural gas dew pointing, hydrogen recovery and purification (Yang, 1987; Ruthven et al., 1994).

Waldron and Sircar (2000) simulated the performance of a pressure swing adsorption process for production of high purity hydrogen from a binary methane-hydrogen mixture, using a detailed, adiabatic PSA model. An activated carbon was used for selective adsorption of methane over hydrogen. The effects of different process design, feed gas pressure and composition, product $H_2$ purity and hydrogen purge gas pressure on process performance were evaluated. Hydrogen recovery and hydrogen productivity per unit amount of adsorbent were treated as dependent variables. It was demonstrated that many different combinations of PSA process steps, their operating and feed gas conditions can be chosen to produce an identical product gas with different hydrogen recovery and productivity.

This was also confirmed by Jiang et al. (2004) in their simulation and optimisation studies on a five-bed hydrogen purification process. $H_2$ recovery and purity were fairly robust objectives and changed only slightly with operating conditions. Thus, some flexibility in

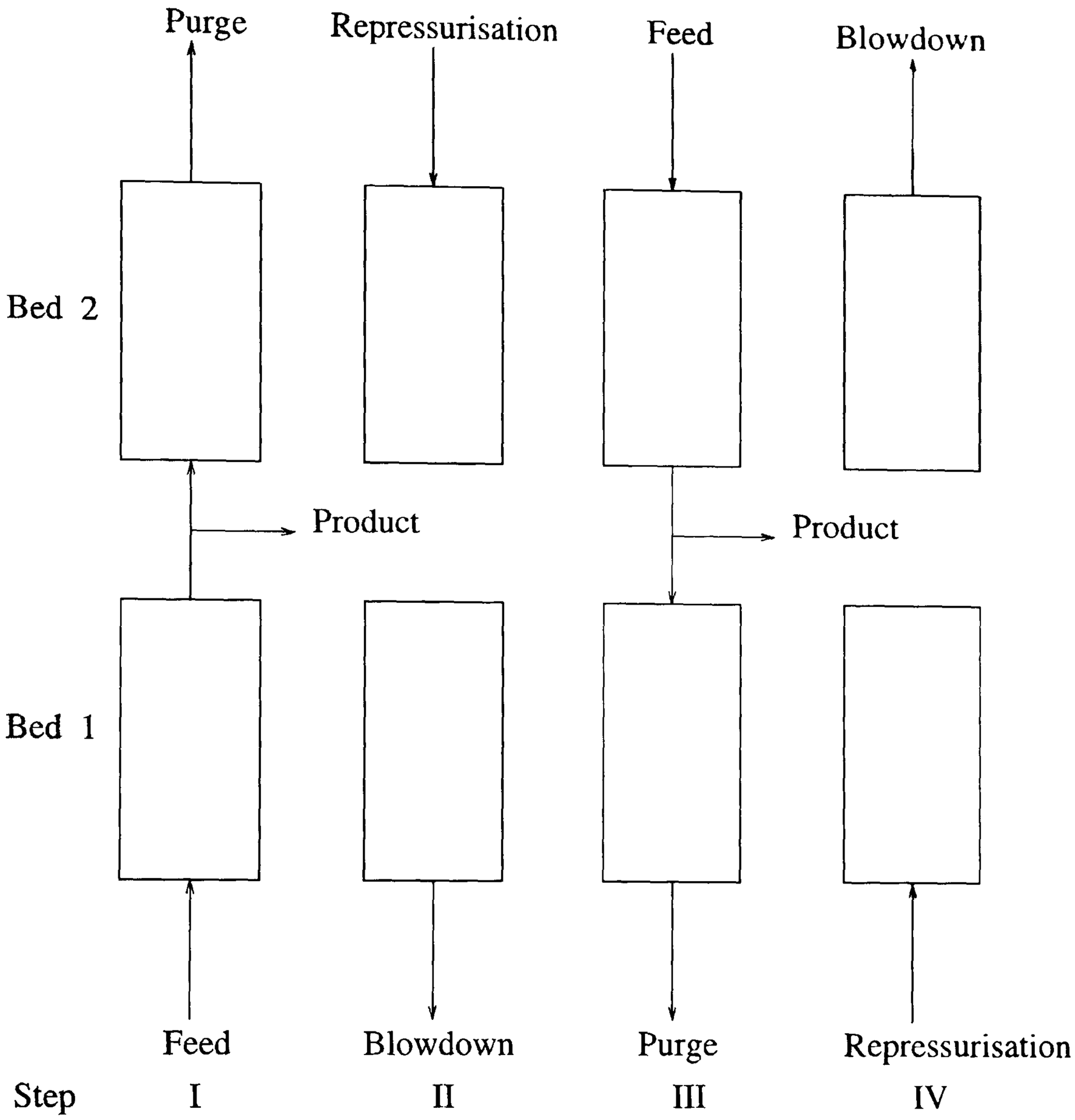



Figure 2.2: Skarstrom pressure swing adsorption cycle.

the design and operation of $H_2$ systems is feasible. Unibed and multibed formulations were both used to describe the five-bed operation. Unibed involves simulation of only one bed and uses storage buffers to mimic the bed interactions. The multibed framework simultaneously treats all beds but only for a portion of the cycle. Multibed simulation truly described the dynamic cycle and accurately predicted both transient and cyclic steady-state behaviours, whereas the unibed framework predicted only cyclic steady-state behaviour and expressed the transient state only approximately.

Through both simulation and experimention. Gomes and Yee (2002) showed the feasibility of applying the PSA process for the removal and recovery of $CO_2$ from exhaust flue gases containing inerts. It was shown that the correction of model equations with multicomponent models in the presence of inerts provided more accurate results, compared to simple corrections involving overall mass balances with input and output inert contents. The simulations for multicomponent sorption showed reasonable agreement with experimental results and the cyclic steady state was found to be established in around three cycles. Furthermore, $CO_2$ purity increased with an increase in cycle time and the optimal cycle time relative to the product purity and recovery was found to be about 300s. Hence, it was indicated that the separation is equilibrium rather than kinetically controlled. This trend was also shown to be valid through experiments. Greater purity was shown to be obtainable with lower feed flow rate and with lower amount of inert component in the mixture. Thus, the process efficiency can be further improved by the reduction of inert content and the optimisation of the feed rate for a given amount of adsorbent. As purity is achieved at the expense of recovery, the determination of complete optimal operating conditions will require an evaluation of desired purity and the corresponding recovery available under feasible conditions.

Recently, Chang et al. (2004) presented a numerical simulation of PSA process with strong adsorbate $CO_2$. The governing equations were converted to dimensionless forms. Dimensionless analysis presumes a representative magnitude for all process variables including the physical properties of the participating components, transport properties between gas and adsorbent phases, geometric dimensions of columns, operating conditions of the process and so forth. The adsorption and concentration profiles of $CO_2$ did not demonstrate much difference regardless of whether the gas–phase accumulation was considered or not. It was indicated that the gas-phase convection mass transfer balances the adsorbent-phase mass accumulation in PSA processes with strong adsorbates. The authors suggested that any algorithm taking the gas-phase accumulation as the main time–derivative term was likely to be subject to considerable stiffness. The algorithm developed was found to reasonably predict the process behaviours even for non-isothermal operations.

### Rapid PSA

The rapid pressure swing adsorption (RPSA) process was initially developed by Turnock and Kadlec (1971). The term "rapid" exemplifies the relatively short step durations (seconds or sub seconds) employed in the pressure swing operation. In PSA, the flow resistance is minimised to reduce pressure drop across the bed by using large adsorbent particles. On the contrary, a typical RPSA bed is usually packed with relatively smaller particles (250-420 $\mu$m), which results in steep and dynamic pressure gradients. This leads to an internal purging mechanism that enhances the regeneration of the adsorbent during the depressurisation step. Because of the high energy requirement created by the large pressure drop incurred, RPSA technology is only economically feasible for small to medium scale operations (Ruthven et al., 1994).

The process consists of a single bed operated in two steps:

- Pressurisation: high pressure feed is introduced to the bed. The strongly adsorbed components are retained in the bed, while the weakly (and/or non-adsorbed) components elute from the bed.
- Depressurisation: the accumulated gas is allowed to exit the bed from both ends. As the bed pressure decreases, the adsorbed components desorb and elute from the bed.

Work by Keller et al. on air separation (Jones et al., 1980; Jones and Keller, 1981) demonstrated that the introduction of a delay step prior to blowdown and a shorter pressurisation step led to higher product recovery (see Fig. 2.3). These modifications improved the performance of the RPSA process in terms of higher product yields but at the expense of higher feed gas pressure.

Alpay et al. (1994b) examined the importance of adsorbent particle size. The authors considered the air separation using RPSA. For a wide range of operating conditions experimental findings showed that an optimal particle size could be identified with respect to product ($O_2$) purity. If, for a selected set of conditions, the particle size was increased,

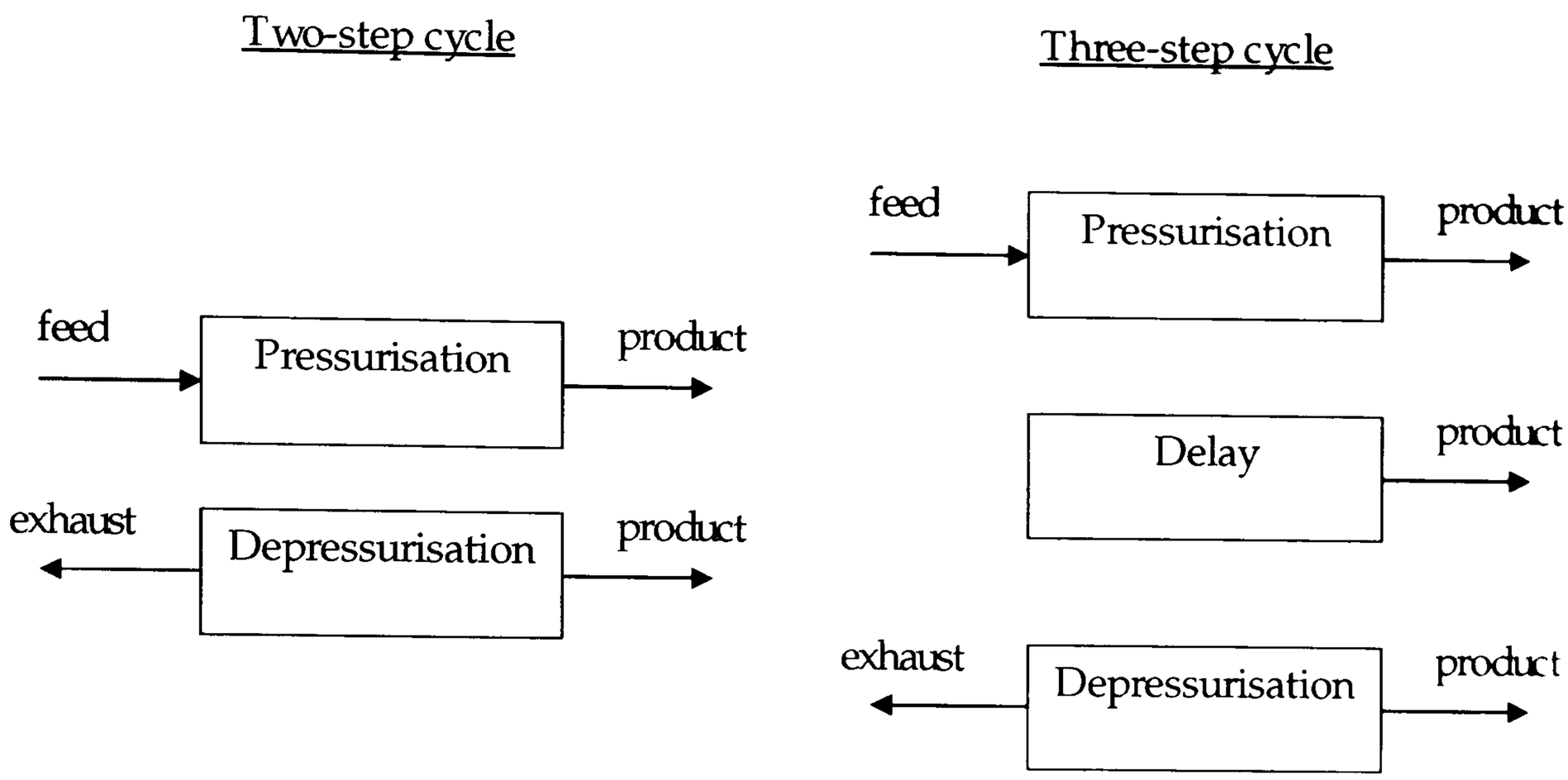



Figure 2.3: Operating steps in RPSA processes.

then the $O_2$ recovery decreased. A theoretical model illustrated that separation performance was limited by ineffective pressure swing for small particles and by intraparticle diffusional resistance for large particles. In cases where small particles were used, the ineffective pressure swing at the product end of the bed resulted in inefficient use of the adsorbent, leading, however, to higher product purity in most cases.

Investigations on both PSA and RPSA processes have been extensively published. Some studies dealt with operational configurations. For example, Bhaumik et al. (1996) reported on a RPSA process that was combined with membrane separation. Suzuki et al. (1996) carried out theoretical work on piston driven, ultra rapid PSA. Optimisation studies of the process include work by Smith and Westerberg (1990), Nilchan and Pantelides (1998) and van Noorden et al. (2003). Issues related to the LDF model and pore diffusion models have also been addressed (Farooq and Ruthven, 1990; Lu et al., 1993; Alpay et al., 1994b; Crittenden et al., 1994). The determination of cyclic steady state and the existence of multiple cyclic steady states have been examined by Ritter and Yang (1991) and LeVan and Croft (1995).

Recently, Kopaygorodsky et al. (2004) developed a dynamic model to determine the vi-

ability of a pulsed Ultra–Rapid PSA (URPSA) air separation process. URPSA involves using a thin bed of monolithic adsorbent and ultra-rapid PSA cycles that consist of two steps: pressurisation and depressurisation (< 3 s). The authors showed the impact of feed pressure, pressurisation time, and depressurisation time on predicted performance characteristics, providing an assessment of the practicability of ultra-rapid cycles and thin monolithic adsorbents for air separation by PSA. The results of their study suggest that URPSA is a viable process that should offer significant advantages over conventional PSA.

In the aforementioned studies, the conventional randomly packed bed of adsorbent particles was used as the mass transfer device for the adsorption processes. However, monolithic adsorbers have been shown to offer important practical advantages over the long-established packed adsorbent columns, especially for applications where the pressure drop has a significant economic impact (Ruthven and Thaeron, 1996, 1997; Ruthven, 2000).

For example, Brandani et al. (2004) studied the adsorption and diffusion of $CO_2$ in two carbon based monoliths, formed by extrusion of an activated carbon adsorbent together with a ceramic material to improve the physical strength. The investigation aimed at characterising the adsorption kinetics and equilibria for $CO_2$ at moderate temperatures. The equilibrium and diffusion parameters were derived by applying two different measurement methodologies and was shown to be consistent. The authors concluded that the dispersion in the monoliths is controlled by mass transfer resistance rather than axial mixing, whereas the diffusion occurs by a combination of the molecular and Knudsen mechanisms, even though the possibility of some additional contribution from micropore resistance cannot be excluded.

### 2.1.2 Adsorption within a solid particle

One of the requirements for solid adsorbents is to provide a large surface area per unit volume in order to adsorb a maximum amount of adsorbate. As a consequence, some commercial adsorbents (e.g. hydrotalcites) are usually derived from microporous materials which enable the gas molecules to diffuse through their pores. The gas molecules are adsorbed onto the solid surface until their concentration in the gas phase is equal to the

equilibrium value corresponding to the adsorbed phase concentration.

A typical porous particle consists of both macropores and micropores (see Figure 2.4). The macropore ($d_{pore} > 200 \times 10^{-10}$ m) is the void space between the microparticles. The micropores ($d_{pore} < 3 \times 10^{-10}$ m) are the pores within the microparticles that contain the active sites for adsorption. For non-equilibrium operations, concentration gradients develop both across the boundary film surrounding the particle as well as within the particle itself. The rate at which the adsorbate is being adsorbed onto the solid surface is directly related to the concentration in the micropores and the availability of free sites.

At the microscopic level, the process of adsorption and desorption can be described by a number of sequential steps:

1. The adsorbate diffuses from the bulk fluid to the external surface of the pellet.
2. The adsorbate diffuses from the external surface of the pellet into and through the macropores.
3. The adsorbate diffuses through micropores.
4. The adsorbate is adsorbed onto the surface of the micropores.
5. The adsorbate is desorbed off the surface of the micropores.
6. The adsorbate diffuses from the micropores into the macropores.
7. The adsorbate diffuses from the macropores to the surface of the pellet.
8. The adsorbate is transported back into the bulk fluid.

For mathematical modelling purposes, it is often useful to identify the rate controlling step, which is assumed to exhibit the highest resistance to mass transfer. All other steps can then be omitted from the model.

The gas phase diffusion occurring in the pores of a particle depends on the relative magnitude of the pore diameter and the mean free path of the adsorbate in the pore under the

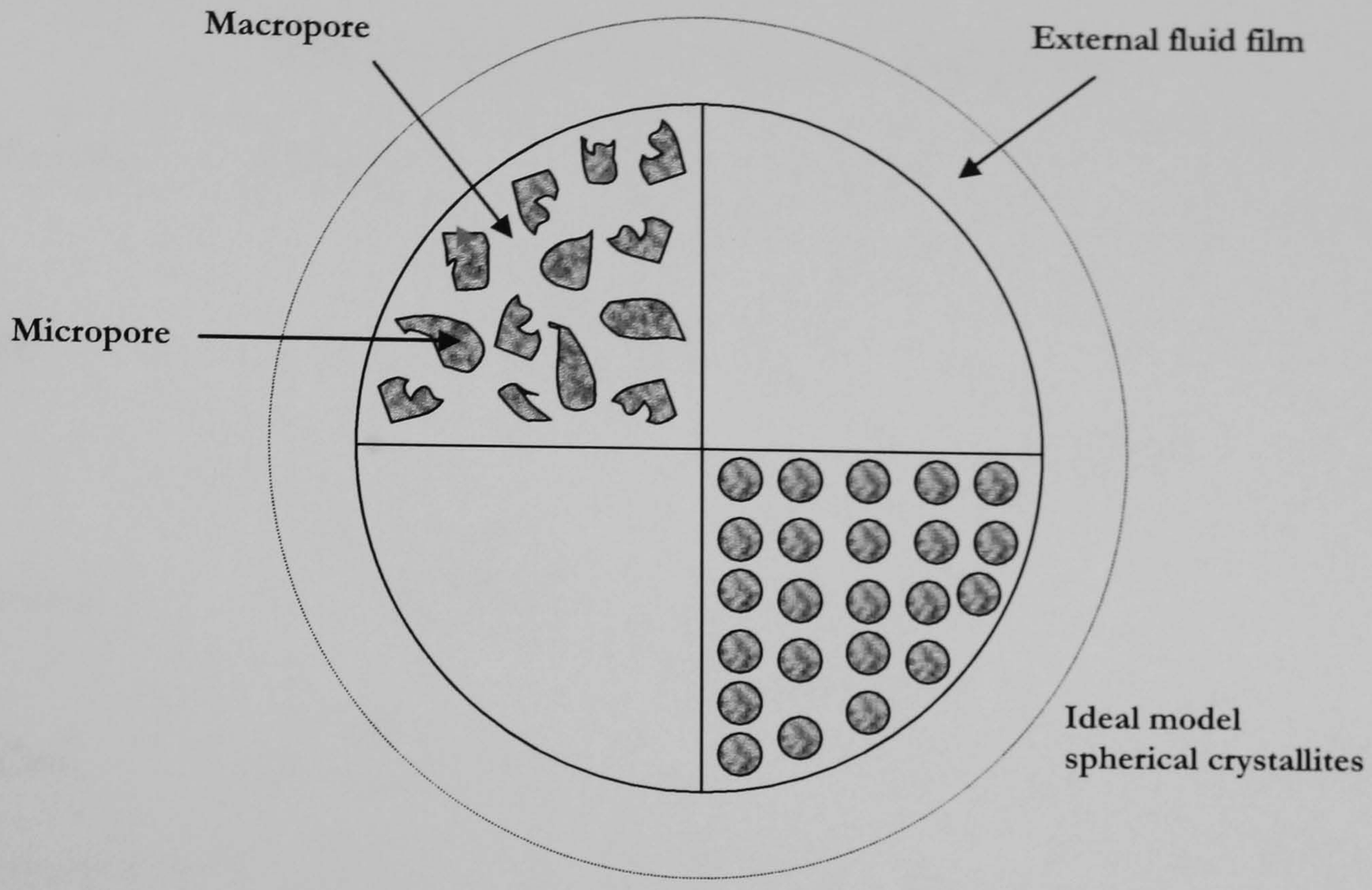



Figure 2.4: Schematic representation of an adsorbent particle (Ruthven, 1984).

operating conditions (Cussler, 1997; Do, 1998). The mechanisms of gas phase diffusion in the pore can be categorised as (see Table 2.2):

1. *Bulk diffusion:* when the pore diameter is much larger than the mean free path of the adsorbate molecule, the collisions among adsorbate molecules are far more frequent than those between the adsorbate molecule the pore wall. Thus, molecular diffusion dominates the transportation.

2. *Knudsen diffusion:* when the mean free path of the adsorbate molecule is much larger that the pore diameter, the collisions between the adsorbate molecules and the pore wall become significant.

3. *Surface diffusion:* in this case the adsorbate molecule diffuses along the micropore wall surface. Many researchers consider surface diffusion to be the dominant mechanism for diffusion in the micropores. For this reason, they often refer to surface diffusion as micropore diffusion (Ruthven, 1984; Yang, 1987).

Table 2.2: Equations for calculation of diffusivities

| Diffusivity | Equation | Comments |
|---|---|---|
| Bulk | $D_m = 0.0018583 \frac{\left[T^3 \left(\frac{1}{M_1} + \frac{1}{M_2}\right)\right]^{1/2}}{P\ \sigma_{12}^2\ \Omega_{D,12}}$ | Chapman–Enskog theory |
| Knudsen | $D_K = \frac{2r}{3}\sqrt{\frac{8RT}{\pi M}}$ | $r$: pore radius |
| Surface | $D_s = \frac{\delta^2}{4\tau}$ (2–D) | $\delta$: distance between two adjacent adsorption sites; $\tau$: occupation time |

In addition to the above–discussed intraparticle diffusion, there is also mass transfer through a stagnant gas layer (or film) around the exterior surface of a particle, commonly known as film diffusion. The corresponding mass transfer coefficient, $k_f$, which is defined as the diffusive flux over the concentration gradient across the film, can be approximated as $k_f = D_m/\delta_f$, where $\delta_f$ is the depth of the film. Since $Sh = (k_f \cdot d_p)/D_m = d_p/\delta_f$, $\delta_f$ can be found if $Sh$ and $d_p$ are known. The characteristic time constant for film diffusion, $t_{FD}$, is defined as $t_{FD} = \delta_f^2/D_m$. For maximum resistance of film diffusion, $Sh = 2$, yielding $t_{FD} = d_p^2/(4 \cdot D_m)$.

### 2.1.3 Adsorbents

The adsorbent acts as a separation medium for the process. As has already been mentioned, a typical adsorbent has a porous structure. The surface area of each pore provides the area for the adsorbate to be deposited. An adsorbent must fulfil the following requirements for effective separation:

1. The adsorbent must selectively retain one or more adsorbates from the fluid either by *equilibrium selectivity* (in which the adsorption of different species depends on the equilibrium affinities) or by *kinetic selectivity* (in which the relative adsorption de-

pends on the differences of intraparticle diffusion rates among different adsorbates).

2. The adsorption of the adsorbate on the adsorbent must be reversible. As time proceeds, the adsorption rate to the adsorbent decreases. Thus the bed must be regenerated for repeated uses either by lowering the concentration (or partial pressure) of the adsorbate or by raising the bed temperature.

3. The adsorbent must be able to adsorb the maximum amount of the adsorbate per unit weight of the adsorbent.

Commercial adsorbents are available in different shapes and sizes. These properties control the mass transfer between gas and solid, the rate of intra–particle diffusion and the pressure drop incurred in the bed. Typical adsorbents are silica gel, alumina, activated carbon, zeolites, carbon activated sieves and organic polymers.

### 2.1.4 Isotherms

Adsorption isotherms can be expressed in the following general mathematical form:

$$[q_i^*]_T = q_i^*(p_i) \tag{2.1}$$

where $q^*$ is the amount of species $i$ adsorbed at equilibrium (mol kg$^{-1}$) at a specified temperature, $T$, and $p_i$ the corresponding gas phase partial pressure (Pa). In other words, the adsorption isotherms relate the amount adsorbed onto the surface of a particular adsorbent at equilibrium to the concentration (or partial pressure) of the adsorbate in the gas phase (see Fig. 2.5). Several models have been proposed in the literature (see Table 2.3) to predict pure and multicomponent isotherms (Ruthven, 1984; Yang, 1987; Do, 1998; Seader and Henley, 2006).

Of the isotherms presented in Table 2.3, the Langmuir–type models are found to be adequately representative of physical adsorption and thus they are most commonly used (see Fig. 2.6). These models are based on the following assumptions:

- Molecules are adsorbed at a fixed number of well-defined localised sites.

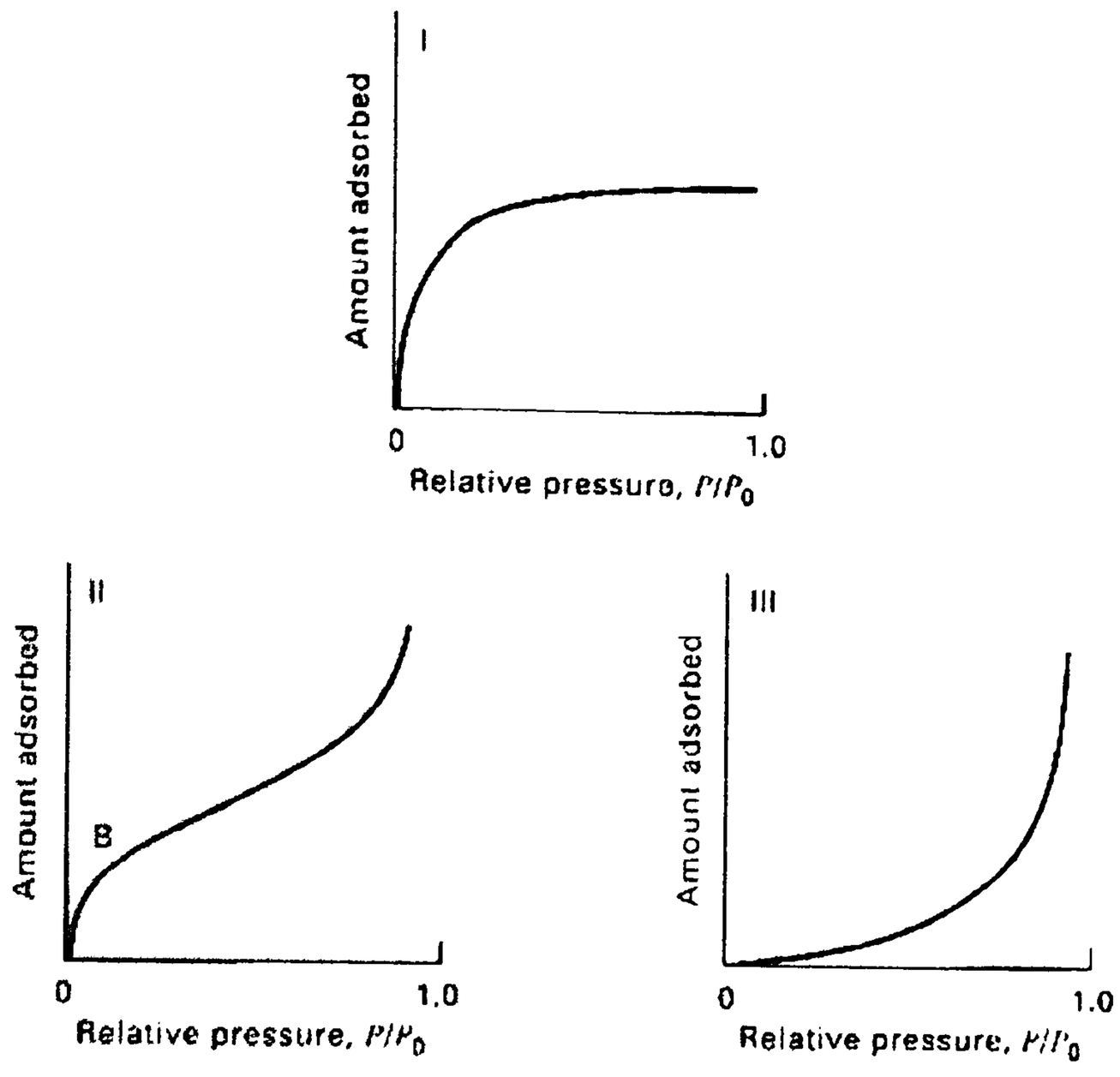



Figure 2.5: Types of adsorption isotherms. Type I: unimolecular adsorption characterised by a maximum limit in the amount adsorbed; Type II: multimolecular adsorption of BET type; Type III: multimolecular adsorption where the heat of adsorption of the first layer is less than that of succeeding layers; Type IV–V: hysteresis phenomena in multimolecular adsorption (see Seader and Henley, 2006, p. 559).

- Each site can hold one adsorbate molecule.
- All sites are energetically equivalent.
- There is no interaction between molecules adsorbed on neighbouring sites.

Table 2.3: Adsorption isotherm equations (general mathematical expressions)

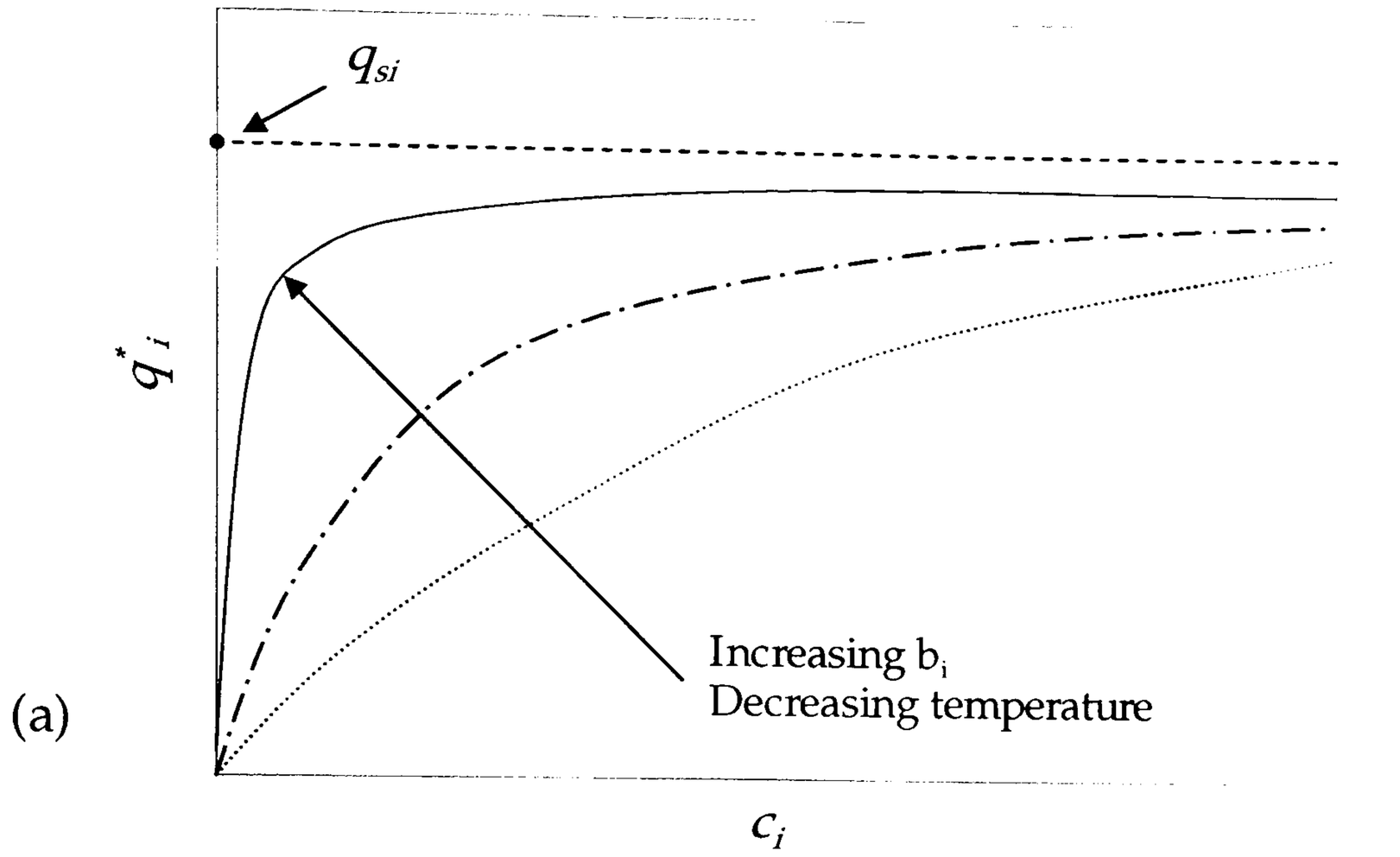
| Name | Equation | Comments |
|---|---|---|
| Henry's law | $\theta = \kappa \cdot p, \qquad \theta = q^*/q_s, \quad \kappa = k_a/k_d$ | $\kappa$: equilibrium constant |
| Langmuir | $\theta = \kappa \cdot p/(1 + \kappa \cdot p)$ | See Eq. 2.2 |
| Freundlich | $\theta = k \cdot p^{1/n}, \qquad n > 1, \quad k, n = fn(T)$ | No adsorption limit |
| BET | $\frac{p}{q^*(p_s - p)} = \frac{1}{q_m c} + \frac{(c-1)}{q_m c} \cdot \frac{p}{p_s}$ | $c$: constant; $q_m$: monolayer adsorbed quantity |

Therefore, of the molecules striking the surface, only those that strike the bare surface are candidates for adsorption, *i.e.*, molecules that strike an adsorbed molecule are elastically reflected. Besides, the probability of desorption of a molecule from the surface is the same whether or not the neighbouring positions on the surface are empty or filled by others molecules (see Fig. 2.7).

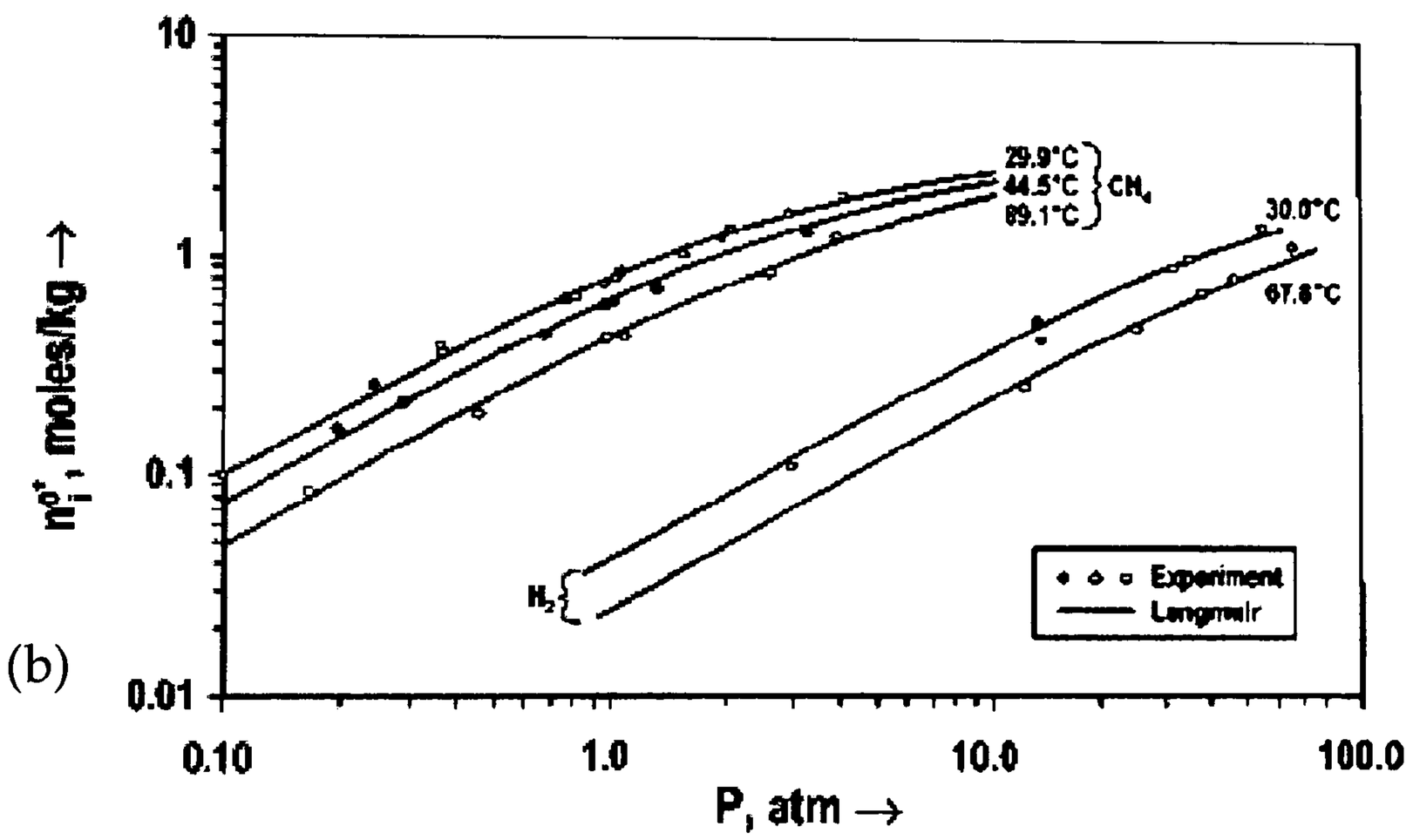
For adsorption of a pure gas adsorbate, $i$, the Langmuir isotherm is given as:

$$\frac{q_i^*}{q_{si}} = \frac{b_i c_i}{1 + b_i c_i} \tag{2.2}$$

where $q_{si}$ denotes the maximum (saturation) amount that can be adsorbed at equilibrium (mol kg$^{-1}$), $b_i$ is the Langmuir constant for the specific adsorption process (m$^3$ mol$^{-1}$) and $c_i$ is the adsorbate concentration in the gas phase (mol m$^{-3}$). The Langmuir adsorption isotherm is restricted to a monomolecular layer, and for a gas mixture of NC components




(a)




(b)

Figure 2.6: (a) The Langmuir isotherm (see Do, 1998, p.16) (b) Pure gas adsorption isotherms for $CH_4$ and $H_2$ on activated carbon (Waldron and Sircar, 2000).

it can be extended to:

$$\frac{q_i^*}{q_{si}} = \frac{b_i c_i}{1 + \sum_{j=1}^{NC} b_j c_j} \tag{2.3}$$

At low gas phase concentrations ($b_i c_i << 1$), the Langmuir–type equations reduce to the

linear form:

$$q_i^* = K_i c_i = m_i p_i \tag{2.4}$$

where $K_i$ is the adsorption equilibrium constant ($m^3\ kg^{-1}$)–the so called Henry's constant– and $m_i$ is usually referred to as the adsorption isotherm gradient ($mol\ kg^{-1}\ Pa^{-1}$). On the other hand, at high adsorbate concentrations ($b_i c_i >> 1$), $q^*$ approaches $q_s$.

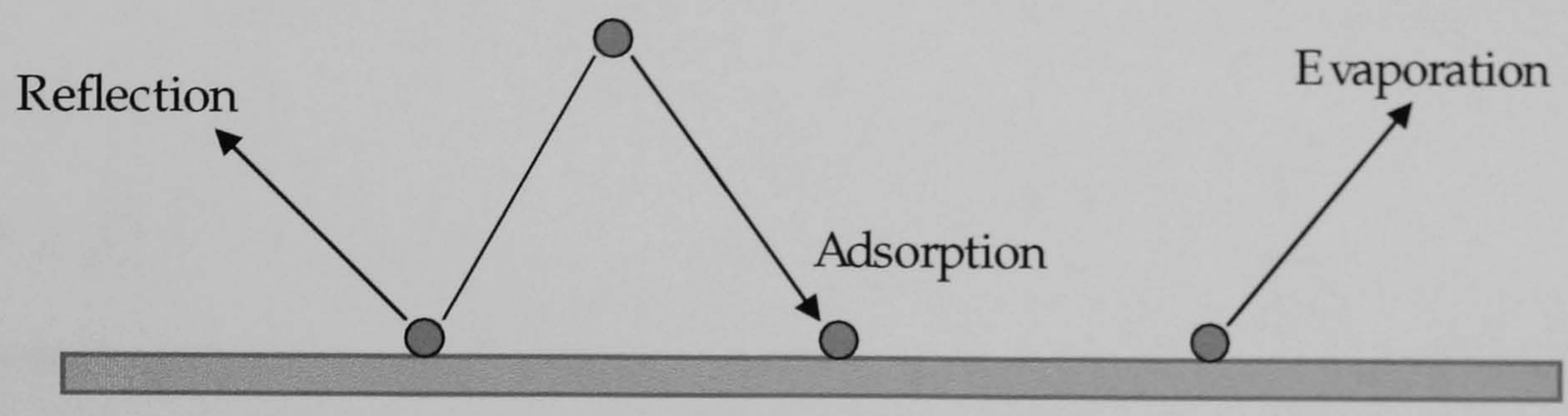



Figure 2.7: Schematic diagram of Langmuir adsorption mechanism on a flat surface (see Do, 1998, p.14).

### 2.1.5 Mass transfer phenomena

The rate at which the adsorbate in the gas phase is transferred to the solid is influenced by the controlling mass transfer resistance. This may be within the adsorbent particle itself, or within an external film surrounding the particle, or a combination of both.

The most widely used models to describe the transportation of the adsorbate to the solid are listed below:

**Linear driving force model (LDF)**

The LDF model is a simplification of the solution to the diffusion equation within a spherical particle (assuming a linear isotherm) expressed by:

$$\frac{\partial q_{ri}}{\partial t} = \frac{D_{ei}}{r^2}\frac{\partial}{\partial r}\left(r^2 \cdot \frac{\partial q_{ri}}{\partial r}\right), \qquad \forall r \in (0, R_p),\ t \geq 0 \tag{2.5}$$

where $q_{ri}$ represents the adsorbed phase concentration of component $i$ (mol kg$^{-1}$). $r$ is the radial position within a spherical particle of radius $R_p$ (m) and $D_{ei}$ the effective diffusivity of component $i$ (m$^2$ s$^{-1}$).

A quantitative description of an actual separation problem requires the simultaneous solution of Eq. 2.5 with the interpellet material balance. It is computationally convenient though to approximate Eq. 2.5 by a simpler expression for the adsorption rate, $\partial q_i/\partial t$, where $q_i$ is the adsorbed phase concentration, $q_{ri}$, averaged over the entire volume of a particle of radius $R_p$:

$$q_i = \frac{3}{R_p^3}\int_0^{R_p} q_{ri}\cdot r^2 dr \tag{2.6}$$

The linear driving force approximation of Glueckauf and Coates (1947) is the simplest and most widely used for mass transfer limited adsorption:

$$\frac{\partial q_i}{\partial t} = k_i(q_i^* - q_i) \tag{2.7}$$

where $q_i^*$ denotes the the adsorbed phase concentration in equilibrium with the local bulk (interpellet) phase concentration and $k_i$ is the mass transfer coefficient (s$^{-1}$), which is given by:

$$k_i = 15\cdot\frac{D_{ei}}{R_p^2} \tag{2.8}$$

For large values of $k_i$, the LDF model approaches the instantaneous local equilibrium model (see below). Although the LDF model it has been formally derived for linear adsorption isotherms, it has been the key tool in adsorptive process studies and design (Yang, 1987; Sircar and Hufton, 2000a) and it has been extensively investigated in the literature (see for example Choong and Scott, 1998; Sircar and Hufton, 2000b; Serbezov and Sotirchos, 2001; Rouse, 2004).

**Instantaneous local equilibrium model**

In cases where the mass transfer resistance between the gas and solid phases can be neglected, the instantaneous local equilibrium model is applied and is expressed by:

$$\frac{\partial q_i}{\partial t} = \frac{\partial q_i^*}{\partial t} \tag{2.9}$$

### Pore diffusion model

The pore diffusion model assumes that the rate of mass transfer is approximated by the fluxes at the pore mouths of the microparticles by solving the diffusion equations for the microparticles (Yang and Doong, 1985). The mass balance for component $i$ inside the pores of a spherical adsorbent particle is:

$$\varepsilon_p \frac{\partial c_{ri}}{\partial t} + \frac{1}{r^2}\frac{\partial}{\partial r}\left(r^2 N_{ri}\right) + \varrho_p \frac{\partial q_{ri}}{\partial t} = 0, \qquad \forall r \in (0, R_p),\ \forall z \in [0, L],\ t \geq 0 \tag{2.10}$$

where $\varepsilon_p$ is the particle porosity, $c_{ri}$ the molar concentration of the gas phase in the pore (mol m$^{-3}$), $N_{ri}$ molar flux of component $i$ into the particle (mol m$^{-2}$ s$^{-1}$) and $\varrho_p$ the particle density (kg m$^{-3}$).

## 2.1.6 Heat transfer phenomena

Adsorption is an exothermic process. The heat generated by adsorption in a packed bed is transferred from the solid particles to the surroundings by conduction between solid particles in both axial and radial directions, and convection from the solid particle to the fluid medium.

The heat transfer resistance for a solid particle subjected to a gas flow can occur either in the external gas film and/or within the particle itself, depending on which one is the controlling resistance. For typical periodic adsorption processes, the rate controlling step is that in the external film (see Ruthven, 1984, pp. 216–217).

When the heat transfer resistance between the solid particle and the gas phase is negligible, instantaneous thermal equilibrium is established between the two phases. When the heat transfer resistance is important, the two phases are of different temperatures requiring a separate energy balance for the description of the heat transport of each phase. In this work, due to the physical properties and the operating nature of the integrated reactor–adsorber, a non–thermal equilibrium model is adopted, since in such a system heat consumption and release by reaction and adsorption may result in a deviation from the instantaneous thermal equilibrium.

## 2.2 Sorption–Enhanced Reaction Process

The investigation of reactor concepts that combine at least two process functionalities synergistically within a single unit has been the subject of considerable attention in both university and industrial research. These conceptualisations are commonly cited as multifunctional reactors (Krishna, 2002). Integration of reaction and separation presents a momentous category of multifunctional reactors (see Fig. 2.8).

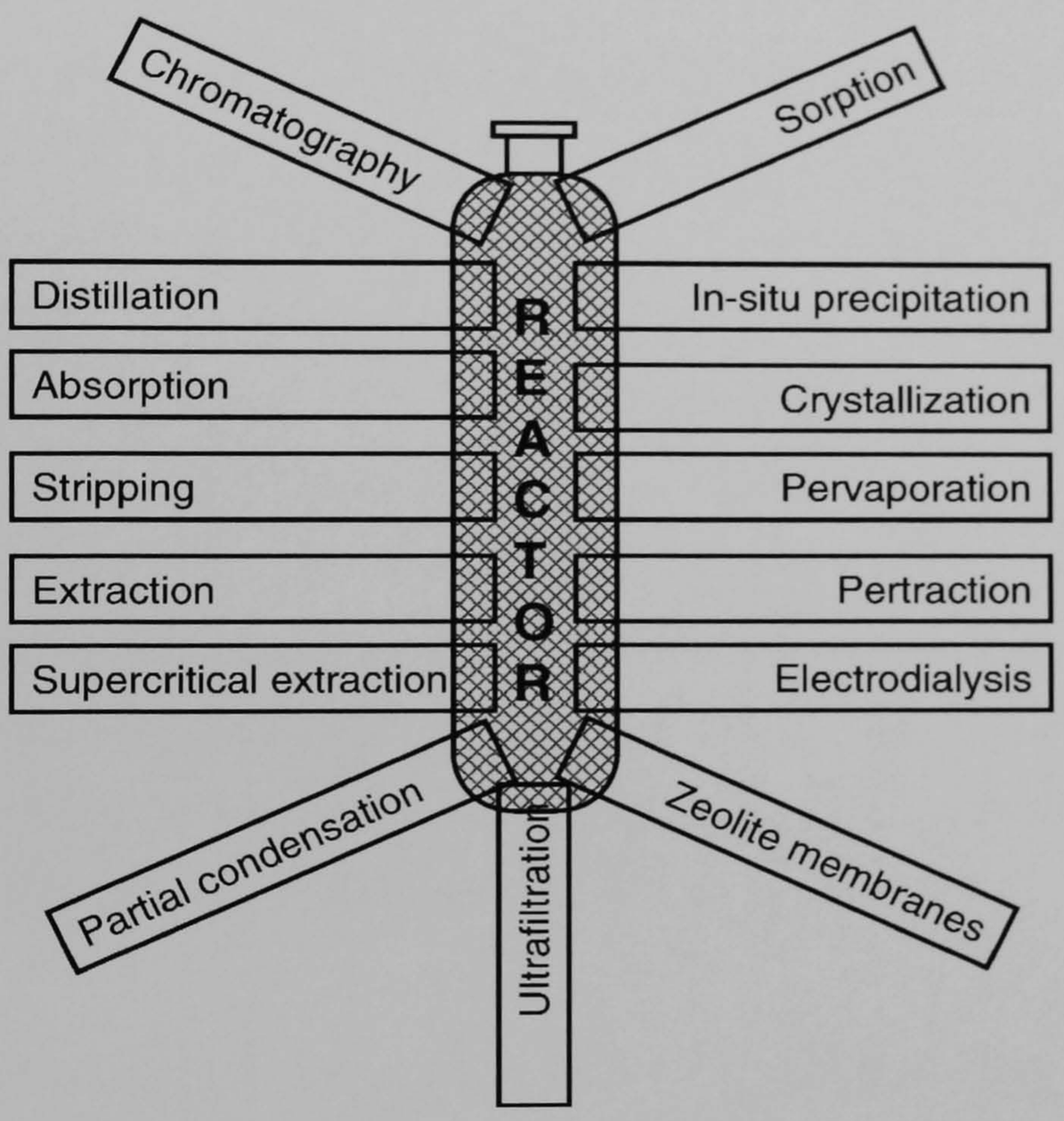



Figure 2.8: *In situ* separation functionalities integrated into the reactor (Krishna, 2002).

The adsorption–based processes of this kind are particularly suitable for large-scale processing under catalytic conditions, mainly due to the established aspects of the process-mechanical design of such systems and to the relatively rapid kinetics associated with adsorptive separations. Besides, a wide choice of natural and synthetic adsorbents exists for attaining the desired separations under the conditions of reaction. The advantages of adsorptive reactors over conventional catalytic reactors include improved reactor performance (e.g. higher conversion and selectivity) and the prospective for primary product

separation. Extensive research has been carried out on the different types of adsorptive reactors, such as chromatographic reactors (Bjorklund and Carr, 1995; Lode et al., 2001; Viecco and Caram, 2006), temperature swing reactors (Yongsunthon and Alpay, 1998, 1999) and pressure swing reactors (Chatsiriwech et al., 1994; Cheng et al., 1998; van Noorden et al., 2003).

The work carried out by Air Product and Chemicals Inc. on PSR[1] systems is of great significance within the scope of this thesis. Carvill et al. (1996) investigated a process for the production of carbon monoxide, referred to as Sorption–Enhanced Reaction Process (SERP), for the equilibrium controlled reverse water–gas shift reaction ($CO_2 + H_2 \rightleftharpoons CO + H_2O$) with the preferential adsorption of $H_2O$. The adsorbent was periodically regenerated by using the principles of pressure swing adsorption. The operation involved five steps in the sequence (see Fig. 2.9): [1] product release (adsorptive reaction); [2] counter-current depressurisation; [3] counter-current purge with a weakly adsorbing extraneous gas; [4] counter-current product (CO) purge with a portion of the CO produced in step [1] in order to remove the weakly adsorbing extraneous gas from the bed void space; and [5] product pressurisation (with CO). The SERP operated at 250°C to achieve 36% conversion, while the equivalent PFR at the same operating temperature was 10%. The obtained product purity exceeded 99% (v/v) at a pressure of 4.8 bar.

Hufton et al. (1999) evaluated the SERP concept for the production of hydrogen by steam-methane reforming (SMR) reaction, using a fixed packed bed column of an admixture of a commercial SMR catalyst and a proprietary chemisorbent to remove carbon dioxide selectively from the reaction zone at a temperature of 450°C and a pressure of 4.8 bar. The reactor directly produced high-purity hydrogen (>95 mol %) at a high methane to hydrogen conversion (>80%) with dilute methane (<5 mol %) and trace carbon oxide (<50ppm) impurities. A conventional SMR reactor needed to be operated at a much higher temperature (>650°C) to achieve the same conversion and produced a much lower purity of hydrogen product (~75 mol %) with a large quantity of carbon oxide (~20 mol %). Continuing this work, Waldron et al. (2001) demonstrated the actual cyclic perfor-

[1]Periodic Separating Reactor or Pressure Swing Reactor

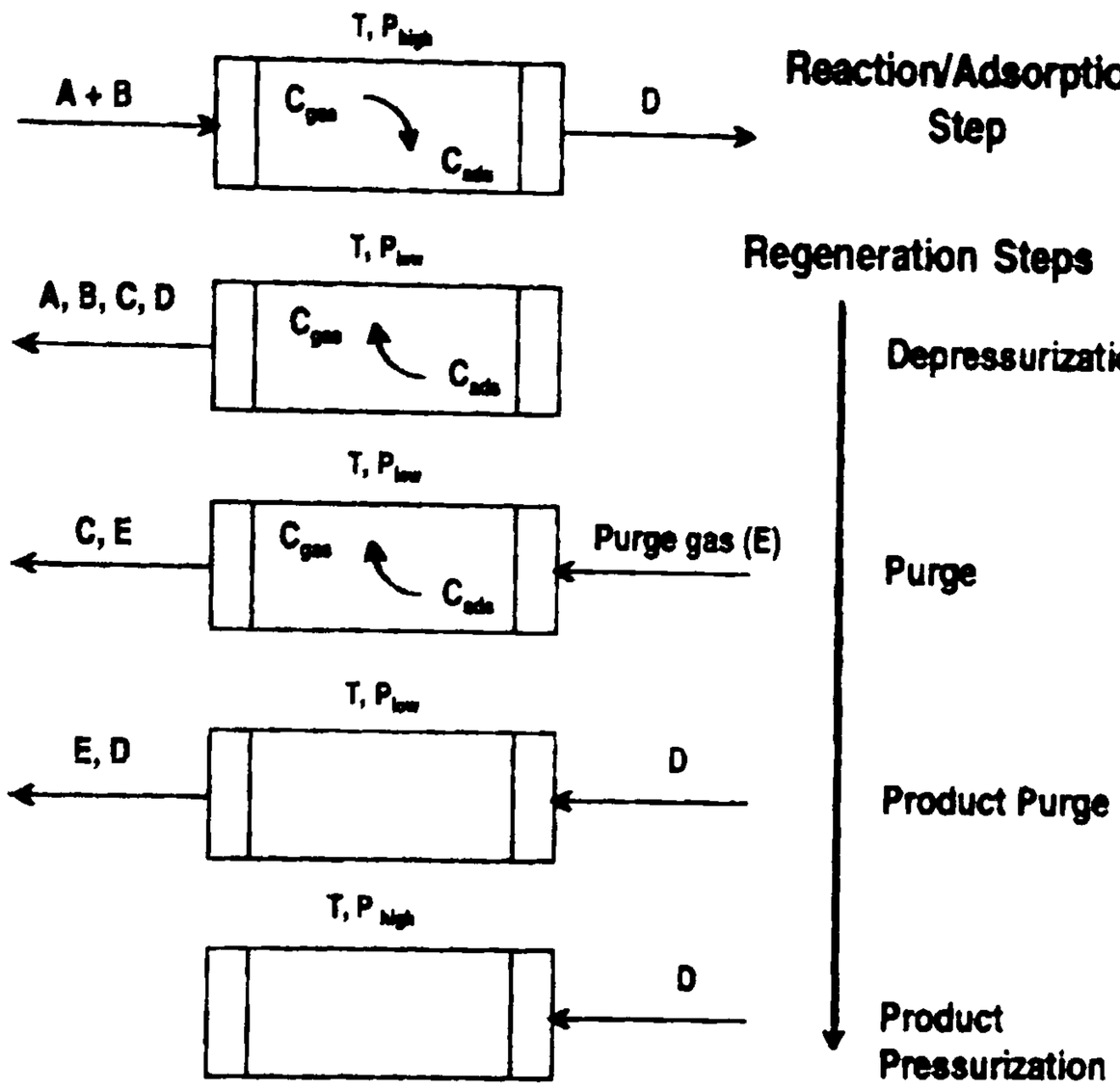



Figure 2.9: Diagram of the sequential SERP steps for the production of CO by the reverse water–gas shift reaction (Carvill et al., 1996).

mance of the SERP concept for hydrogen production using a pilot scale apparatus with a proprietary SMR catalyst this time. Steady–state performance data were reported for a reaction temperature of 490°C and pressures ranging from 1.8 to 4.5 bar. The process was capable of directly producing 88-95% hydrogen with methane as the primary impurity. It was also indicated that the concentrations of carbon oxides could be kept below 40 ppm by controlling the operating conditions of the process, whereas the conversion of methane to hydrogen could be much larger than that dictated by thermodynamics by catalyst- alone reactor.

Recently, numerous theoretical and experimental studies on adsorptive reactor concepts for hydrogen production through steam methane reforming have been published. An inclusive review is given below.

### 2.2.1 Sorption–enhanced SMR

Ding and Alpay (2000b) proposed a non-isothermal and non-isobaric dynamic model for the aforementioned process, which was found to accurately predict the observed species elution profiles from the reactor packed with an admixture of a Ni–based SMR catalyst and hydrotalcite adsorbent. The authors investigated the influence of some key operating parameters on the degree of reaction (conversion) enhancement. Their work led to the following conclusions: (i) a high reactor space time is favourable for minimising the effects of adsorbent intraparticle mass transfer resistances and, of course, for overcoming kinetic limitation to reaction, (ii) for a given conversion of methane or yield of carbon dioxide, the SE-SMR process enables operation with lower steam-to-methane ratios, and/or higher operating pressures, and (iii) under the conditions of SE-SMR operation, negligible deactivation of the catalyst occurs.

Xiu et al. (2002a) theoretically analysed the five–step one–bed SERP, using data from the earlier works of Hufton et al. (1999) and Ding and Alpay (2000a,b). A detailed mathematical model was developed and used to determine suitable operating conditions of this periodic process that allow the production of a sufficiently high $H_2$ purity (average purity over 80%) with traces of CO and $CO_2$, high methane conversion, fast adsorbent regeneration and cyclic steady–state operation. The simulation results were found to be in reasonable agreement with experimental data from the literature (Hufton et al., 1999; Ding and Alpay, 2000a) for SE–SMR. The authors suggested that for the specified system, increasing the packing density, the adsorbent/catalyst ratio and the residence time in the adsorptive reactor can improve methane conversion and favour the production of high purity hydrogen. They concluded that there is scope for improvement of the adsorbent regeneration method, since simulations showed that a longer reactor produces purer $H_2$ product gas, but, on the other, hand pressure losses during the regeneration step limit the process performance.

In their subsequent study, a modification of the aforementioned process was theoretically investigated, in which reactive regeneration (through methanation and reverse water gas shift reactions) was used to improve $CO_2$ desorption (Xiu et al., 2002b). A four step one–

bed process was proposed: [1] high pressure reaction/adsorption at high temperature; [2] depressurisation; [3] low pressure reactive regeneration with a mixture of 10% $H_2$ in $N_2$ at low temperature and purge with steam at high temperature; and [4] pressurisation with steam at high temperature. The operating temperature during the regeneration step was lowered to thermodynamically favour the methanation reaction. It was shown that this mode of operation resulted in considerably shorter regeneration times, while maintaining high $H_2$ purity and production rate. The model results qualitatively agreed with experimental data reported by Waldron et al. (2001). The authors also demonstrated that the *in situ* separation and reaction concept could be extended to possibly integrate sequential reaction systems involving simultaneous endothermic and exothermic reactions.

The above authors later presented a non–isothermal, non–adiabatic and non–isobaric model for the SE–SMR that takes into account the effects of intraparticle diffusion limitations on the reactions and $CO_2$ adsorption processes (Xiu et al., 2003a). The Fickian diffusion model was adopted and the mechanism of the adsorption–enhanced SMR was studied by analysing the profiles of the bed concentrations, temperature, velocity, pressure, reaction and adsorption rates. It was found that the adsorbent is saturated gradually with $CO_2$ from the inlet part of the adsorptive reactor, propagating to the outlet with time. Correspondingly, the adsorption–enhanced reaction (AER) zone moves ahead along the bed and sharp peaks of the AER rates were predicted at the adsorption front edge. The authors also pointed out that the effectiveness factors were difficult to be evaluated in comparison with conventional reactor. However, they proposed that the presented method can be used to estimate the average effectiveness factors that may be subsequently applied in a simpler model (e.g. LDF model for $CO_2$ adsorption combined with average effectiveness factor for the catalyst).

Consequently, Xiu et al. (2003b, 2004) applied the subsection–controlling strategy to the design of the adsorptive reactor to improve the SE-SMR. They used subsection–packing ratio of adsorbent and catalyst and subsection–controlling wall temperature (see Fig. 2.10). In the case of the subsection–controlling wall temperature, there is a lower operating temperature zone at the outlet of the adsorptive reactor where the remaining CO and $CO_2$

concentrations in the gas stream can be decreased further by the principle of temperature–induced equilibrium shift. In the inlet zone of the adsorptive reactor, the SMR is more intensive, and the reaction rate is fast, so it is packed with more catalyst than the middle section. In the second section the sorption-enhanced SMR is dominant and thus it may be packed with more adsorbent. A mathematical model for this process was developed and at low operating pressures a product gas with $H_2$ purity above 85% and traces of $CO_2$ (<300 ppm) and CO (<30 ppm) can be continuously produced with higher hydrogen productivity by a four-step one-bed (a 6 m long adsorptive reactor) pressure swing sorption-enhanced SMR cyclic process.

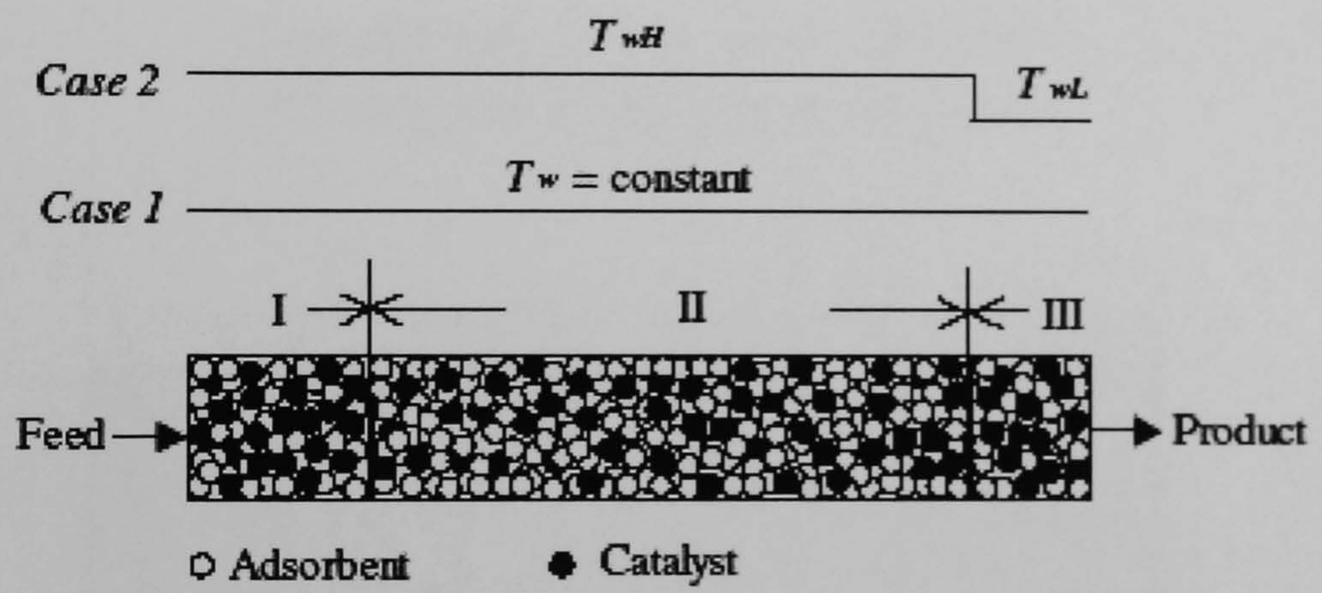



Figure 2.10: Schematic of sorption–enhanced reactor with subsection–controlling strategy (Xiu et al., 2003b).

More recently, the same research group recommended that the models by Ding and Alpay (2000b) and Xiu et al. (2002a), albeit realistic for process description, do not provide directly comprehensible results due to the highly nonlinear interactions involved. They therefore proposed a simplified and conceptually more compact model for facilitating the process analysis (Wang and Rodrigues, 2005). More specifically, a two–section reactor model was developed, the first part containing the catalyst alone (equilibrium section) and the second packed with an admixture of the catalyst and the $CO_2$ adsorbent (adsorption reforming section). It was assumed that the bed length of the first section required for achieving equilibrium conversion is negligible, compared to the relatively long bed length of the adsorption reforming section (see Fig. 2.11). Additionally, thermodynamic consistency

of the model was accomplished by assuming isothermal and isobaric operation for both sections. This approach allows the contribution from the equilibrium conversion and the sorption enhancement to be quantitatively identified. The authors showed the bed residence time to have a significant impact on the sorption enhancement, with longer residence times being suitable for promoting $H_2$ purity and controlling CO concentration. A comparison between the two alternatives for extending residence time indicated that increasing bed length can result in higher $H_2$ productivity than lowering gas velocity.

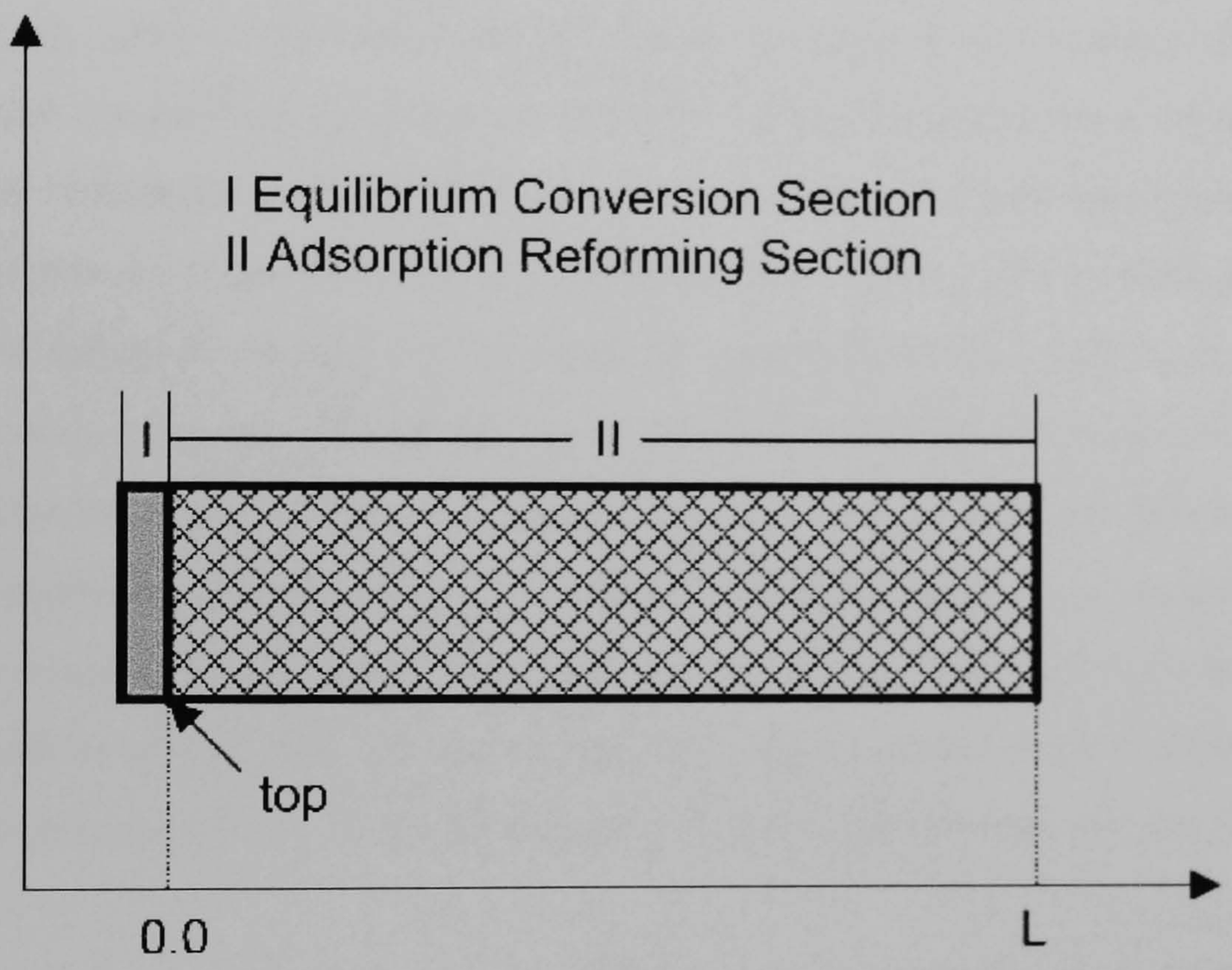



Figure 2.11: The conceptual scheme for the two–section model proposed by Wang and Rodrigues (2005).

Lee et al. (2004) analysed the transient behavior of the catalytic SMR over a Ni–catalyst coupled with simultaneous $CO_2$ removal by carbonation of CaO pellets in a packed bed reactor for hydrogen production through a mathematical model and reaction experiments for model verification. A dynamic model was developed to describe the process at non–isothermal, non–adiabatic, and non–isobaric operating conditions assuming that the rate of CaO carbonation in a local zone of the packed bed is governed by kinetic limitation or by mass transfer limitation of the reactant $CO_2$. The model was used to investigate

the effects of major operating parameters on the transient behavior of the *in situ* CaO carbonation-enhanced SMR. The bed temperature was found to be the most important parameter for determining the amount of $CO_2$ removed, while higher temperatures resulted in higher CO production during the pre–breakthrough period. The authors concluded that operation at high pressure, high steam to methane feed ratio and decreased feed rate at a given temperature are favorable for increasing the degree of the overall utilisation of CaO pellets in the reactor bed, and for lowering the CO concentration in the product.

Rajasree et al. (2006) proposed a reactor design strategy that considers the combination of tubular packed–bed microreactor (TPBM) operation and catalyst dilution by $CO_2$ adsorbent for enhancement of the SMR process. A dynamic 2–dimensional pseudohomogeneous model was developed and used to investigate the improvement in SMR performance pertaining to effects of varying reactor diameter, extent of catalyst dilution by adsorbent, and solids packing density. The simulation results indicated that the improved heat transfer characteristics of the TPBM combined with the effects of catalyst dilution and $CO_2$ adsorption complement each other. As a result, enhanced reactor performance in terms of methane conversion and hydrogen purity was predicted. The authors concluded that the simultaneous optimisation of reactor diameter and adsorbent loading could contribute towards the cost reduction and miniaturisation of fuel processors for fuel cell applications.

Discussion so far considered fixed–bed adsorptive reactors, which represent the predominant configuration in the literature for both experimental and modelling investigations of the SE–SMR process. Fluidised bed reactor systems for hydrogen production by adsorption–enhanced SMR will now be reviewed. Fluidised beds are commonly used in processes, which involve continuous catalyst regeneration, e.g. fluid catalytic cracking. Their advantages over packed bed reactors include enhanced heat transfer, temperature uniformity and higher catalyst effectiveness factors.

Kurdyumov et al. (1996) used a specially treated form of dolomite as adsorbent (active CaO with chemically inert MgO) in a continuous fluidised bed reactor containing microspheres of nickel on alumina catalyst. Freshly regenerated particles of the adsorbent were

fed to the fluidised bed in a direction countercurrent to reactant gas flow. Large adsorbent particles were used so that they could travel due to gravity through the fluidised catalyst particles toward the feed gas end of the bed. The size and density differences between the adsorbent and catalyst materials allowed complete separation between them at the gas inlet end. The adsorbent particles were pneumatically carried to a thermal regenerator for $CO_2$ desorption. A significant enhancement of $CH_4$ conversion to $H_2$, compared to that achieved by using catalyst alone, was reported at a reaction temperature of 650°C, pressure 2 MPa and $H_2O/CH_4$ molar ratio equal to 6. The product gas leaving the fluidised bed contained 97–98% $H_2$ and virtually no carbon oxides.

Prasad and Elnashaie (2004) proposed and modelled a novel reactor–regenerator configuration in which a CaO–based adsorbent was added to assist hydrogen permselective membranes in "breaking" the thermodynamic equilibrium of SMR. The authors chose a fast fluidised bed as reformer and found that increasing the adsorbent particle size by incorporating a slip factor into their model, resulted in higher hydrogen yield, as the residence time for carbonation increased.

More recently, Johnsen et al. (2006a) carried out an experimental study of SE SMR in a bubbling fluidised bed reactor with dolomite as $CO_2$ acceptor. The bed was operated cyclically and batchwise, alternating between reforming/carbonation conditions and higher–temperature calcination conditions for adsorbent regeneration (see Fig. 2.12). The catalyst was not separated from the adsorbent between the cycles. An equilibrium $H_2$ concentration of ~98% on dry basis was reached at 600°C and atmospheric pressure. Particular attention was given to the multi–cycle performance of both the catalyst and the adsorbent. Multiple reforming/regeneration cycles showed that hydrogen concentration remained at 98–99 vol % after 4 cycles. The total production time was reduced with an increasing number of cycles due to loss of $CO_2$–uptake capacity of the dolomite, but the reaction rate seemed to be unaffected for the conditions investigated.

Based on the above experimental findings, theoretical analysis of a dual bubbling fluidised bed reactor system was conducted (Johnsen et al., 2006b). A steady- state model was

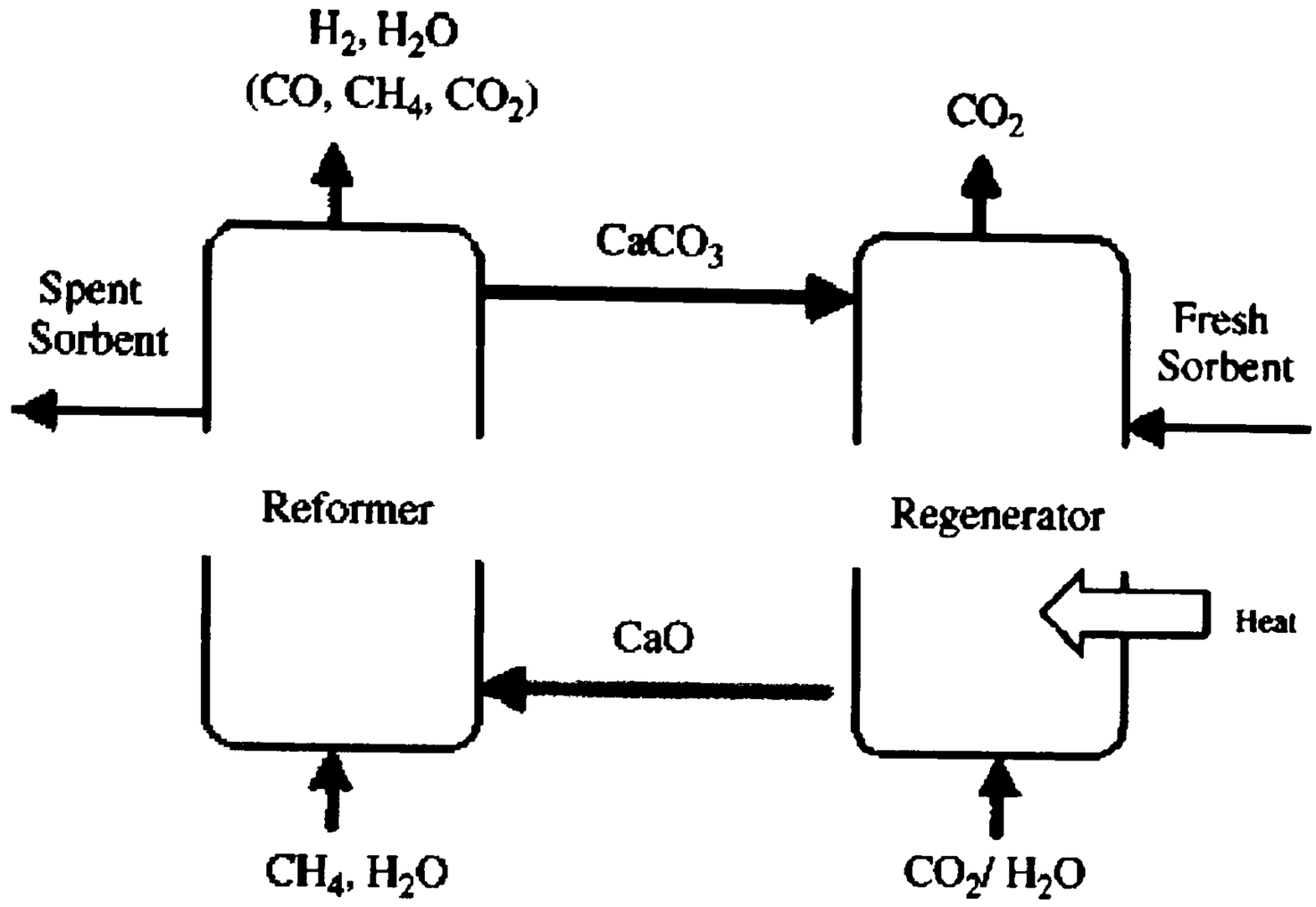



Figure 2.12: Simplified schematic of the sorption–enhanced SMR process proposed by Johnsen et al. (2006a).

developed and used to predict the product composition with focus on the expected energy efficiency and carbon capture performance of a continuous system. Dry $H_2$ concentrations above 98% were predicted for temperatures of 600°C and a superficial gas velocity of 0.1 m $s^{-1}$. Simulation results also showed that the reformer temperature should not be lower than 540°C or above 630°C for carbon capture efficiencies to exceed 90%. Calculations showed that operating at relatively high solids circulation rates results in higher system efficiency, whereas the addition of fresh adsorbent reduces the efficiency of the system. The authors concluded that the cycling capacity property of any chosen adsorbent is of great importance in terms of practicality and optimisation of the process.

### 2.2.2 $CO_2$ adsorbents for SE–SMR

The equilibria and kinetics of $CO_2$ adsorption over various adsorbents have been extensively studied, especially at low temperatures (273–400K) and low partial pressures (0 1bar) of operation, in which $CO_2$ is the only adsorbate. However, for the scope of the sorption–enhanced steam methane reforming, it is more important to study the adsorption of $CO_2$ on adsorbent materials at high temperature. For use in such a process, the

adsorbent material should fulfill the following requirements (Reijers et al., 2006):

- It should exhibit sufficient $CO_2$ capacity in the temperature range 650–850K and in the pressure range 1–40bar.
- It should be able to withstand the high $p_{steam}/p_{CO_2}$ ratios (typically $> 20$) under reforming conditions, where $p_{steam}$ and $p_{CO_2}$ are the partial pressures of steam and gaseous $CO_2$ respectively.
- It should be stable enough, both chemically as well as mechanically, for extended periods under these conditions.
- Adsorption and desorption kinetics should be sufficiently fast.

From a literature search it follows that there are three groups of materials within the interest of SERP , namely hydrotalcites (see Fig. 2.13), lithium metal oxides (e.g. lithium zirconates) and metal oxides (e.g. dolomite, CaO).

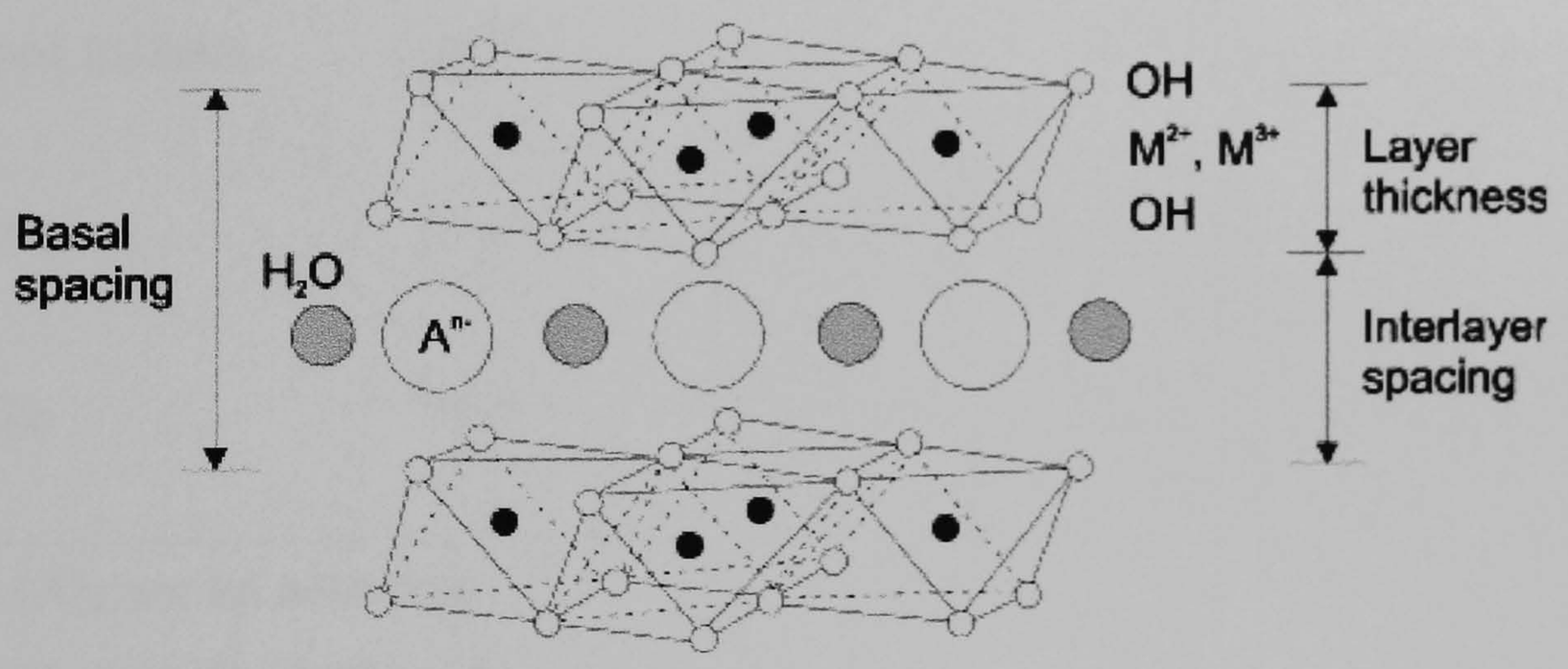



Figure 2.13: Structure of hydrotalcite–like compounds (Hutson et al., 2004).

Hydrotalcites exhibit relatively low adsorption capacities and have been intensively studied for high temperature $CO_2$ capture (Ding and Alpay, 2000a; Reijers et al., 2006). Lithium zirconates have been characterised by high adsorption capacity, but kinetic limitation have also been reported (Xiong et al., 2003). CaO–based adsorbents are promising for $CO_2$ capture at high temperatures, and the enhancement of their uptake capacity and

reversibility has attracted research attention (Lu et al., 2006). Hydrotalcites may be regenerated by pressure swing since the heat of adsorption is rather low. Materials of the other two groups are preferably regenerated using temperature swing since they react with $CO_2$ through a strongly exothermic reaction. Clearly, the choice of adsorbent material, as well as the desorption mode, is of great significance for the system configuration and efficiency of a SE–SMR process. Key properties of typical adsorbents for SE–SMR are provided in Table 2.4.

Table 2.4: Properties of typical $CO_2$ adsorbents for SE–SMR

| Adsorbent | Capacity | $\Delta H_{298}$ (kJ mol$^{-1}$) | Reference |
|---|---|---|---|
| K–promoted HTlc | 0.65[a] | -17 | Ding and Alpay (2000a) |
| Mg–Al–$CO_3$ HTlc | 0.89[a] | – | Hutson et al. (2004) |
| CaO | 49.5[b] | -178 | Ochoa-Fernández et al. (2007) |
| $Li_2ZrO_3$ | 27.1[b] | -160 | Ochoa-Fernández et al. (2007) |
| K–doped $Li_2ZrO_3$ | 20.7[b] | – | Ochoa-Fernández et al. (2007) |
| $Na_2ZrO_3$ | 16.3[b] | -149 | Ochoa-Fernández et al. (2007) |
| $Li_4SiO_4$ | 22.9[b] | -143 | Ochoa-Fernández et al. (2007) |

[a]mol $CO_2$ per kg adsorbent

[b](g $CO_2$ / g adsorbent)×100

Yong et al. (2002) have provided an inclusive review on the adsorption of $CO_2$ at high temperature. Adsorbent materials including carbon–based adsorbents, metal oxide sorbents, zeolites and hydrotalcite–like compounds (HTlcs) for $CO_2$ at high temperature were discussed. The authors identified some key issues related to the development of $CO_2$ adsorbents at high temperature, such as understanding the adsorption mechanism of $CO_2$ on different types of adsorbent materials; finding the best chemical reagent to modify adsor-

bents for enhanced adsorption of $CO_2$; studying the adsorption and desorption kinetics of $CO_2$ on the adsorbents; and choosing the optimal technological conditions for industrialisation. They also concluded that although chemically modified carbon–based adsorbents, zeolites, HTlcs, and basic alumina can all directly be used as adsorbents for the removal and recovery of $CO_2$ from power plant fuel gases, only HTlcs and basic alumina have enough adsorption capacity of $CO_2$ to be used in the sorption–enhanced reaction process.

The equilibria and kinetics of high temperature $CO_2$ adsorption on hydrotalcite adsorbent have been studied by Ding and Alpay (2000a), using semi–technical and bench–scale elution apparatus. The chosen conditions of measurements depicted those of the SE SMR process, *i.e.*, temperatures up to 753K and in the presence of water vapour. At 753K and in the presence of water vapour, adsorption saturation capacities of ~0.58 mol $kg^{-1}$ were measured and found to be insensitive to the actual concentration of feed water. Under dry feed conditions, a small reduction in the capacity of the fresh adsorbent (~10%) was observed, however, both dry and wet feed cases were adequately described by Langmuir models. A mathematical model based on a LDF description of mass transfer, in which the non–linearity of the isotherm was incorporated, was found to give a good description of the key operating steps of the PSR process. The work also highlighted the complexities of $CO_2$ adsorption on hydrotalcite in which, for example, pre–adsorbed layers of water and $CO_2$ may alter the capacity of the material, and possibly generate adsorption sites for physisorption. For adsorbent previously not contacted with steam or $CO_2$ feed, an initial strong adsorption of material was observed, implying a chemisorption mechanism.

Yong et al. (2001a) have investigated the adsorption capacities of $CO_2$ on six commercial hydrotalcite–like compounds and the main factors (aluminum content, anion type, water content and heat treatment temperature) influencing their adsorption capacities at high temperatures. The findings indicated an optimal aluminium content heat treatment temperature, when HTlcs are to be used as adsorbents for $CO_2$ at elevated temperatures. The authors suggested that the $CO_2$ adsorption capacity is mainly dependent on the microporous volume, interlayer spacing and layer charge density of the HTlcs. The same group later proposed that the adsorption capacity of carbon dioxide on a carbon-based

adsorbent at high temperature can be greatly enhanced by simple chemical treatments, which introduced metal oxides and a heteroelement. They concluded that the chemically-modified carbon–based adsorbent is very promising for use in sorption–enhanced reaction process when its adsorption capacity is improved (Yong et al., 2001b).

A worthnoting finding of the above studies was that the $CO_2$ adsorption capacity followed the trend $Q_{300} > Q_{20} > Q_{200}$, where $Q_T$ is the adsorption capacity at 1 atm and temperature T, °C (Yong et al., 2001a). The authors suggested that this is due to a decrease of the interlayer spacing (see Fig. 2.13) between ambient temperature and 200°C, resulting in less void space, thus inhibiting $CO_2$ adsorption. They further proposed that dehydroxylation and decarbonation of the HTlc at 300°C results in structural modifications, increased porosity and an enhanced adsorption capacity. Hutson et al. (2004) characterised the structural changes of a synthetic HTlc (see Table 2.4) upon heating to 200 and 400°C. These changes were particularly related to observed behaviour with respect to the physisorption and chemisorption of $CO_2$ at 200°C (see Table 2.5). The authors concluded that HTlcs are very open to physical and chemical manipulation and therefore they may conceivably be synthesised and tailored for use in high–temperature $CO_2$ capture processes. Hence, the effect of the adsorbent characteristics on the performance of the proposed process is accommodated in this work (see §4.2).

Table 2.5: Adsorption capacities (at 200°C and 107 kPa) for HTlc after heating to 200 and 400°C in vacuum (Hutson et al., 2004)

| | $CO_2$ adsorption capacity, mol $kg^{-1}$ | | | |
|---|---|---|---|---|
| sample | combined | physisorption | chemisorption | chemisorption contribution |
| HTlc–200 | 0.604 | 0.274 | 0.330 | 54.6% |
| HTlc–200 | 0.896 | 0.731 | 0.165 | 18.4% |

Ochoa-Fernández et al. (2005) developed a novel soft chemical method, which was found to significantly improve the $CO_2$ adsorption kinetics and stability of lithium zirconate. The $CO_2$ adsorption properties were evaluated using a tapered element oscillating microbalance. A kinetic equation for the adsorption of $CO_2$ as a function of $CO_2$ partial pressure and the temperature was determined. The derived expression was used for the simulation of SE–SMR by a dynamic 1–D pseudo–homogeneous fixed–bed reactor model. Simulation results showed that the process is capable of directly producing $H_2$ purer than 95 mol % with methane as the main side product and less than 0.2 mol % of CO.

Readman and Blom (2005) reported on the investigation of dolomite as a potential reversible high–temperature $CO_2$ adsorbent, using *in situ* powder X–ray diffraction. Dolomite was treated in inert atmosphere at 900°C resulting in its decomposition into separate CaO and MgO rich phases and it was never reformed upon $CO_2$ sorption. The experiments showed that the calcined dolomite could go through several cycles of $CO_2$ adsorption/desorption in a reversible manner, but the sorption capacity diminished with each cycle. Only calcium seemed to be involved in the $CO_2$ sorption, while MgO acted as a carrier for the calcium phase. The authors concluded that the development of reversible high–temperature $CO_2$ adsorbents is not a trivial task and there are still many key factors influencing the sorption properties of even well–known materials, such as dolomite.

More recently, Ochoa-Fernández et al. (2007) presented a comparative study of five different high–temperature $CO_2$ scavengers (see Table 2.4). Their work showed that none of the adsorbents completely fulfill all the requirements for use in SE–SMR. CaO was found to be the most favourable material from the thermodynamic point of view leading to the highest $H_2$ yields. However, the authors suggested that its stability must be improved, advocating that $Na_2ZrO_3$ may be a promising alternative.

## 2.3 Monolithic type reactors

Monolithic structures or monolithic reactors (see Fig. 2.14) are relatively new compared to other more customary types of heterogeneous reactors such as fixed–bed or fluidised

bed reactors. In the last thirty years, substantial work has been done on the analysis of monolithic reactors, of which most important applications include automotive exhaust gas emissions control as an afterburning reactor for the combustion of hydrocarbons and CO, catalytic combustion and selective catalytic reduction, the most widely used catalytic $NO_x$ removal technology (Hayes and Kolaczkowski, 1994; Santos et al., 1998). A monolithic reactor resembles a honeycomb structure consisting of hundreds of individual parallel passageways of the order of one millimetre inside dimension and a variety of cross sectional shapes (Williams, 2001). The wall (substrate) may be either ceramic or metal and can be either coated with a high surface area washcoat (e.g. alumina) of 10 to 50$\mu$m that contains the dispersed catalyst or may itself contain the catalyst as an integral part of its structure (Leung et al., 1996; Kolaczkowski, 1999). Such a monolith support structure combines a relatively high surface to volume ratio with a low pressure drop and is, thus, preferred to a packed-bed reactor (Kolaczkowski, 1995).

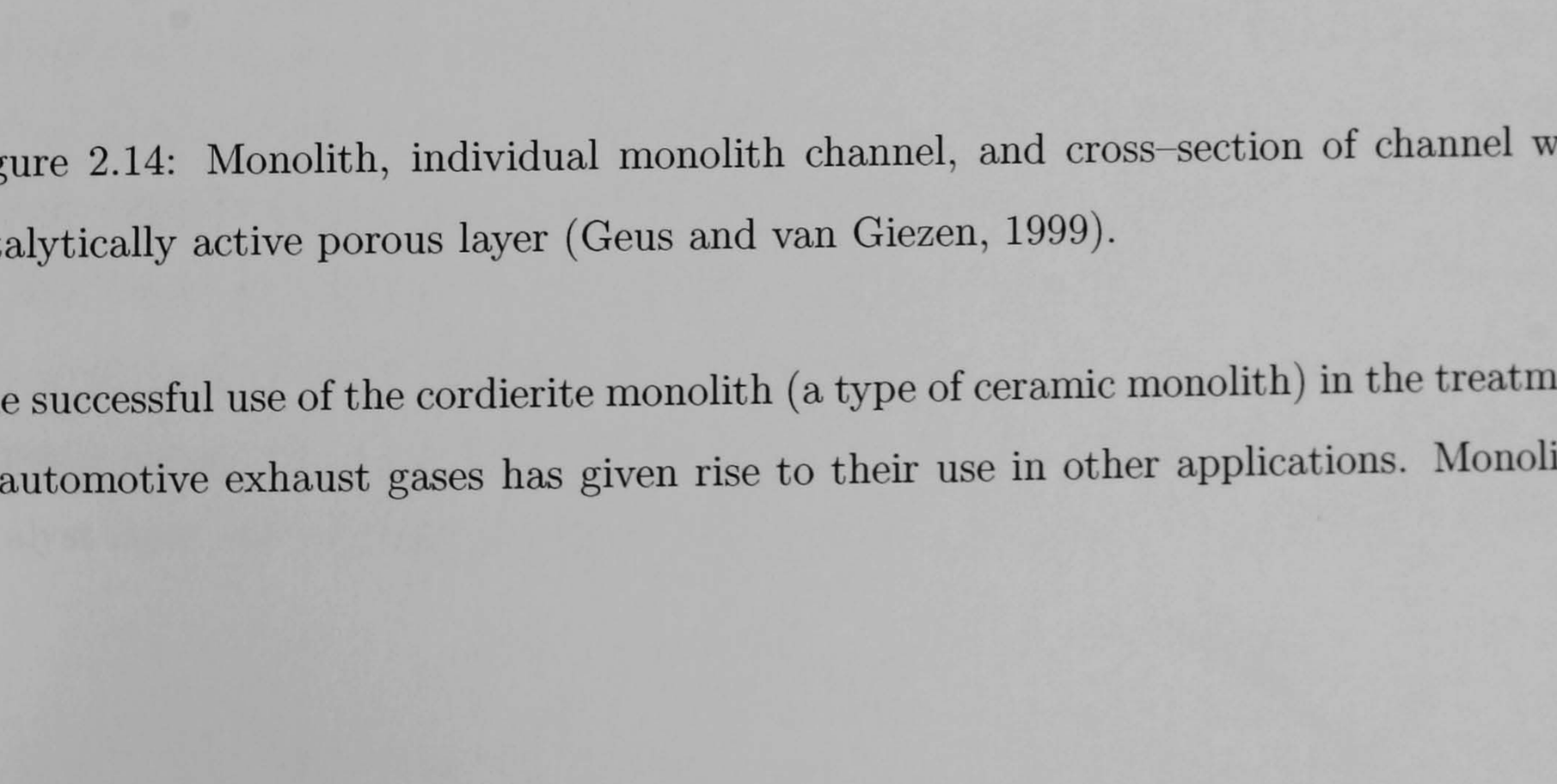



Figure 2.14: Monolith, individual monolith channel, and cross–section of channel with catalytically active porous layer (Geus and van Giezen, 1999).

The successful use of the cordierite monolith (a type of ceramic monolith) in the treatment of automotive exhaust gases has given rise to their use in other applications. Monoliths

are increasingly under development and evaluation for many new reactor applications, e.g. chemical process and refining industries, ozone abatement and industrial heat recovery. The utilisation of other substrate materials and designs in many of these applications may be promising, since the process requirements are not as demanding as these of automotive emissions control. Additionally, because of the high cost of a monolithic catalyst, only processes in which the catalysts are sensibly stable and/or easy to regenerate are practicable, such as liquid phase hydrogenations, oxidations of organic compounds and biotechnology processes (Cybulski and Moulijn, 1998).

However some disadvantages of the monolith may restrain extensive use outside the environmental applications. The parallel channel monolith is essentially an adiabatic reactor limiting the control of temperature. For many exothermic or endothermic chemical or petroleum reactions, selectivity is ruled by temperature and as a result these types of monoliths are not suitable. A metal heat exchanger or metallic foam can be employed, in order to control temperature, but the quantity of catalyst on the walls in a specified volume of monolith is much less than a comparable volume of small diameter beads or extrudates. Hence, for chemical controlled reactions, the monolith may not contain enough catalyst to yield the desired conversion efficiencies (Heck et al., 2001).

### 2.3.1 Modelling of monolith reactors

The modelling of the monolithic reactors has attracted a lot of research attention and, thus, has been extensively investigated and published. In order to illustrate the interactions that may take place in a catalytic coated channel, the case of a monolith type combustor is considered (see Fig. 2.15). As the fuel and air flow down the channel, the reactants (i.e. methane and oxygen) are transported to the catalyst surface, where they diffuse into the porous structure and react on catalytically active sites. The products of the reaction, though, diffuse through that porous structure and into the gas phase, which continues to flow down the channel. Concurrently, a rise in temperature occurs, as the highly exothermic combustion reaction proceeds in the catalyst layer. The gas phase temperature increases due to the energy convection, driven by the temperature difference between the catalyst layer and the bulk gas. Heat conduction through the walls and radiation between

the walls also arise in the axial direction (Kolaczkowski, 1999).

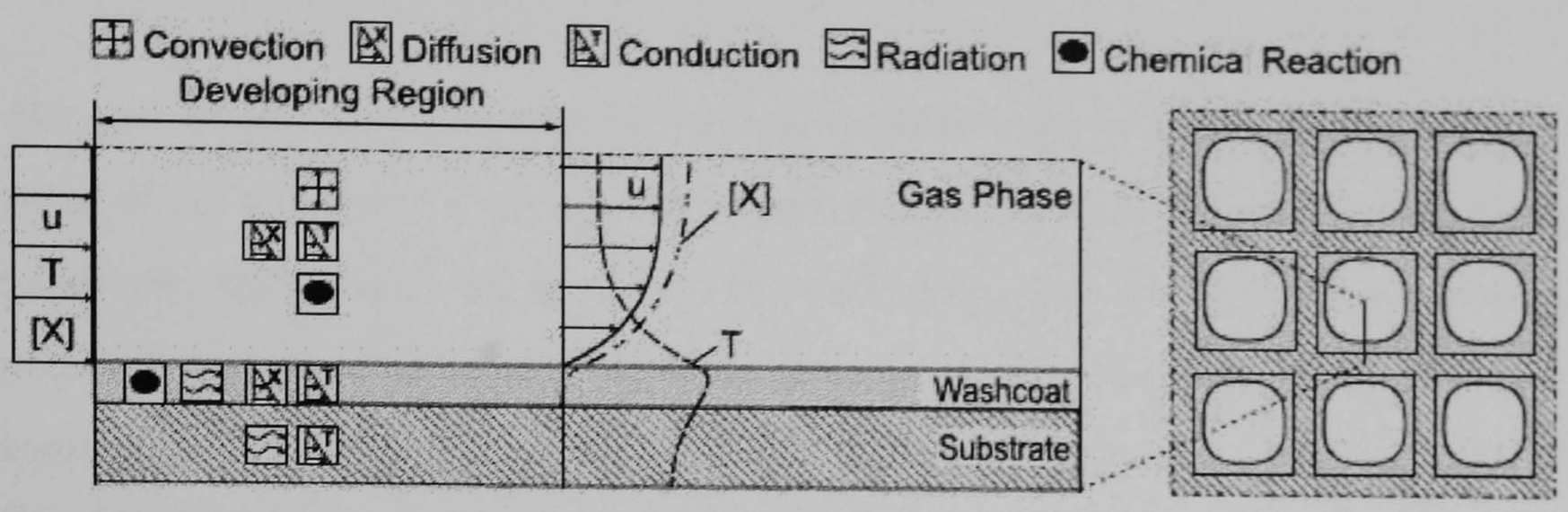



Figure 2.15: Sketch of a monolith channel indicating the relevant physical and chemical phenomena in the gas phase, washcoat, and substrate (Holder et al., 2006).

In automobile exhaust applications, typical monolithic reactors operate in the laminar flow regime and have a negligible pressure drop. The hydrodynamic entrance region is usually a small fraction of the overall reactor length and fully developed flow can be assumed in the main part of the monolith channel (Hayes et al., 1992; Hayes and Kolaczkowski, 1994). Despite the laminar flow, a monolithic reactor can essentially be modelled as a plug–flow reactor due to the considerable radial diffusion in the narrow channels (Hoebink and Marin, 1998). This approach is also adopted in this work (see §3.2).

Modelling of the mass and heat transfer processes in the monolithic reactors, adjoined with heterogeneous and/or homogeneous reactions can be realised through distributed or lumped parameters models. In the literature the typical modelling procedure involves splitting the computational domain into parts and treating each part singly. On average, the domain is split into the gas and solid phase and each one of them can be modelled as a one–dimensional (Heck et al., 1976; Sincule and Hlavacek, 1978; Tronconi et al., 1992; Groppi et al., 1995b; Nakhjavan et al., 1995; Choi et al., 1996; Kirchner and Eigenberger, 1996, 1997; Tomasic et al., 2004), two–dimensional (Young and Finlayson, 1976a,b; Lee and Aris, 1977; Groppi et al., 1995a; Leung et al., 1996; Hayes and Kolaczkowski, 1999; Wanker et al., 2000; Tomasic and Gomzi, 2004) or even three–dimensional system (Jahn et al., 1997; Roduit et al., 1998; Papadias et al., 2000). One–dimensional models are

generally preferred to multi–dimensional ones as the latter are more difficult to solve and require more computational time.

For the gas phase, one–dimensional models consider merely variations along the axial direction of the channel. This type of models rely on average radial concentrations and temperatures, while mass and heat transfer coefficients are introduced to account for the discontinuities at the wall. On the other hand, two–dimensional models consider gas-phase mass and heat variations both in the axial and radial directions and it is possible to impose flux boundary conditions. Thus, these coefficients are not necessary. In reality, such mass and heat transfer coefficients, in the forms of Sherwood (Sh) and Nusselt (Nu) dimensionless numbers, are commonly calculated from the radial concentration and temperature gradients obtained by two–dimensional models (Leung et al., 1996; Wanker et al., 2000). However, as it will be seen later in this section, there is some controversy over the correct value of these dimensionless numbers in a monolith channel under reacting conditions.

Several gas phase models can be developed, based on various assumptions. Some researchers assumed constant physicochemical properties of the gas phase (Lee and Aris, 1977; Sincule and Hlavacek, 1978), while others considered that these may be temperature and/or concentration dependent. Mass and heat axial dispersion has been either considered (Hayes and Kolaczkowski, 1994) or neglected (Groppi et al., 1995a).

The issue of the velocity profile has also been addressed by several investigations. In a laminar flow reactor, there is a radial velocity profile, leading to the development of radial concentration and temperature gradients, with the velocity at the centreline being twice the average velocity. The magnitude of these gradients depends upon the relative rates of mass and heat transfer and chemical reaction (Hayes and Kolaczkowski, 1999). Groppi et al. (1995b) assumed an invariant radial parabolic shape profile of axial velocity, since enhancement of gas–solid heat transfer due to hydrodynamic development was minor compared to other phenomena under the conditions studied. In other works, fully developed laminar velocity profiles, varying with both radial and axial positions, were considered in two–dimensional models (Hayes and Kolaczkowski, 1994). For transient simulation, a

quasi–static approximation is usually made, based on the fact that the thermal capacities of solids are much larger than those of gases, thus the solid phase dominates the transient behaviour of the system (Young and Finlayson, 1976a; Heck et al., 1976).

As for the solid phase, several approaches have been adopted. It is often assumed that the reactions are taking place on the wall-gas interphase, since the catalytic layers are very thin compared to the monolith walls. Hence, there is no need to take the solid phase mass balance into account (Young and Finlayson, 1976a). As for the heat balance, the radial heat effects occurring in the solid phase are often not taken into account, and a heat balance equation in the axial direction is simply used. As a result, the radial heat conduction in the solid phase is *a priori* neglected and the washcoat is assumed to be isothermal at each point along the reactor (Hayes and Kolaczkowski, 1994; Wanker et al., 2000; Tomasic and Gomzi, 2004). Some models consider axial heat dispersion (Sinclue and Hlavacek, 1978; Hayes and Kolaczkowski, 1994) or heat transfer by radiation (Lee and Aris, 1977; Hayes and Kolaczkowski, 1994). Lee and Aris (1977) studied the effect of wall conduction and showed that radiative heat transfer could be accounted by properly increasing the wall heat conduction coefficient. Two–dimensional models have been developed, considering axial conduction, radiation and catalytic reaction at the wall (Hayes et al., 1992; Groppi et al., 1995a,b; Leung et al., 1996). Groppi et al. (1995a,b) concluded that the contributions of wall conduction and radiation could be reasonably neglected in the simulation of ceramic monoliths, so computational time could be saved. Hayes et al. (1992) demonstrated that the axial conduction in the solid has a bigger effect than radiation.

The diffusion process is another issue that the research on monolithic reactors has addressed. This can involve intraphase diffusion within the coating and interphase diffusion from the gas phase to the washcoat. It is generally recognised that diffusion within the porous structure of a catalyst pellet can restrict the rate of reaction. In a washcoat, for example, if the catalytic reaction rate constant is very large, the concentration at the washcoat–support wall may be much lower than the average bulk concentration. Under these circumstances the reaction is said to be mass transfer controlled. On the other hand,

the concentration at the wall is comparable to the bulk concentration value if the kinetic rate constant is small. In this case, the reaction is said to be kinetically controlled. Given that reaction rate constants are exponentially dependent on temperature, in automobile exhaust applications it is commonly believed that the reaction is kinetically controlled in one region of the reactor and mass transfer controlled in the other one. The transition from kinetic to mass control is usually referred to as the light–off point, with which a sharp temperature rise is normally associated (see Fig. 2.16).

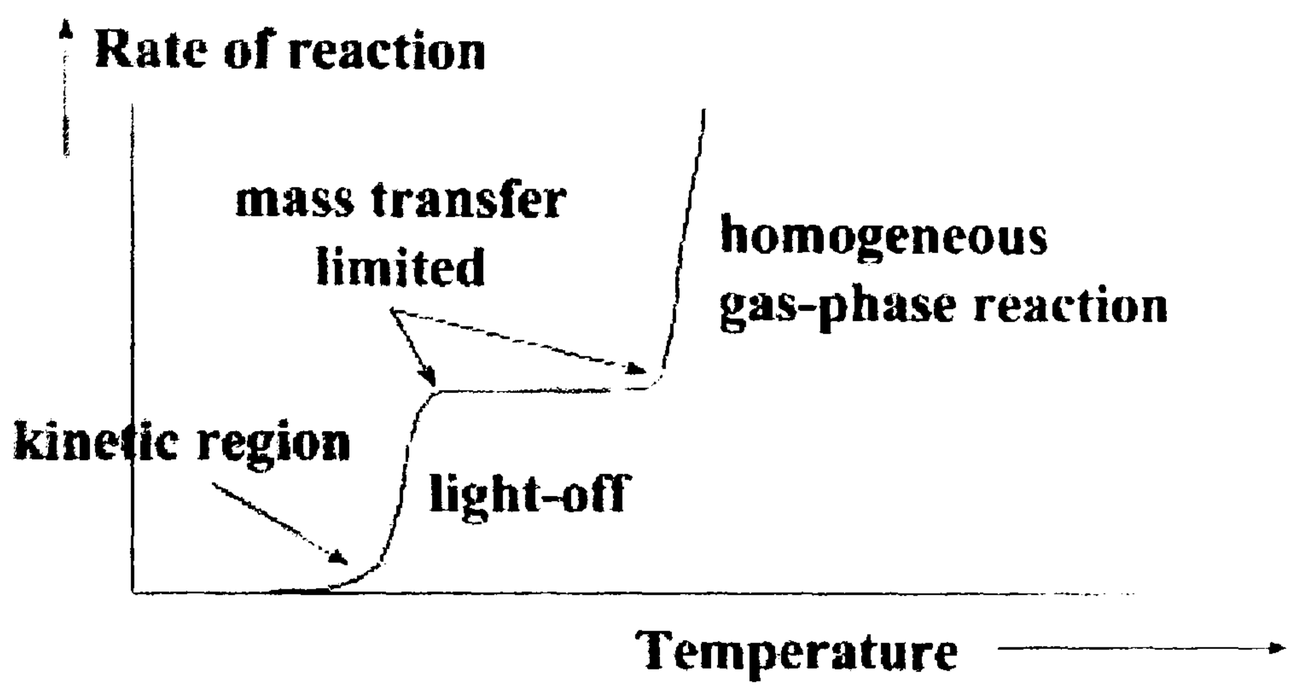



Figure 2.16: Idealised plot of reaction rate (or conversion) versus temperature exhibiting the possible rate–controlling regimes for monolithic reactors (Geus and van Giezen, 1999).

At typical monolithic reactor operating temperatures, diffusion resistances in the catalyst washcoat are likely to be significant (Zygourakis and Aris, 1983; Hayes and Kolaczkowski, 1994; Kolaczkowski and Serbetcioglou, 1996). An effectiveness factor is normally used in order to describe this mass transfer limitation. Numerous studies have assumed that the washcoat layer is so thin that the diffusion resistances are not important and used an effectiveness factor equal to 1 (Heck et al., 1976; Lee and Aris, 1977). However, as shown in several studies (Zygourakis and Aris, 1983; Nakhjavan et al., 1995; Leung et al., 1996; Kolaczkowski and Serbetcioglou, 1996; Santos et al., 1998), diffusion limitations can be considerable even at low temperatures, depending on the type of fuel and/or the catalyst/washcoat properties. Kolaczkowski (1999) underlined that false conclusions may be drawn about the activity of a certain catalyst when diffusion limitations are neglected. In

such a case, higher rates of reaction may be achieved by just decreasing the thickness of the catalyst layer, while simultaneously increasing the geometric surface area per unit volume of the monolith. When modelling monoliths, the effect of pore diffusion can be included in the mass and energy balances via the boundary conditions at the gas–washcoat interphase. This is frequently addressed by including the aforementioned effectiveness factor in the rate expression for the heterogeneous reaction. In the case of a rectangular slab porous catalyst, the diffusion/reaction problem in the washcoat can be solved analytically, assuming isothermal conditions, infinite geometry, first–order irreversible chemical reaction, no flux across the centre of the slab and steady–state conditions (Groppi et al., 1995a; Wanker et al., 2000).

Several numerical and experimental investigations on the interphase mass and heat transfer have also been published (Bennett et al., 1991). Many correlations for the calculation of Nusselt (Nu) and Sherwood (Sh) dimensionless numbers have been proposed and discussed (see Table 2.6).

Table 2.6: Indicative correlations for Nu and Sh numbers

| Nu = | Sh = | Reference |
|---|---|---|
| $\frac{k_h d_c}{\lambda}$ | $\frac{k_m d_c}{D_m}$ | Hoebink and Marin (1998); Balakotaiah and West (2002) |
| $0.0767\left(1+Pe_H\frac{d_c}{L}\right)^{0.829}$ | $0.0767\left(1+Pe_M\frac{d_c}{L}\right)^{0.829}$ | Bennett et al. (1991) |
| $3.66\left(1+0.095\frac{d_c}{L}Pe_H\right)^{0.45}$ | $3.66\left(1+0.095\frac{d_c}{L}Pe_M\right)^{0.45}$ | Hayes and Kolaczkowski (1999) |

Such correlations can be for laminar or developing flow and for different shapes of channels (square, circular and triangular); see for example Balakotaiah and West (2002); Bhat-

tacharya et al. (2004). The calculation of these numbers is often based on the assumption of either constant wall temperature or constant wall heat flux, whereas the most correlations available are for non–reacting conditions. It should also be noted that most of the correlations available predict average values for the entire reactor length and not a local value as would be more useful (Hayes and Kolaczkowski, 1999). An illustrative example is the oxidation of CO in a monolithic reactor, which is characterised by a jump in the Nu and Sh values when sudden light–off occurs. The light–off point is usually preceded and followed by two asymptotic Nu and Sh values. Many numerical investigations predicted Nu and Sh values in the range of 3.0–4.5 for the fully developed region under steady state conditions and for an adiabatic cylindrical system (same order of magnitude applies to other geometries). A comprehensive study on this subject was published by Hayes and Kolaczkowski (1994, 1999). The authors reported on the transition from the kinetic to the mass transfer control in a monolith reactor with laminar flow. They suggested that this transition is dependent on the inlet conditions, the value of the kinetic rate constants and their form of expression (e.g. the diffusion coefficient and the reactor length and diameter). The transition between the two regimes may be sharp or gradual, depending on the nature of the rate expression. The controversy over the controlling mechanism in the literature has led to some uncertainty concerning the values of Nu and Sh numbers in a monolith reactor channel under reaction conditions. For transient conditions, if the transition is sharp, the value of these numbers will exhibit discontinuities.

## 2.4 Concluding remarks

The fundamental physical and mathematical basis of this thesis has been reviewed in this chapter. Some overall conclusions can now be drawn and thereby motivate the work to be presented in the subsequent parts of the thesis.

From a physical point of view, the adsorption phenomena and processes are now relatively well understood and characterised. The fundamentals of the adsorption have been presented, which included brief discussions on adsorption isotherms, mass and heat transfer aspects, adsorbent regeneration and adsorbent characteristics. Major investigations

on the areas of TSA, PSA and RPSA have been provided. Moreover, several process configurations that couple SMR systems with $CO_2$ adsorption for hydrogen production (SERP) have been examined. Additionally, a brief synopsis of monolithic reactors and their applications has been presented and the interactions between the various physical and chemical processes occurring within the reactor have been described. Then, a short literature review in modelling of monolithic reactors has been provided.

From a mathematical point of view, it is evident that the construction of quite accurate models for the prediction of the behaviour of adsorptive reactors and monoliths is possible. Such systems are spatially distributed and therefore their models comprise mixed systems of differential and algebraic equations (DAEs). Fortunately, there is now a wide variety of reliable numerical techniques and modelling tools for the simulation and optimisation of such problems (see §3.9).

An extra degree of complication emerges from the nature of the newly–proposed process (see §3.1), *i.e.*, pneumatic transport of adsorbent particles, $CO_2$ adsorbent characteristics and optimal process design/operation. A mathematical framework will be presented in the next chapter addressing these new challenges.

# Chapter 3

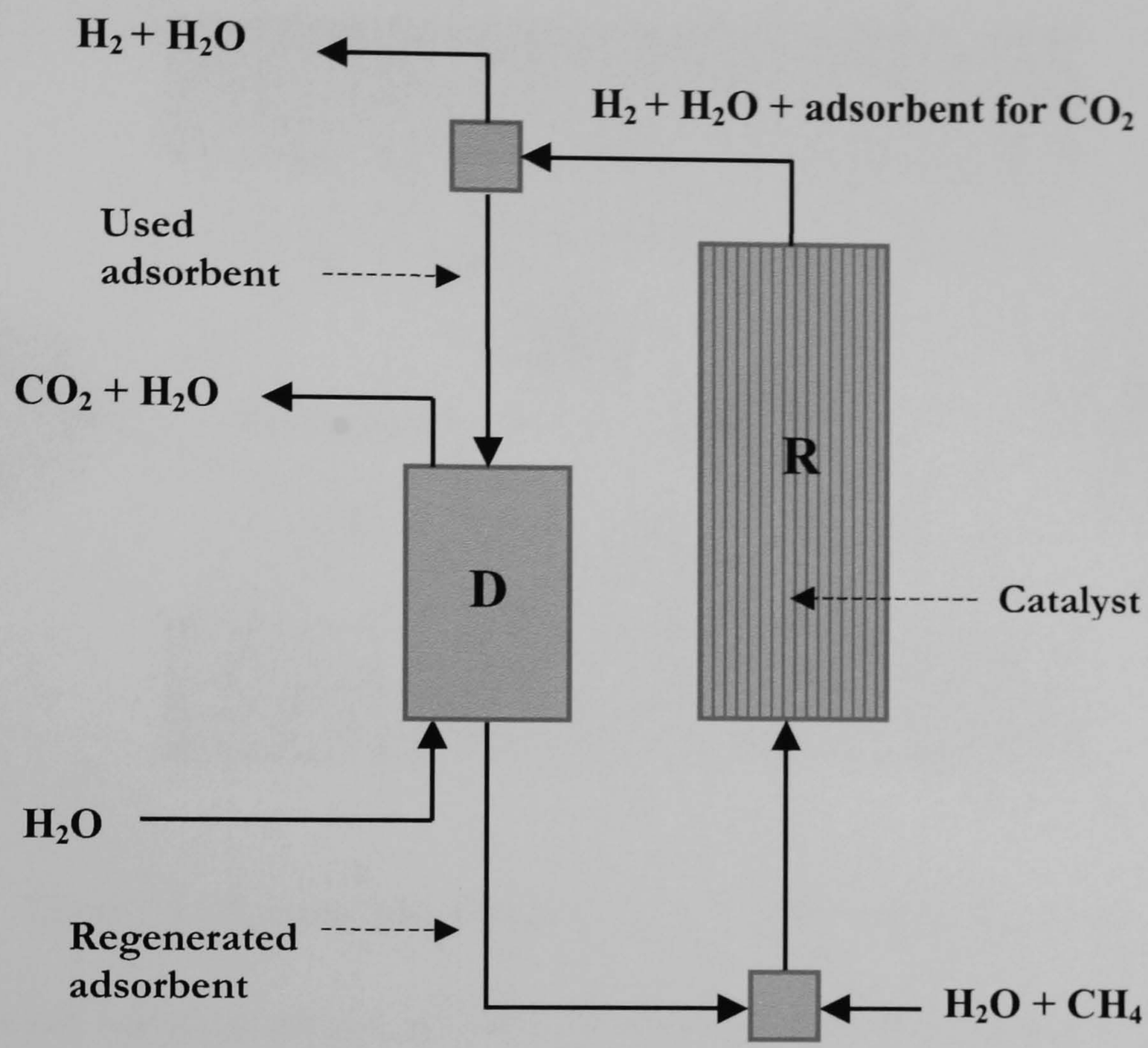
# Mathematical modelling

## 3.1 Process scheme

As shown schematically in Fig. 3.1, the process consists of a reactor/adsorber unit and a regeneration (desorption) unit. The novelty of this approach is the use of mobile $CO_2$ adsorbent flowing through a stationary SMR catalyst phase. Adsorbent regeneration is carried out in an external regeneration unit, thus decoupling the reaction and adsorbent regeneration steps. The hot regenerated adsorbent is passed back to the reactor unit, so heat for reaction is also supplied via the regeneration unit, *i.e.*, via the thermal capacitance of the adsorbent. As a result effective energy integration is possible between the reactor and regeneration units. A continuous mode of operation is also enabled.

## 3.2 Model assumptions

A schematic diagram of the monolith channel coated with reforming catalyst, wherein $CO_2$ adsorbent particles are pneumatically conveyed through, is shown in Fig. 3.2. The key model assumptions include steady state and non-isothermal (adiabatic) operation, perfect gas behaviour, adsorption kinetics described by the linear driving force model (LDF) and a Langmuir isotherm for the $CO_2$ adsorption equilibrium. The general reaction kinetic model proposed by Xu and Froment (1989) is employed. $CO_2$ is considered as the only adsorbate and $CO_2$ adsorption is assumed to take place on the flowing adsorbent particles.




**Column R: Reactor/Adsorber**
**Column D: Desorber**

Figure 3.1: Schematic diagram of the proposed process.

Additional model assumptions are summarised below:

- all monolith channels are identical and thus it is only necessary to model a single channel
- a circular channel geometry
- negligible pressure drop along the monolith channel
- reactions occur heterogeneously on the catalytic material in the solid phase
- ideal plug flow

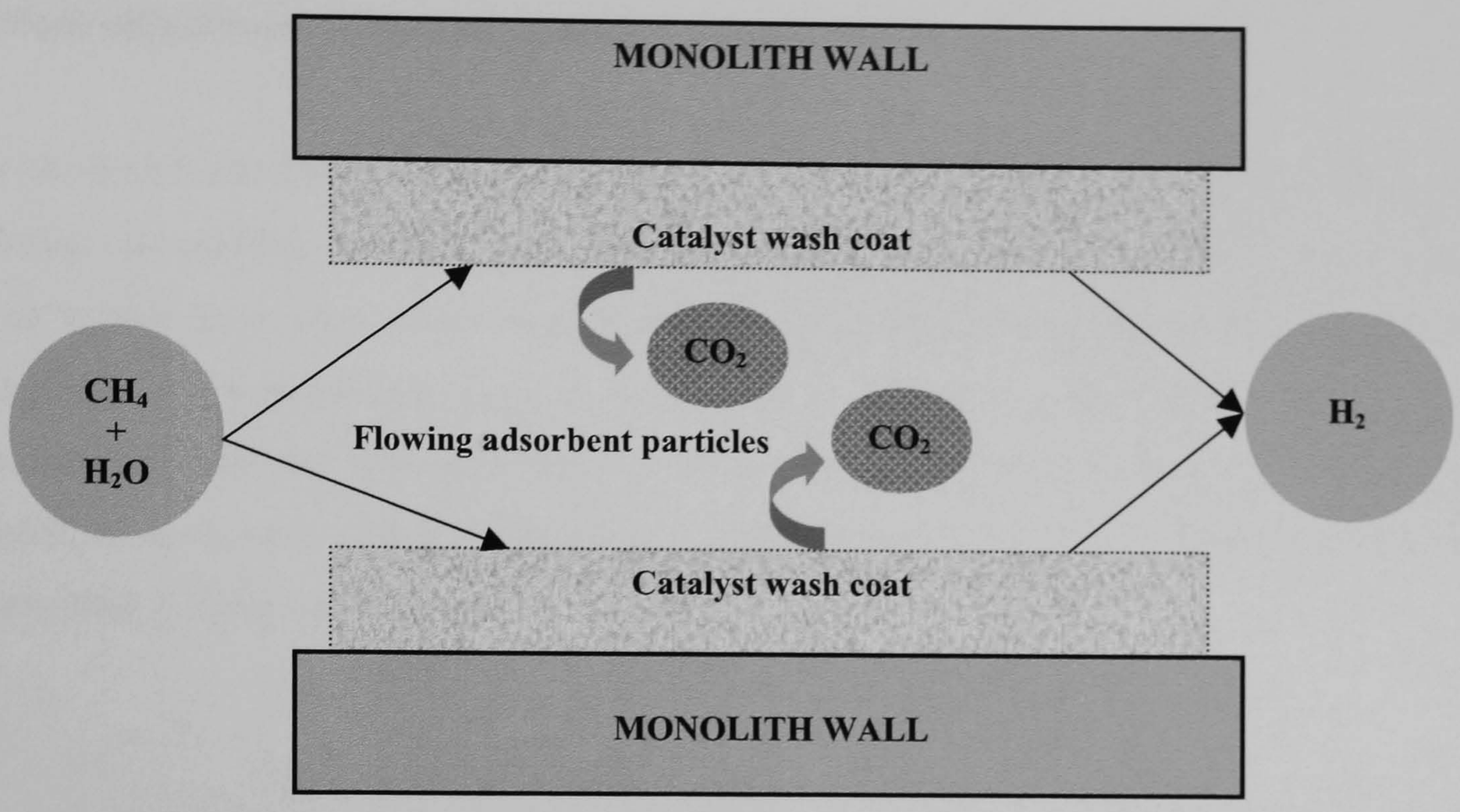



Figure 3.2: Reaction and adsorption in an idealised monolith channel.

- gas and adsorbent particle velocities are assumed constant and equal

The integration domain has been split into the solid (catalyst) phase and the flowing two–phase gas–solid (adsorbent) mixture (see Fig. 3.2). Given the small radial dimension, radial concentration and temperature gradients in the flowing gas–adsorbent mixture are neglected. The investigation of this type of flow through narrow monolithic channels is rather limited in the literature and extensive work is necessary to gain a meaningful insight into the true behaviour of the gas–solid mixture (see Ding et al., 2005, 2006). It has been shown that for pure gas flow, the laminar–to–turbulent transition in monolith channels may occur at a Reynolds number of ~620, much lower than the conventional transition criterion of 2200 for large pipes (Ding et al., 2005). Both non–uniform gas and solids velocity distribution as well as non–uniform solids concentration distribution have been reported (Ding et al., 2006; Ding, 2006). However, the approximations of ideal plug flow and same (and constant) interstitial velocities of gas and adsorbent particles can be used within the scope of this work (Ding, 2006). Necessary quantitative calculations are provided in Table 3.1. As for the catalytic washcoat, a one–dimensional reactor model is implemented, in which the diffusion transport within the wash coat is described by a

simple effectiveness factor, set at unity for this particular study.

It should be noted that Fickian diffusion is assumed instead of the more rigorous Maxwell Stefan formulation, which may be more appropriate for diffusion–dominated flows as the one in this work (non–dilute system involving non–equimolar counter diffusion of $H_2$). However, its computational cost is considerably elevated, and the Fick's law has been proved adequate for modelling systems of this nature (Stutz and Poulikakos, 2005). Finally, no volumetric change of flow due to reaction and adsorption is taken into account, assuming a mean velocity value.

Table 3.1: Calculations in support of model assumptions

| | |
|---|---|
| $Re = \frac{(2R_c)u_g\varrho_g}{\mu_m} = 48$ | Laminar flow regime |
| $\frac{D_m L}{u_g(2R_c)^2} \simeq 45 \gg \frac{1}{28}$ | Approximation of laminar flow by plug flow with axial dispersion, which can be neglected (see Hoebink and Marin, 1998) |

Use of $Sh$ and $Nu$ to describe the mass and heat transfer from the bulk flow toward the catalytic wash coat

$$Nu = 3.65 \qquad \text{if} \qquad \frac{z}{R_c} \geq 0.1RePr = 3.43 \qquad Pr = \frac{\mu_m c_{p,g}}{\lambda_m} = 0.71$$

It is valid to assume that this condition holds $\forall z \in [0, L]$, $L = 1$ m and $R_c = 1 \times 10^{-3}$ m (see Hoebink and Marin, 1998)

## 3.3 Governing equations

Based upon the aforementioned assumptions, the component mass balances and the energy balances for the monolithic adsorptive reactor are presented below. Detailed derivations of the governing are presented in the Appendices.

### 3.3.1 Component balance equations

**Gas phase**

$$-u_g \frac{dc_{i,g}}{dz} - \varepsilon\varphi\varrho_{ads} r_{ads} - k_m \frac{2}{R_c}\varepsilon(c_{i,g} - c_{i,c}) = 0 \tag{3.1}$$

where $u_g$ (m $s^{-1}$) is the superficial gas velocity; $c_{i,g}$ and $c_{i,c}$ (mol $m^{-3}$) are the molar concentrations of component $i$ in the gas and catalyst phase respectively; $\varepsilon$ is the monolithic reactor voidage; $\varphi$ is the adsorbent loading defined as the volumetric ratio of the adsorbent in the two–phase gas–solid mixture; $\varrho_{ads}$ (kg $m^{-3}$) is the adsorbent density; $r_{ads}$ (mol $kg^{-1}$ $s^{-1}$) denotes the rate of adsorption; $k_m$ (m $s^{-1}$) is the gas–washcoat mass transfer coefficient; and $R_c$ (m) is the radius of the monolithic channel.

**Solid (catalyst) phase**

$$k_m \frac{2}{R_c}\left(\frac{\varepsilon}{1-\varepsilon}\right)(c_{i,g} - c_{i,c}) + \eta\varrho_c r_i = 0 \tag{3.2}$$

where $\eta$ is the catalyst effectiveness factor; $\varrho_c$ (kg $m^{-3}$) the density of the catalyst phase; and $r_i$ (mol $kg^{-1}$ $s^{-1}$) the formation (or consumption) rate of component $i$.

**Adsorbent phase**

$$-u_{ads} \frac{dq_i}{dz} + \varepsilon\varphi r_{ads} = 0 \tag{3.3}$$

where $u_{ads}$ (m $s^{-1}$) is the superficial adsorbent particle velocity; and $q_i$ (mol $kg^{-1}$) the adsorbent–phase concentration of component $i$.

### 3.3.2 Energy balance equations

**Gas phase**

$$-u_g \frac{d}{dz}(c_g c_{p,g} T_g) + k_h \frac{2}{R_c}\varepsilon(T_c - T_g) + k_{h,ads}\frac{6}{d_p}\varepsilon\varphi(T_{ads} - T_g) = 0 \tag{3.4}$$

where $c_g$ (mol $m^{-3}$) is the gas–phase density; $c_{p,g}$ (J $mol^{-1}$ $K^{-1}$) the gas heat capacity; $T_g$ (K) the gas temperature; $k_h$ (J $m^{-2}$ $s^{-1}$ $K^{-1}$) the gas–washcoat heat transfer coefficient; $T_c$ (K) the catalyst temperature; $k_{h,ads}$ (J $m^{-2}$ $s^{-1}$ $K^{-1}$) the gas–adsorbent heat transfer coefficient; $d_p$ (m) the adsorbent particle diameter; and $T_{ads}$ (K) the adsorbent temperature.

**Solid (catalyst) phase**

$$\lambda\frac{d^2T_c}{dz^2} + k_h\frac{2}{R_c}\left(\frac{\varepsilon}{1-\varepsilon}\right)(T_g - T_c) + \sum_{j=I}^{III}\varrho_c\eta(-\Delta H_{R_j})R_j = 0 \tag{3.5}$$

where $\lambda$ (J $m^{-1}$ $s^{-1}$ $K^{-1}$) is the catalyst thermal conductivity; $\Delta H_{R_j}$ (J $mol^{-1}$) and $R_j$ (mol $kg^{-1}$ $s^{-1}$) are the heat and rate of reaction $j$ respectively.

**Adsorbent phase**

$$-u_{ads}\varrho_{ads}c_{p,ads}\frac{dT_{ads}}{dz} + k_{h,ads}\frac{6}{d_p}\varepsilon\varphi(T_g - T_{\text{ads}}) + \varrho_{ads}(-\Delta H_{ads})\varepsilon\varphi r_{ads} = 0 \tag{3.6}$$

where $c_{p,ads}$ (J $kg^{-1}$ $K^{-1}$) is the adsorbent heat capacity; and $\Delta H_{ads}$ (J $mol^{-1}$) the heat of adsorption.

It should be reminded that $q_i$ and $r_{ads}$ are equal to zero for non–adsorbing components, *i.e.*, i $\neq CO_2$.

### 3.3.3 Boundary conditions

The following boundary conditions are used in the simulations:

**Reactor entrance** (z = 0)

$$c_{i,g} = c_{i,f} \tag{3.7}$$

$$q_i = 0 \tag{3.8}$$

$$T_g = T_f \tag{3.9}$$

$$T_c = T_f \tag{3.10}$$

$$T_{ads} = T_f + \vartheta \tag{3.11}$$

**Reactor outlet** (z = L)

$$\frac{\partial T_c}{\partial z} = 0 \tag{3.12}$$

The subscript $f$ denotes the feed conditions (concentrations and temperatures) and $\vartheta$ represents the temperature difference between the adsorbent and the gas at the reactor entrance. The feed gas is assumed to consist of a mixture of steam and methane at a ratio of 6:1. As a result, no carbon–producing reactions (see Introduction) are incorporated in the reaction kinetics model.

## 3.4 Reaction kinetics

Several studies have been published on the kinetics of steam methane reforming. There is a general agreement that the reaction is first order to methane, but there is some controversy over other kinetic parameters. This is partially due to the use of different catalysts or

experimental conditions, but also to the lack of appreciation of diffusion and heat transfer limitations. In this work, the intrinsic rate equations, derived by Xu and Froment (1989a), for the steam reforming of methane on a Ni–based catalyst are used. These rate models are considered to be the most general and reliable expression for the SMR process and have been extensively studied in the literature (Ding and Alpay, 2000a).

Xu and Froment (1989a,b) extensively studied the kinetic and mechanistic details of steam methane reforming in a conventional tubular reactor at the temperature range 523–823K and for pressure varying between 300 and 1000 kPa. They developed a model based on a Langmuir–Hinshelwood reaction mechanism, which includes 13 reaction steps. The following three key reactions of the SMR process are considered in the model:

Reaction I $\quad CH_4 + H_2O \leftrightarrows CO + 3H_2,\ \Delta H_{298} = 206 kJ/mol$

Reaction II $\quad CH_4 + 2H_2O \leftrightarrows CO_2 + 4H_2,\ \Delta H_{298} = 164.9 kJ/mol$

Reaction III $\quad CO + H_2O \leftrightarrows CO_2 + H_2,\ \Delta H_{298} = -41 kJ/mol$

Amongst the large number of reaction schemes developed, two were proposed to represent the steam reforming system kinetics. The two schemes proposed differ in the appearance of CO and $CO_2$. Rate equations were written for the rate–determining step of each of the three global reactions I–III in terms of the concentrations of the adsorbed species. The concentrations were then eliminated by means of the Langmuir equilibrium relations and a balance to the active sites, including those covered by adsorbed species and and those remained vacant. The resulting rate equations, in terms of accessible gas–phase partial pressures, are given below:

$$R_I = \frac{k_1}{P_{H_2}^{2.5}} \left( P_{CH_4} P_{H_2O} - \frac{P_{H_2}^3 P_{CO}}{K_I} \right) (DEN)^{-2} \ ,\ kmol \cdot kg_{cat}^{-1} \cdot h^{-1} \tag{3.13}$$

$$R_{II} = \frac{k_2}{P_{H_2}^{3.5}} \left( P_{CH_4} P_{H_2O}^2 - \frac{P_{H_2}^4 P_{CO_2}}{K_{II}} \right) (DEN)^{-2} \ ,\ kmol \cdot kg_{cat}^{-1} \cdot h^{-1} \tag{3.14}$$

$$R_{III} = \frac{k_3}{P_{H_2}} \left( P_{CO} P_{H_2O} - \frac{P_{H_2} P_{CO_2}}{K_{III}} \right) (DEN)^{-2} \ , \ kmol \cdot kg_{cat}^{-1} \cdot h^{-1} \tag{3.15}$$

where $DEN = 1 + K_{CO}P_{CO} + K_{H_2}P_{H_2} + K_{CH_4}P_{CH_4} + K_{H_2O}P_{H_2O}/P_{H_2}$, representing the adsorption of reacting species. Since the three reactions are assumed to occur on the same active sites, the three rate equations have the same denominator.

The rate coefficients, $k_j$, and the adsorption constants, $K_i$, were parameterised according to Eqs. 3.16 and 3.17.

Table 3.2: Parameters for equations 3.16 and 3.17

| Activation energy (kJ $mol^{-1}$) | | | Enthalpy change of adsorption (kJ $mol^{-1}$) | | | |
|---|---|---|---|---|---|---|
| $E_1$ | $E_2$ | $E_3$ | $\Delta H_{CH_4}$ | $\Delta H_{H_2O}$ | $\Delta H_{H_2}$ | $\Delta H_{CO}$ |
| 240.1 | 243.9 | 67.13 | -38.28 | 88.68 | -82.9 | -70.65 |

$$k_j = k_{j,T_r} \exp\left[ -\frac{E_j}{R} \left( \frac{1}{T} - \frac{1}{T_r} \right) \right] \ , \ j = 1, \ 2, \ 3 \tag{3.16}$$

$$K_i = K_{i,T_r} \exp\left[ -\frac{\Delta H_i}{R} \left( \frac{1}{T} - \frac{1}{T_r} \right) \right] \ , \ i = CH_4, \ H_2O, \ H_2, \ CO \tag{3.17}$$

where $T_r$ is reference temperature, equal to 648K for $k_j$, $K_{H_2}$, and $K_{CO}$, and 823K for $K_{CH_4}$, and $K_{H_2O}$. $R$ is the universal gas constant, equal to 8.314472 J $mol^{-1}$ $K^{-1}$. The values of activation energies, $E_j$, and adsorption enthalpies, $\Delta H_j$ are given in Table 3.2.

The resulting expressions for the rate and adsorption constants, $k_j$ and $K_i$ respectively, are given below:

$$k_1 = 1.82 \times 10^{-4} \exp\left[ 28878.0 \left( \frac{1}{T} - \frac{1}{648} \right) \right] \ , \ \mathrm{mol} \cdot \mathrm{bar}^{0.5} \cdot \mathrm{kg}_{\mathrm{cat}}^{-1} \cdot \mathrm{h}^{-1} \tag{3.18}$$

$$k_2 = 2.193 \times 10^{-5} \exp\left[29336.0\left(\frac{1}{T} - \frac{1}{648}\right)\right] \ , \ \mathrm{mol \cdot bar^{0.5} \cdot kg_{cat}^{-1} \cdot h^{-1}} \tag{3.19}$$

$$k_3 = 7.558 \exp\left[8074.3\left(\frac{1}{T} - \frac{1}{648}\right)\right] \ , \ \mathrm{mol \cdot kg_{cat}^{-1} \cdot h^{-1} \cdot bar^{-1}} \tag{3.20}$$

$$K_{CH_4} = 0.1791 \exp\left[4604.3\left(\frac{1}{T} - \frac{1}{823}\right)\right] \ , \ \mathrm{bar^{-1}} \tag{3.21}$$

$$K_{H_2O} = 0.4152 \exp\left[-10666.35\left(\frac{1}{T} - \frac{1}{823}\right)\right] \ , \ \mathrm{dimensionless} \tag{3.22}$$

$$K_{H_2} = 0.0296 \exp\left[9971.13\left(\frac{1}{T} - \frac{1}{648}\right)\right] \ , \ \mathrm{bar^{-1}} \tag{3.23}$$

$$K_{CO} = 40.91 \exp\left[8497.71\left(\frac{1}{T} - \frac{1}{648}\right)\right] \ , \ \mathrm{bar^{-1}} \tag{3.24}$$

The temperature dependent expressions for the equilibrium constants, $K_I$, $K_{II}$ and $K_{III}$, are taken by Twigg (1996):

$$K_I = \frac{1.026}{\exp\left(0.2513Z^4 - 0.3665Z^3 - 0.58101Z^2 + 27.1337Z - 3.2770\right)} \ , \ bar^2 \tag{3.25}$$

$$K_{II} = K_I \cdot K_{III} \ , \ bar^2 \tag{3.26}$$

$$K_{III} = \exp\left(-0.29353Z^3 + 0.63508Z^2 + 4.1778Z + 0.31688\right) \ , \ \mathrm{dimensionless} \tag{3.27}$$

where $Z = 1000/T - 1$.

The rate of formation or consumption of component $i$, $r_i$, is then calculated by using Eqs. 3.13–3.15 as follows:

$$r_i = \sum_{j=I}^{III} \upsilon_{ij} R_j \ , \ i = CH_4,\ H_2O,\ H_2,\ CO_2,\ CO \tag{3.28}$$

where $\upsilon_{ij}$ is the stoichiometric coefficient of component $i$ in reaction $j$. In case $i$ refers to a reactant, $\upsilon_{ij}$ is negative, whereas for a product $\upsilon_{ij}$ is positive. Thus, the disappearance rates for $CH_4$ and $H_2O$ and the formation rates for $H_2$, $CO_2$ and $CO$ are given by the following equations:

$$r_{CH_4} = -R_I - R_{II} \tag{3.29}$$

$$r_{H_2O} = -R_I - 2R_{II} - R_{III} \tag{3.30}$$

$$r_{H_2} = 3R_I + 4R_{II} + R_{III} \tag{3.31}$$

$$r_{CO_2} = R_{II} + R_{III} \tag{3.32}$$

$$r_{CO} = R_I - R_{III} \tag{3.33}$$

Partial pressure of hydrogen is a critical parameter in Xu and Froment's model, because if the feed is hydrogen free, then the initial rate of reactions I–III (see equations 3.13- 3.15) is infinite. To overcome this obstacle, a very small amount of hydrogen is used in the feed. The arbitrary value of hydrogen feed molar fraction is set at $10^{-4}$. Sensitivity analysis shows that there are no significant discrepancies in the results in the range $10^{-6} - 10^{-2}$ of hydrogen molar fraction.

## 3.5 Adsorption equilibria and kinetics

The Langmuir model for $CO_2$ adsorption, as proposed by Ding and Alpay (2000a,b), can be written as:

$$q^*_{CO_2} = \frac{m_{CO_2} b_{CO_2} P_{CO_2}}{1 + b_{CO_2} P_{CO_2}} \tag{3.34}$$

where $m_{CO_2}$ represents the adsorbent capacity (mol of $CO_2$ per kg adsorbent) under wet conditions, and $b_{CO_2}$ is a temperature dependent parameter:

$$b_{CO_2} = 2.36 \times 10^{-4} \exp\left[\frac{17000}{R}\left(\frac{1}{T} - \frac{1}{673}\right)\right] \ , \ Pa^{-1} \tag{3.35}$$

The adsorption rate into an adsorbent particle is approximated by the LDF model:

$$r_{ads} = k_{LDF}(q^*_{CO_2} - q_{CO_2}) \tag{3.36}$$

where $k_{LDF}$ is the effective mass transfer coefficient (see Eq. 2.8); $q^*_{CO_2}$ and $q_{CO_2}$ are the equilibrium and the local adsorbed phase concentration (average over an adsorbent particle). The direct relation between $q_{CO_2}$ and the gas–phase $CO_2$ concentration is lumped in the above formulation and the term, $r_{ads}$, is used in the corresponding governing equations. Fast adsorption kinetics are assumed because of the small adsorbent particle diameter ($d_p$ = 55$\mu$m), since $k_{LDF} \propto 1/R_p^2$. The value of $k_{LDF}$ is arbitrarily set equal to 1 $s^{-1}$ for a base case (given the specific reactor design, e.g. residence time). A detailed parametric study is presented in §4.2 regarding the effect of the adsorption kinetics on the process performance. For further details on Langmuir and LDF parameters of $CO_2$ adsorption on hydrotalcite adsorbent, see Ding and Alpay (2000a,b).

## 3.6 Regeneration unit

The adsorbent regeneration is assumed to take place in a well-mixed, continuous flow desorption unit with a mean residence time $\tau$, operating at steady state under isobaric conditions; see Fig. 3.3. The mass and energy balances of the regeneration unit can be written as:

$$(q_{in} - q) = r_{des}\tau \tag{3.37}$$

$$Fc_{CO_2} = r_{des}\tau N_c \dot{m} \tag{3.38}$$

$$Fc_g c_{p,g}(T_{in} - T) + N_c \dot{m} \cdot (c_{p,ads}(T_{in} - T) + \Delta H_{ads} r_{des} \tau) = 0 \tag{3.39}$$

Note that the residence time of the adsorbent particles, $\tau$ (s), is given by:

$$\tau = \frac{M}{\dot{m} N_c} \tag{3.40}$$

where $M$ (kg) is the total mass of adsorbent in the regeneration unit.

The rate of desorption, $r_{des}$, is provided by the LDF model, while the equilibrium adsorbent phase concentration, $q^*$, is obtained by the Langmuir model for $CO_2$ adsorption. It should be mentioned that the proposed design is limited only to this particular study, in order to facilitate an initial overall process evaluation. Therefore, the effects of adsorbent hydrothermal ageing and/or attrition on the regeneration efficiency (e.g. loss of capacity, alteration in $\varrho_{ads}$ value) are not considered.

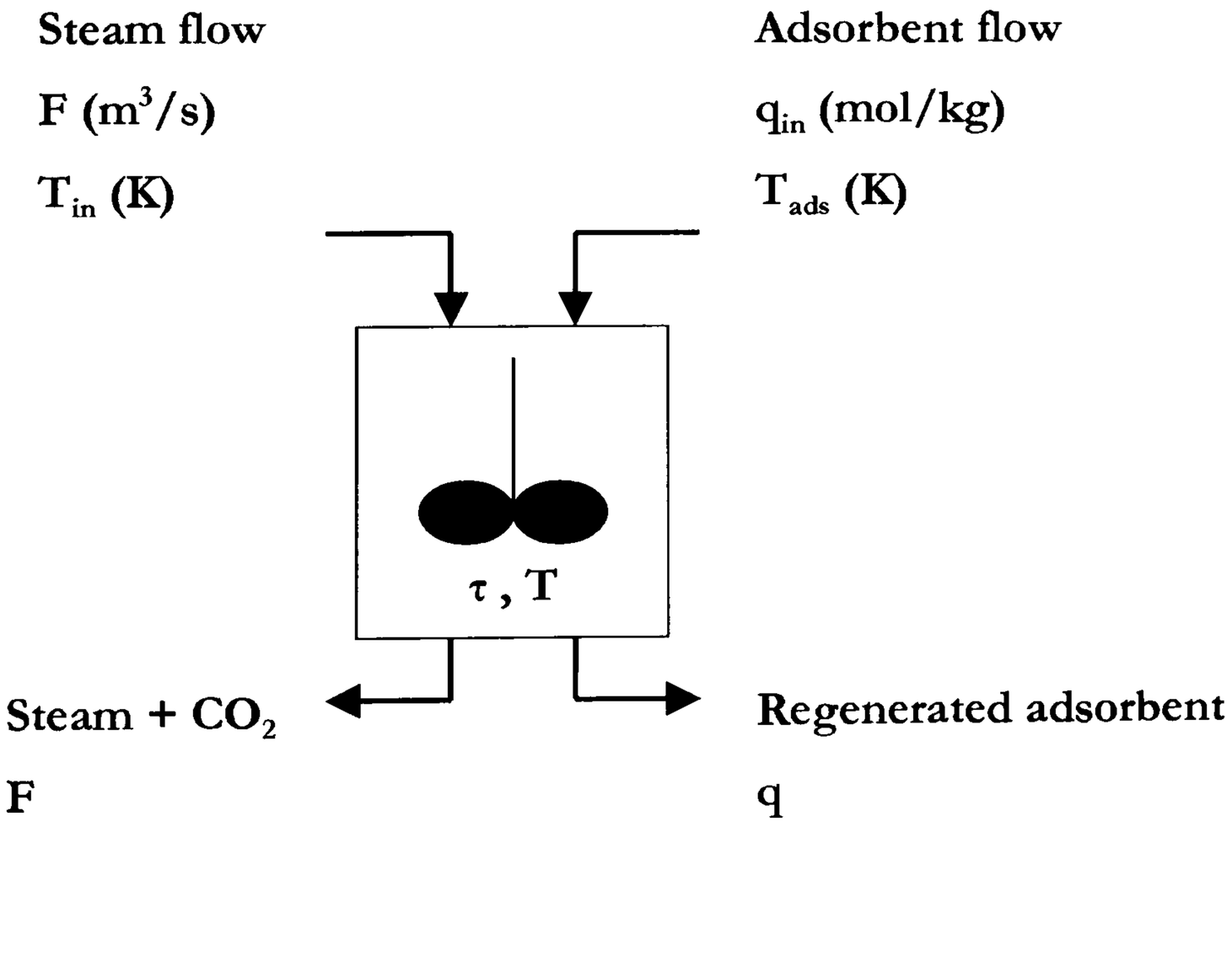



Figure 3.3: Schematic diagram of the well-mixed continuous flow desorber.

## 3.7 Other process parameters

From §3.3 it can be seen that the derived model has some additional parameters that determine the behaviour of the system. These are – in the first instance – the mass and heat transfer coefficients for the film between the gas phase and the catalytic coated wall, $k_m$ and $k_h$ respectively. The aforementioned coefficients are estimated, assuming Nu and Sh numbers equal to 3.65, since the predicted values for these numbers are in the range 3.0–4.5 for the fully developed region and steady–state conditions.

Therefore, the mass transfer coefficient can be obtained by (Hoebink and Marin, 1998):

$$k_m = \frac{Sh \times gaseous\ diffusivity}{2R_c} \tag{3.41}$$

and the heat transfer coefficient by:

$$k_h = \frac{Nu \times gaseous\ thermal\ conductivity}{2R_c} \tag{3.42}$$

where $R_c$ is the radius of the reactor channel (m).

The calculation of the thermal conductivity of the gaseous mixture is based on the Eucken semi–empirical formula as follows (Reid et al., 1987):

$$\lambda_m = \sum_i \left( \frac{y_i \lambda_i}{\sum_j y_j \varphi_{ij}} \right) \ , \ \lambda_i = \left( c_{p,i} + \frac{5}{4} \frac{R}{M_i} \right) \mu_i \tag{3.43}$$

with the Chapman–Enskog parameter

$$\varphi_{ij} = \frac{1}{\sqrt{8}} \left( 1 + \frac{M_i}{M_j} \right) \left[ 1 + \left( \frac{\mu_i}{\mu_j} \right)^{1/2} \left( \frac{M_j}{M_i} \right)^{1/4} \right] \tag{3.44}$$

and the dynamic viscosity of an individual component, assuming **monoat**omic gases, $\mu_i$ given by:

$$\mu_i = 2.6693 \times 10^{-6} \frac{\left(10^3 M_i T\right)^{1/2}}{\sigma_i^2 \Omega_{\mu,i}} \tag{3.45}$$

The diffusivity of the gas mixture is estimated using the Chapman–Enskog theory for binary mixtures:

$$D_{ij} = 0.018829 \left[T^3 \left(\frac{10^{-3}}{M_i} + \frac{10^{-3}}{M_j}\right)\right]^{1/2} \left(P\, \sigma_{ij}^2\, \Omega_{D,ij}\right)^{-1} \tag{3.46}$$

Note that $\sigma_{ij} = (\sigma_i + \sigma_j)/2$, while the parameters $\Omega_{\mu,i}$ and $\Omega_{D,ij}$ are functions of temperature; see Reid et al. (1987) for more details.

The above gas phase properties are considered constant throughout the reactor. Binary mixtures are chosen from the two highest concentrations of the gas mixture at the inlet and outlet of the channel. Average values are then taken, which apply throughout the system (a reasonable assumption, given the uncertainty associated with these estimates). The resulting values of $k_m$ and $k_h$ used in the simulations are listed in Table 3.3. It should be mentioned that the coefficient of heat transfer between the gas phase and the adsorbent particle, $k_{h,ads}$, is assumed equal to $k_h$ (see §5.3 for a sensitivity analysis on this assumption).

The gas phase heat capacity is obtained from:

$$c_{p,g} = \sum_i y_i c_{p,i} \ , \ c_{p,i} = A_i + B_i T + C_i T^2 + D_i T^3 + E_i T^4 \ (\mathrm{Jmol^{-1}K^{-1}}) \tag{3.47}$$

Note that $i = CH_4,\ H_2O,\ H_2,\ CO_2,\ CO$ and the parameters $A_i,\ B_i,\ C_i,\ D_i,\ E_i$ at the above polynomial function of temperature, $T$, are extracted by Reid et al. (1987).

The heat of each reaction $j = I - III$ is then given by:

$$\Delta H_{R_j}(T) = \Delta H_{R_j}(298) + \int_{298}^{T} \Delta c_{pj} dT \tag{3.48}$$

Heat capacity changes for the three SMR reactions are given by:

$$\Delta c_{pI} = 3c_{p,H_2} + c_{p,CO} - c_{p,H_2O} - c_{p,CH_4} \tag{3.49}$$

$$\Delta c_{pII} = 4c_{p,H_2} + c_{p,CO_2} - 2c_{p,H_2O} - c_{p,CH_4} \tag{3.50}$$

$$\Delta c_{pIII} = 4c_{p,H_2} + c_{p,CO_2} - c_{p,H_2O} - c_{p,CO} \tag{3.51}$$

As mentioned in §3.2, the actual gas and adsorbent velocities are assumed equal, *i.e.*, $u_g^{int} = u_{ads}^{int}$. The interstitial gas velocity, $u_g^{int}$, is given by:

$$u_g^{int} = \frac{\dot{V}_g}{(1-\varphi)\varepsilon A}$$

where $\dot{V}_g$ ($m^3\ s^{-1}$) is the gas volumetric flowrate and $A$ ($m^2$) the total cross sectional area of the monolithic channel. The superficial gas velocity, $u_g$, is as follows:

$$u_g = \frac{\dot{V}_g}{A}$$

As a result

$$u_g^{int} = \frac{u_g}{(1-\varphi)\varepsilon}$$

Similarly, for the adsorbent particles:

$$u_{ads}^{int} = \frac{\dot{m}}{\varepsilon\varphi\varrho_{ads}A}\ ,\ u_{ads} = \frac{\dot{m}}{\varrho_{ads}A} \quad \text{giving} \quad u_{ads}^{int} = \frac{u_{ads}}{\varepsilon\varphi}$$

where $\dot{m}$ ($kg\ s^{-1}$) is the adsorbent mass flowrate.

Clearly, the adsorbent superficial velocity can be expressed as a function of the superficial gas velocity, $u_g$, and the adsorbent loading, $\varphi$, as follows:

$$u_{ads} = \left(\frac{\varphi}{1-\varphi}\right) u_g \tag{3.52}$$

In reality, it is likely that there is some slip. Sensitivity analysis shows that the overall process performance is not affected (see §5.3).

## 3.8 Process performance indices

Adsorption–enhanced processes can be assessed in terms of reaction performance such as the reactant conversion and the overall yield of a key component, and in terms of separation performance such as the purity and recovery of a key component.

In order to carry out a detailed parametric investigation of the proposed process, the methane conversion and its enhancement factor, as well as the $CO_2$ recovery are introduced as measures of its performance. Specific definitions of these criteria are now given.

Methane conversion is defined as the ratio between converted methane at the reactor exit (or at any position along the monolithic channel) and the inlet flux of methane. It reads:

$$X(\%) = 100 \cdot \frac{\dot{n}^{in}_{CH_4} - \dot{n}^{out}_{CH_4}}{\dot{n}^{in}_{CH_4}} \tag{3.53}$$

The conversion enhancement factor can be quantified by the normalised conversion of methane in the presence (AD) and absence (NAD) of $CO_2$ adsorption (Ding and Alpay, 2000b), *i.e.*:

$$E(\%) = 100 \cdot \frac{X_{AD} - X_{NAD}}{X_{NAD}} \tag{3.54}$$

The recovery of $CO_2$ is obtained by the overall mass balance. and given by:

$$R(\%) = 100 \cdot \frac{\dot{n}_{CO_2}^{recov}}{\dot{n}_{CO_2}^{total}} \tag{3.55}$$

where $\dot{n}_{CO_2}^{recov}$ is the flowrate of $CO_2$ recovered at the purge steam of the desorption step and $\dot{n}_{CO_2}^{total}$ is the total amount of $CO_2$ produced.

Additional performance measures, used mainly for process optimisation, include the hydrogen purity and yield and the reactor efficiency. The product gas $H_2$ purity is expressed as mol % on a dry basis. The hydrogen yield is expressed as the moles of hydrogen produced per mole of methane fed, *i.e.*:

$$Y_{H_2} = \frac{\dot{n}_{H_2}^{prod}}{\dot{n}_{CH_4}^{in}} \tag{3.56}$$

The evaluation of the reactor efficiency is based on methodologies previously applied to similar systems (see Johnsen et al., 2006b; Ryden, 2006). In particular, a $H_2$–equivalent term, $H_{2,eq}$, is firstly introduced to describe the amount of hydrogen remaining per mole of methane fed, if the process energy demands were to be met by utilising the produced hydrogen for this purpose. Hence:

$$H_{2,eq} = Y_{H_2} - \left(\frac{Q_H}{LHV_{H_2}}\right) \cdot 10^{-3} \tag{3.57}$$

The reformer efficiency, $\Upsilon$, is then defined as:

$$\Upsilon(\%) = 100 \cdot H_{2,eq} \cdot \left(\frac{LHV_{H_2}}{LHV_{CH_4}}\right) \tag{3.58}$$

where $Q_H$ is the heat demand of the process in J (mol $CH_4$)$^{-1}$. The lower heating values

(LHVs) for hydrogen and methane are equal to 241.8 and 802.3 kJ $mol^{-1}$ respectively (Johnsen et al., 2006b). The energy demand of the process, $Q_H$, is quantified as follows:

$$Q_H = \frac{Q_r + Q_{reg}}{\dot{n}^{in}_{CH_4}} \tag{3.59}$$

where

$$Q_r = \dot{n}_g c_{p,g} (T_f - 298) \tag{3.60}$$

is the energy input rate for the reactor, defined as the heat supply (J $s^{-1}$) required to raise an inlet stream from ambient temperature (298K) to the reactor gas inlet temperature, $T_f$. The corresponding requirement for the regeneration unit is given by:

$$Q_{reg} = \dot{m} (c_{p,ads} (T_{ads}|_{z=0} - T_{ads}|_{z=L}) - \Delta H_{ads} \cdot q_{CO_2}|_{z=L}) \tag{3.61}$$

where $\dot{m}$ is the adsorbent mass flowrate in kg $s^{-1}$. $Q_{reg}$ (J $s^{-1}$) denotes the energy required: to increase the adsorbent temperature from its value at the reactor exit ($T_{ads}|_{z=L}$) up to the specified temperature at the reactor entrance ($T_{ads}|_{z=0} = T_f + \vartheta$); and to fully "clean" the adsorbent. The above expression provides a quantitative measure of the energy requirement for the regeneration stage, while bypassing any uncertainties involved in the design of the regeneration unit.

## 3.9 Numerical discretisation and model solution

The equations described above were coded and solved in the gPROMS modelling environment (Process Systems Enterprises Ltd.). The finite difference approach is used to replace the continuous problem domain by a grid, in which the dependent variables from the continuous domain exist only at a finite number of discrete points. As a result, the domain is divided into equidistant intervals involving a finite number of discrete (grid) points; see Fig. 3.4. Finite differences equations can be established by approximating the spatial derivatives in terms of the values of the corresponding variables at the grid points. This can be achieved using a number of different ways, for example:

1. Taylor–series expansion

2. Polynomial approximation

3. Integral method

4. Control volume approach

Traditionally the derivation of finite differences is achieved by Taylor–series expansion, and this method is also adopted in this work. Discretisation to the spatial dimension reduces the derived system of ordinary differential and algebraic equations to a large set of non-linear algebraic equations, which is then solved using a sophisticated implementation of a Newton–type method.

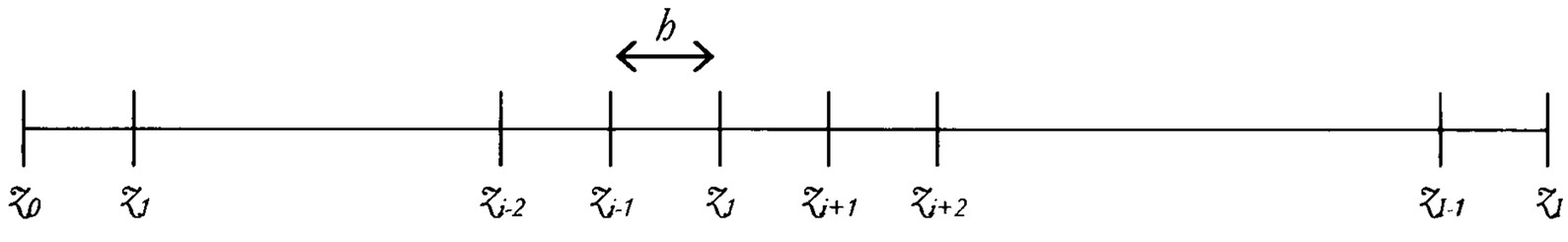



Figure 3.4: Equidistant finite difference grid.

With reference to Fig. 3.4, consider a distributed dependent variable $\theta(z_i)$: the Taylor series for $\theta(z_{i+1})$ and $\theta(z_{i-1})$ can be written as:

$$\theta(z_{i+1}) = \theta(z_i) + \frac{\partial\theta(z_i)}{\partial z}h + \frac{\partial^2\theta(z_i)}{\partial z^2}\frac{h^2}{2!} + \frac{\partial^3\theta(z_i)}{\partial z^3}\frac{h^3}{3!} + \ldots \tag{3.62}$$

$$\theta(z_{i-1}) = \theta(z_i) - \frac{\partial\theta(z_i)}{\partial z}h + \frac{\partial^2\theta(z_i)}{\partial z^2}\frac{h^2}{2!} - \frac{\partial^3\theta(z_i)}{\partial z^3}\frac{h^3}{3!} + \ldots \tag{3.63}$$

Eq. 3.62 can be rearranged and divided by $h$ to obtain the first order *forward* difference approximation to the partial derivative $\frac{\partial\theta(z_i)}{\partial z}$:

$$\frac{\partial\theta(z_i)}{\partial z} = \frac{\theta(z_{i+1}) - \theta(z_i)}{h} + O(h) \tag{3.64}$$

The first order *backward* difference approximation to the partial derivative $\frac{\partial\theta(z_i)}{\partial z}$ can be obtained in a similar manner using Eq. 3.63:

$$\frac{\partial\theta(z_i)}{\partial z} = \frac{\theta(z_i) - \theta(z_{i-1})}{h} + O(h) \tag{3.65}$$

Note that the accuracy of these first order approximations is of order $h$ ($O(h)$). To improve the approximation accuracy, one ought to consider additional neighbouring points, namely $\theta(z_{i+2})$ and $\theta(z_{i-2})$, the Taylor series of which are given by:

$$\theta(z_{i+2}) = \theta(z_i) + \frac{\partial\theta(z_i)}{\partial z}2h + \frac{\partial^2\theta(z_i)}{\partial z^2}\frac{(2h)^2}{2!} + \frac{\partial^3\theta(z_i)}{\partial z^3}\frac{(2h)^3}{3!} + ... \tag{3.66}$$

$$\theta(z_{i-2}) = \theta(z_i) - \frac{\partial\theta(z_i)}{\partial z}2h + \frac{\partial^2\theta(z_i)}{\partial z^2}\frac{(2h)^2}{2!} - \frac{\partial^3\theta(z_i)}{\partial z^3}\frac{(2h)^3}{3!} + ... \tag{3.67}$$

Then a one–sided derivative that is correct to $O(h^2)$ can be developed by four times Eq. 3.62 minus Eq. 3.66 (thereby eliminating the $\frac{\partial^2\theta(z_i)}{\partial z^2}$ terms) to yield the second order *forward* difference approximation to the partial derivative $\frac{\partial\theta(z_i)}{\partial z}$:

$$\frac{\partial\theta(z_i)}{\partial z} = \frac{-3\theta(z_i) + 4\theta(z_{i+1}) - \theta(z_{i+2})}{2h} + O(h^2) \tag{3.68}$$

The analogous formula in the other direction, *i.e.*, the second order *backward* approximation to the partial derivative $\frac{\partial\theta(z_i)}{\partial z}$ can be obtained from Eq. 3.63 and Eq. 3.67 as:

$$\frac{\partial\theta(z_i)}{\partial z} = \frac{\theta(z_{i-2}) - 4\theta(z_{i-1}) + 3\theta(z_i)}{2h} + O(h^2) \tag{3.69}$$

Additionally, Eqs. 3.62 and 3.63 can be combined to result in a *centered* difference approximation:

$$\frac{\partial\theta(z_i)}{\partial z} = \frac{-\theta(z_{i-1}) + \theta(z_{i+1})}{2h} + O(h^2) \tag{3.70}$$

The second order partial derivative $\frac{\partial^2\theta(z_i)}{\partial z^2}$ can be obtained by similar algebraic manipulations (eliminating the $\frac{\partial\theta(z_i)}{\partial z}$), *i.e.*, *forward* difference: Eq. 3.66 minus two times Eq. 3.62:

$$\frac{\partial^2\theta(z_i)}{\partial z^2} = \frac{\theta(z_i) - 2\theta(z_{i+1} + \theta(z_{i+2}))}{h^2} + O(h^2) \tag{3.71}$$

*centered* difference: Eq. 3.62 plus Eq. 3.63:

$$\frac{\partial^2\theta(z_i)}{\partial z^2} = \frac{\theta(z_{i-1}) - 2\theta(z_i) + \theta(z_{i+1}))}{h^2} + O(h^2) \tag{3.72}$$

*backward* difference: Eq. 3.66 plus Eq. 3.63:

$$\frac{\partial^2\theta(z_i)}{\partial z^2} = \frac{\theta(z_{i-2}) - 2\theta(z_{i-1}) + \theta(z_i))}{h^2} + O(h^2) \tag{3.73}$$

The involvement of a larger number of neighbouring points leads to higher order accuracies for the approximation.

It should be noted that a normalised space co–ordinate $\zeta \in [0, 1]$ is introduced replacing $z \in [0, L]$, as follows:

$$\zeta \equiv z/L \tag{3.74}$$

All derivatives can then be expressed in terms of this new independent variable:

$$\frac{\partial}{\partial z} = \frac{1}{L}\frac{\partial}{\partial \zeta} \; ; \; \frac{\partial^2}{\partial z^2} = \frac{1}{L^2}\frac{\partial^2}{\partial \zeta^2} \tag{3.75}$$

The spatial derivatives involved in the governing equations and boundary conditions are modified as indicated by the the above expressions. The transformed model equations hold over the domain $\zeta \in (0, 1)$. The corresponding boundary conditions hold at $\zeta = 0$ and $\zeta = 1$.

In this work, the normalised spatial domain is discretised using centred finite differences of second order over a uniform grid of typically 80–100 intervals. This approach is found to give a converged solution in which component balance errors (associated with the numerical integration) are negligible. The convergence of the solution is checked by varying the number of grid points along $\zeta$ and by using the internal criteria of the gPROMS integrator. In particular, a system of $n$ equations $f(x)$ in $n$ unknowns $x$ is assumed to have converged when the norm of the equations:

$$||f(x)|| \equiv \max_{i \in [1,n]} |fi(x)|$$

falls below $10^{-5}$. Other key criteria include the maximum number of evaluations of the vector of equations $f(x)$ that is permitted during solution (equal to $10^6$), the maximum number of iterations without a reduction in the norm of the equation vector (see above) before the solver takes corrective action (equal to 10) and the maximum number of iterations that the solver is allowed to take (equal to $10^3$). The solver also attempts to take certain corrective actions if no improvement in the equation norm is achieved within a certain number of consecutive iterations. If such corrective action is attempted more than 10 times in a row (*i.e.*, having to return to the same $x^{best}$ in all cases), then the solver terminates its operation unsuccessfully.

A summary of parameters (constants) used for the simulations is given in Table 3.3. The flowrates and dimensions are characteristic of a laboratory-scale reactor rig (Ding et al., 2005; Ding, 2006).

Table 3.3: Parameters (constants) used in the simulations

| Parameter | Value | Unit |
|---|---|---|
| Adsorbent heat capacity, $c_{p,ads}$ | 850 [a] | J $kg^{-1}$ $K^{-1}$ |
| Adsorbent particle diameter, $d_p$ | $55\times10^{-6}$ [b] | m |
| Feed steam/$CH_4$ ratio | 6 [c] | - |
| Heat of adsorption, $\Delta H_{ads}$ | $-17\times10^{3}$ [a] | J $mol^{-1}$ |
| Gas–coating heat transfer coefficient, $k_h$ | 170 | J $m^{-2}$ $s^{-1}$ $K^{-1}$ |
| Gas–adsorbent heat transfer coefficient, $k_{h,ads}$ | 170 | J $m^{-2}$ $s^{-1}$ $K^{-1}$ |
| LDF mass transfer coefficient, $k_{LDF}$ | 1 | $s^{-1}$ |
| Mass transfer coefficient, $k_m$ | 0.15 | m $s^{-1}$ |
| Reactor length, $L$ | 1 [b] | m |
| Mass of adsorbent in the regenerator, $M$ | 2 [b] | kg |
| Langmuir model constant, $m_{CO_2}$ (wet condition) | 0.65 [a] | mol $kg^{-1}$ |
| Number of monolith channels, $N_c$ | 1000 | – |
| Pressure | 5 | bar |
| Monolith channel radius, $R_c$ | $1\times10^{-3}$ [b] | m |
| Reactor feed temperature, $T_f$ | 723 [c] | K |
| Superficial gas velocity, $u_g$ | 0.46 [b] | m $s^{-1}$ |
| Monolithic reactor voidage, $\varepsilon$ | 0.5 [b] | – |
| Catalyst effectiveness factor, $\eta$ | 1 | |
| Thermal conductivity, $\lambda$ | 5 [d] | J $m^{-1}$ $s^{-1}$ $K^{-1}$ |
| Adsorbent density, $\varrho_{ads}$ | 1563 [a] | kg $m^{-3}$ |
| Wash coat (catalyst) density, $\varrho_c$ | 785 | kg $m^{-3}$ |

[a] Data from Ding and Alpay (2000a,b)

[b] Data from Ding et al. (2005); Ding (2006)

[c] Data from Xiu et al. (2002a)

[d] Data from Koci et al. (2004)

# Chapter 4

# Simulation results

The mathematical model presented in Chapter 3 is used for detailed fundamental analysis of the process. Initially, the feasibility of the proposed reactor concept is investigated, focusing on the identification of important operating parameters. Subsequently, the overall process performance and the interaction between the reaction and regeneration stages are examined. Finally the effect of the adsorbent characteristics – $CO_2$ capacity and sorption kinetics – on both the reactor and overall process performance are systematically investigated. Typical simulation outputs include concentration and temperature profiles along the reactor as well as performance characteristics, namely methane conversion, enhancement factor and $CO_2$ recovery.

## 4.1 Process analysis

### 4.1.1 Performance of the adsorptive reactor

The influence of the adsorbent on the reactor performance is investigated by considering three cases. In the first, the adsorbent loading is set to zero, thus simulating "pure" SMR in hollow monolith channels. In the second case, adsorbent is considered to flow through the monolith channels, but the adsorption capacity of the particles is set to zero. However, the "adsorbent" in this case, acts as a heat carrier. In the third case, the adsorbent has its normal adsorption capacity, as well as being a heat carrier. Such simulations enable the analysis of the individual contributions of the adsorption and heating effects of the

adsorbent. With reference to Fig. 4.1, in which axial methane conversion profiles for these three cases are shown, the thermodynamic equilibrium constraint of SMR is evident for the first two cases. As expected, higher methane conversion is achieved in the second one due to the extra heat supplied by the flowing particles. However, the thermodynamic equilibrium is shifted to give even higher conversion by removing $CO_2$ in the third case. Hence, the contribution of the adsorbent is indicated to be two–fold: separation enhancement and additional heat supply for the endothermic reaction. Consequently, the adsorbent loading and the adsorbent inlet temperature are two important operating parameters. The former dictates the separation capacity available in the reactor, whilst the latter is a means of providing the heat for the endothermic reaction.

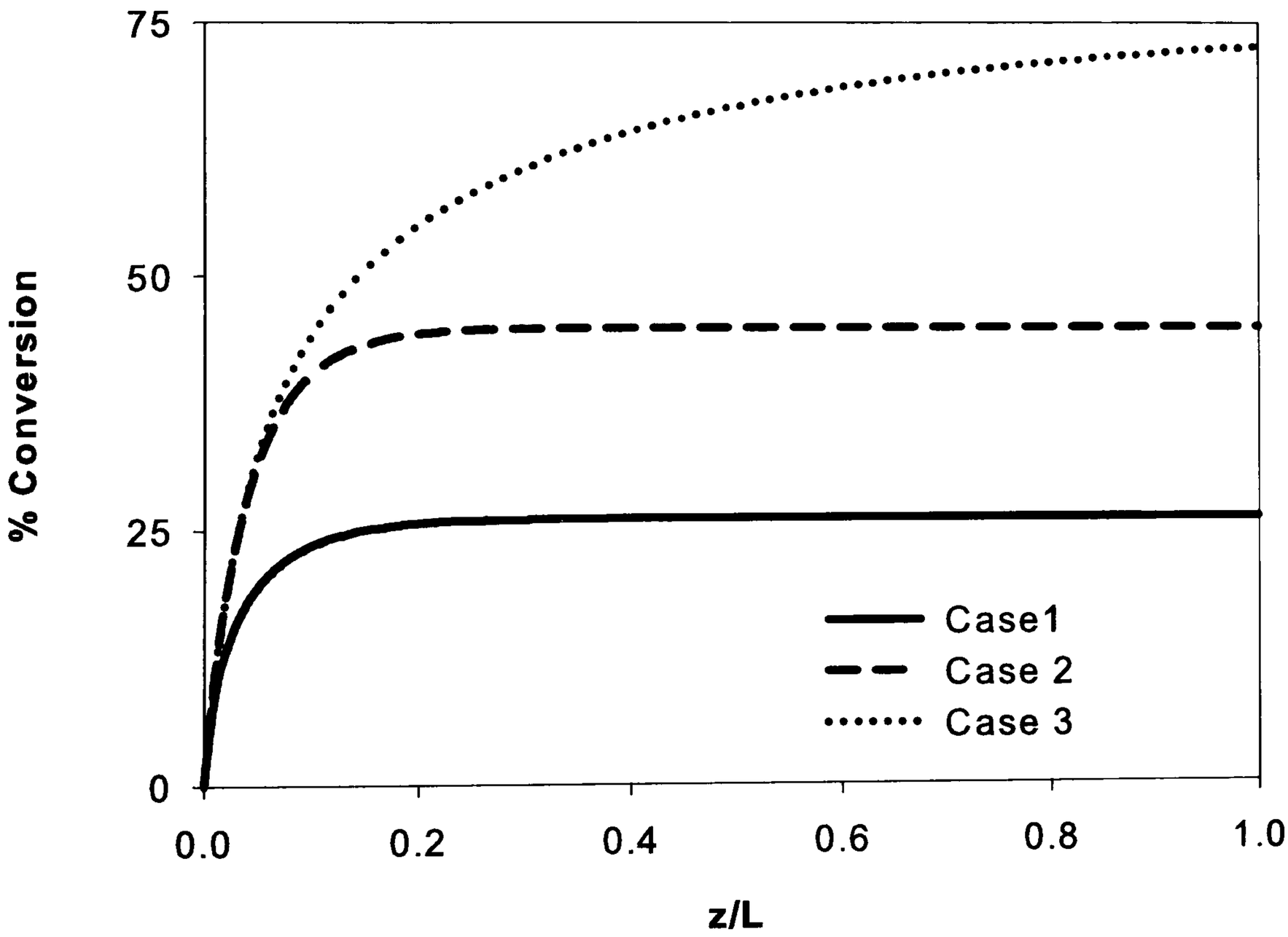



Figure 4.1: Axial methane conversion profiles (Case 1: $\varphi = 0$; Case 2: $\varphi = 0.1$, $m_{CO_2} = 0$; Case 3: $\varphi = 0.1$, $m_{CO_2} = 0.65$ mol kg$^{-1}$).

The effect of the adsorbent inlet temperature on the conversion enhancement at different

adsorbent loadings is shown in Fig. 4.2. Calculations showed a substantial degree of reaction enhancement in the range from 55% to 75% at about 750K, depending on the adsorbent loading. Generally, the temperature range for adsorption-enhanced SMR is relatively narrow (typically within 700–800K), denoting the lower limit of catalyst activity and the upper limit of the adsorbent working temperature. Calculations indicated a lower degree of reaction enhancement at higher temperatures. At temperatures above 750K the separation enhancement effect decays, resulting in comparable enhancement factors for 5% and 10% adsorbent loading at temperatures above 800K.

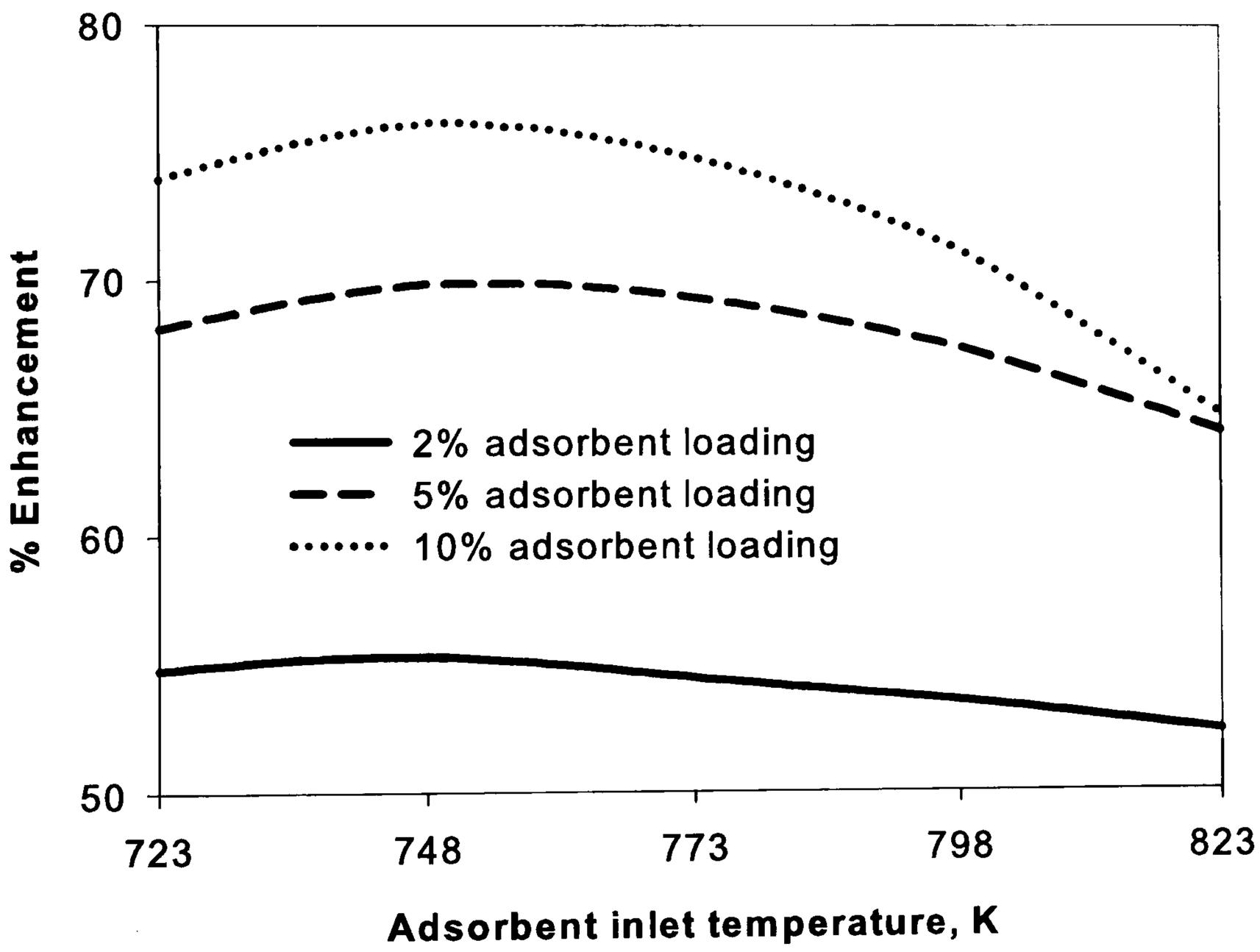



Figure 4.2: Effect of the adsorbent inlet temperature on the conversion enhancement.

Axial profiles of $CO_2$ concentration in the gas phase at different adsorbent loadings with $T_{ads} = 750K$ are shown in Fig. 4.3. As expected, $CO_2$ concentration within the reactor decreases at higher adsorbent loadings. Calculations also showed that there is no significant reduction in $CO_2$ concentration at the second half of the reactor.

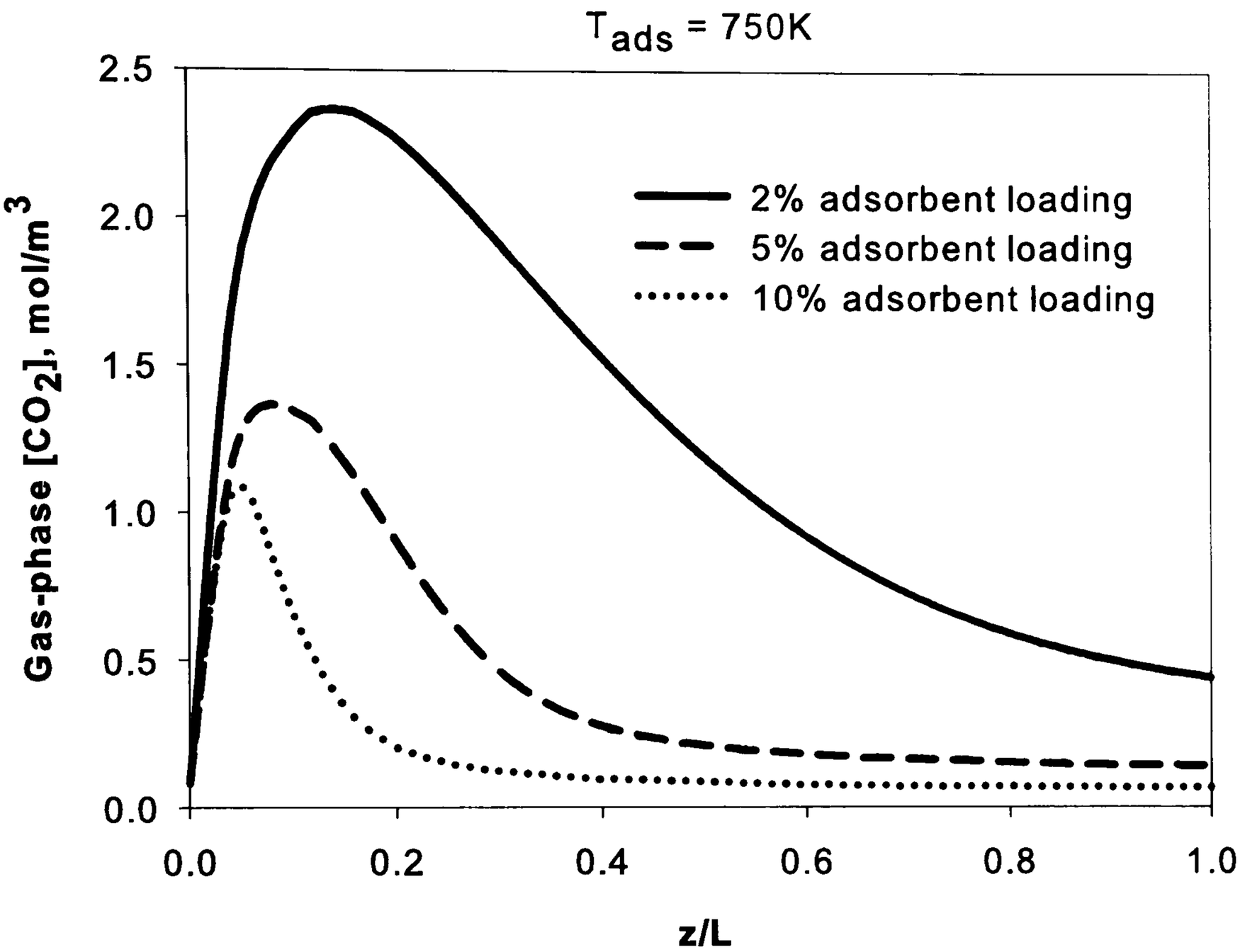



Figure 4.3: $CO_2$ concentration profiles along the adsorptive reactor.

This finding is also confirmed by Fig. 4.4, in which calculated temperature profiles along the reactor are presented. A sharp wash coat temperature gradient at the reactor entrance was predicted because of the strongly endothermic reaction. Still, farther within the monolithic channel, results indicated that thermal equilibration occurs, and hence almost isothermal conditions are reached. However, the adsorbent–phase $CO_2$ concentration keeps increasing, as shown in Fig. 4.4, indicating that $CO_2$ adsorption still takes place in the second half of the reactor. This result also explains the constantly increasing $CH_4$ conversion for the third case ($\varphi = 0.1$, $m_{CO_2} = 0.65$ mol kg$^{-1}$), as shown in Fig. 4.1.

It is evident that the temperature of the adsorbent and its loading in the reactor determine the reaction temperature (Fig. 4.4). Larger adsorbent loadings at higher inlet temperatures result in higher reaction temperature and thus conversion, but as already shown, the enhancement effect weakens. As a result, there is a trade–off between the two objectives of

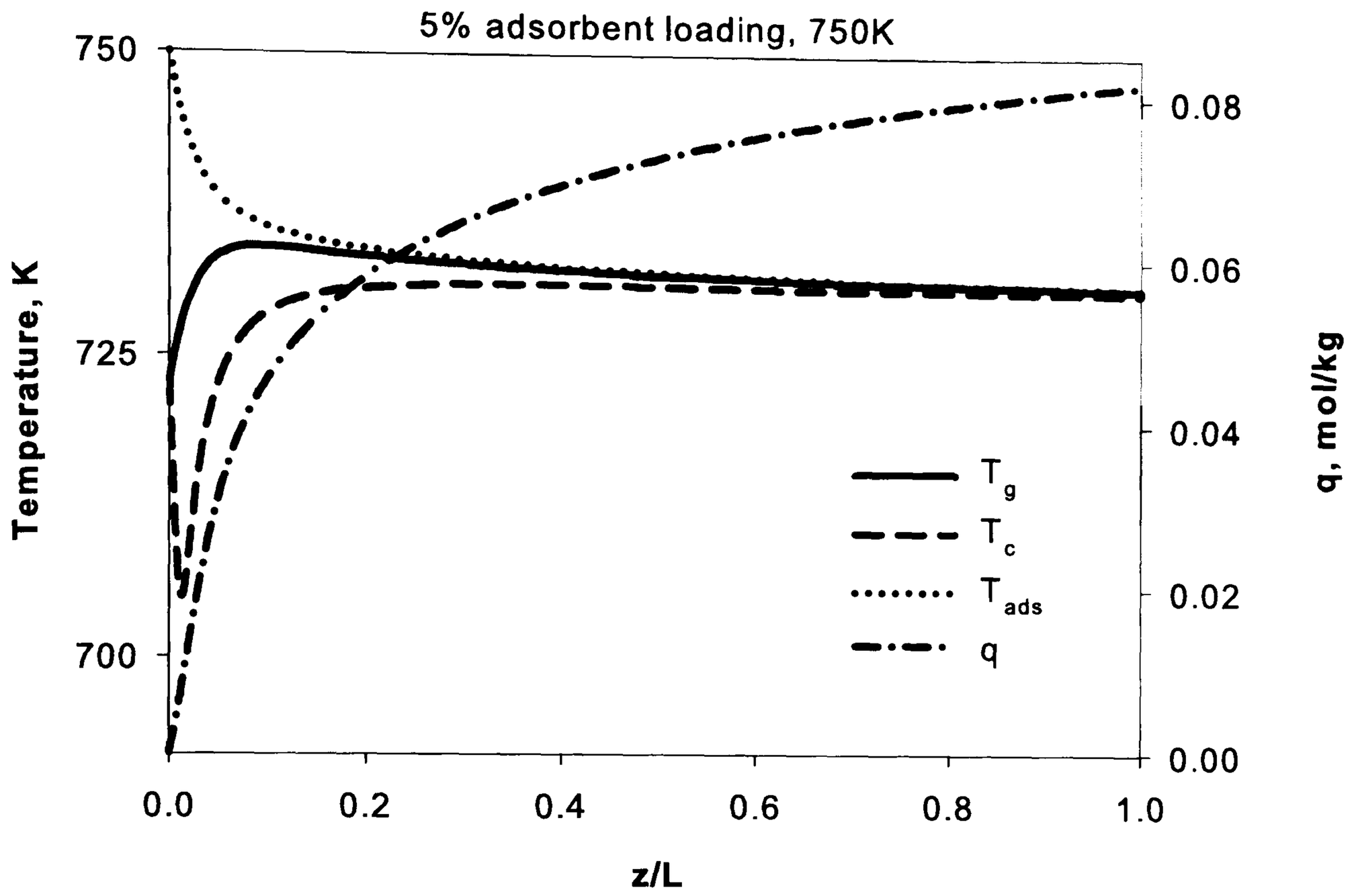



Figure 4.4: Temperature ($T_g, T_c, T_{ads}$) and adsorbent-phase $CO_2$ concentration ($q$) profiles along the adsorptive reactor.

separation versus reaction. The adsorbent mass flux, which is a function of the superficial gas velocity, determines the adsorption enhancement. On the other hand, although a high adsorbent inlet temperature leads to higher conversion, it reduces the capture of $CO_2$ on the adsorbent.

### 4.1.2 Overall process performance

The adsorbent loading and reactor inlet temperature are directly related to the operation of the regeneration unit. Thus, the operating conditions of the desorber are of great importance for the analysis of the overall sorption–enhanced SMR process. For example, the purge steam inlet temperature and flow rate directly influence the adsorbent loading and temperature at reactor inlet. The relation between the adsorbent temperature at the desorber outlet (T) and the steam inlet temperature ($T_{in}$) as a function of steam flow rate

through the desorber (F) at different adsorbent loadings is presented in Fig. 4.5.

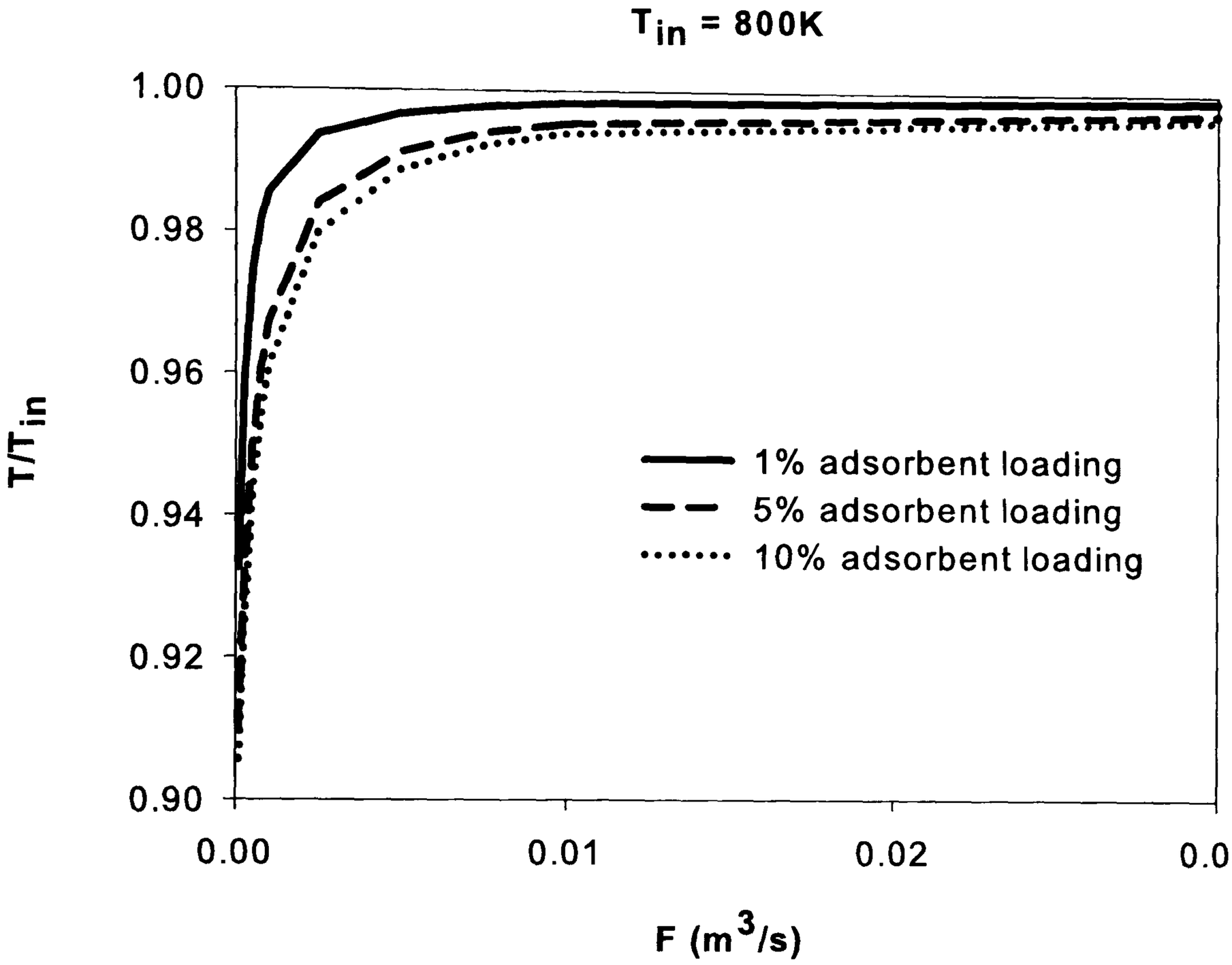



Figure 4.5: Ratio of adsorbent temperature at the desorber outlet ($T$) over steam inlet temperature ($T_{in}$) as a function of steam flow rate ($F$) at different adsorbent loadings.

As shown, heating–up the adsorbent particles can be achieved even at relatively low steam flow rates. However, in terms of $CO_2$ desorbed, higher flow rates are required, especially at higher adsorbent loadings; see Fig. 4.6. These findings imply that $CO_2$ desorption is probably driven by concentration rather than temperature swing in this case.

In connection to the performance of the adsorptive reactor, the methane conversion and enhancement factor as functions of the steam flow rate are shown in Fig. 4.7 & 4.8. Conversion and enhancement steadily increase with the steam flow rate, until a plateau is reached. In Table 4.1 the calculated asymptotic values of conversion and enhancement

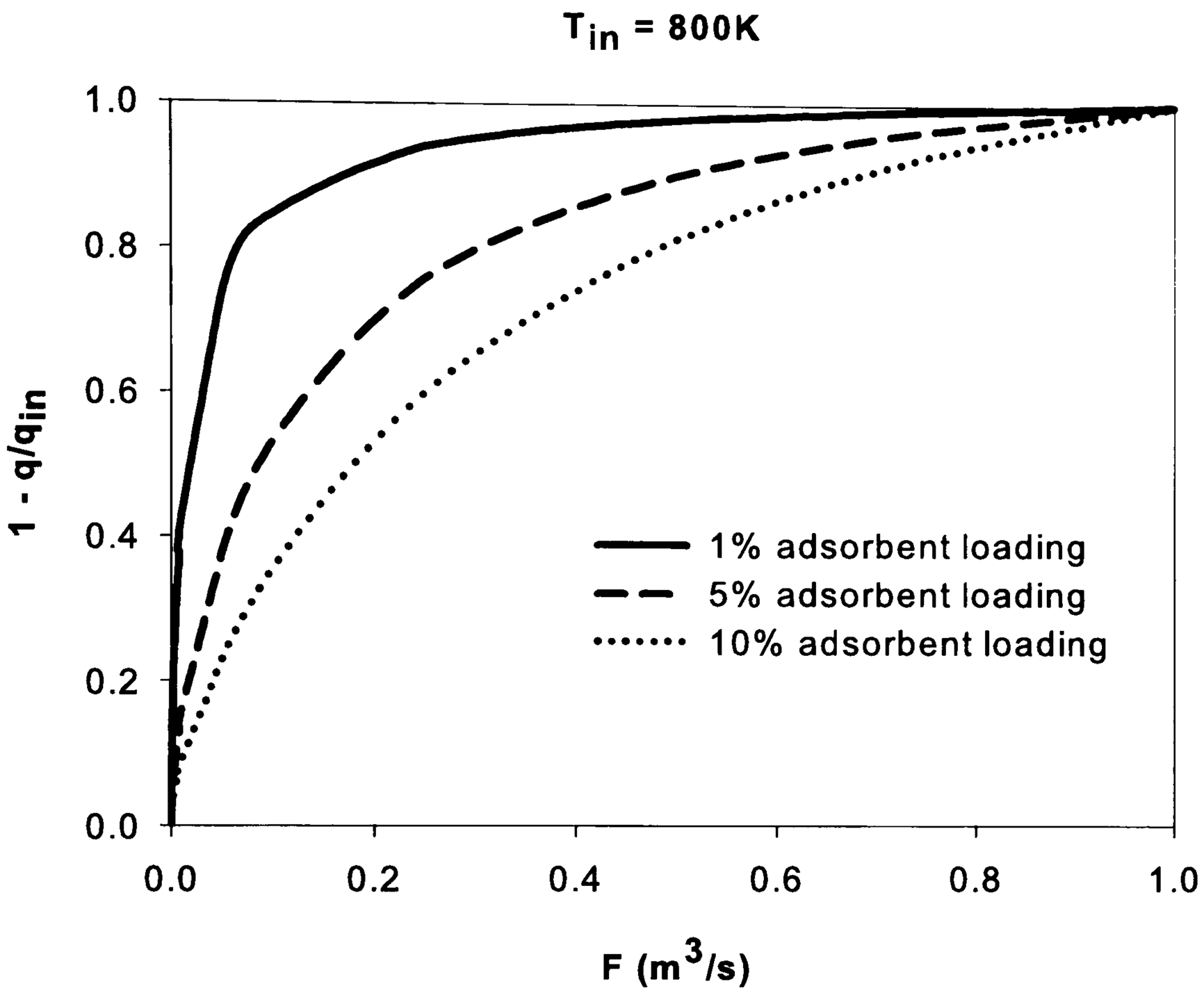



Figure 4.6: Relative amount of $CO_2$ desorbed $(1 - q/q_{in})$ as a function of steam flow rate $(F)$ at different adsorbent loadings.

factor at several adsorbent loadings and steam inlet temperatures are summarised.

Similarly, the $CO_2$ recovery at the outlet of the regenerator increases with the steam flow rate; see Fig. 4.9. However, the steam inlet temperature is not significant for $CO_2$ recovery, as shown in Table 4.1, e.g. approximately 97.3% recovery was calculated at 5% adsorbent loading. These results strengthen the findings presented in Fig. 4.5 and Fig. 4.6.

In connection to the findings presented in Figs. 4.7–4.9, the methane conversion as a function of the $CO_2$ molar fraction at the gaseous purge stream of the desorber is presented in Fig. 4.10. Higher conversion, therefore improved overall process performance, is associated with lower molar fractions of recovered $CO_2$, resulting from higher consumption of

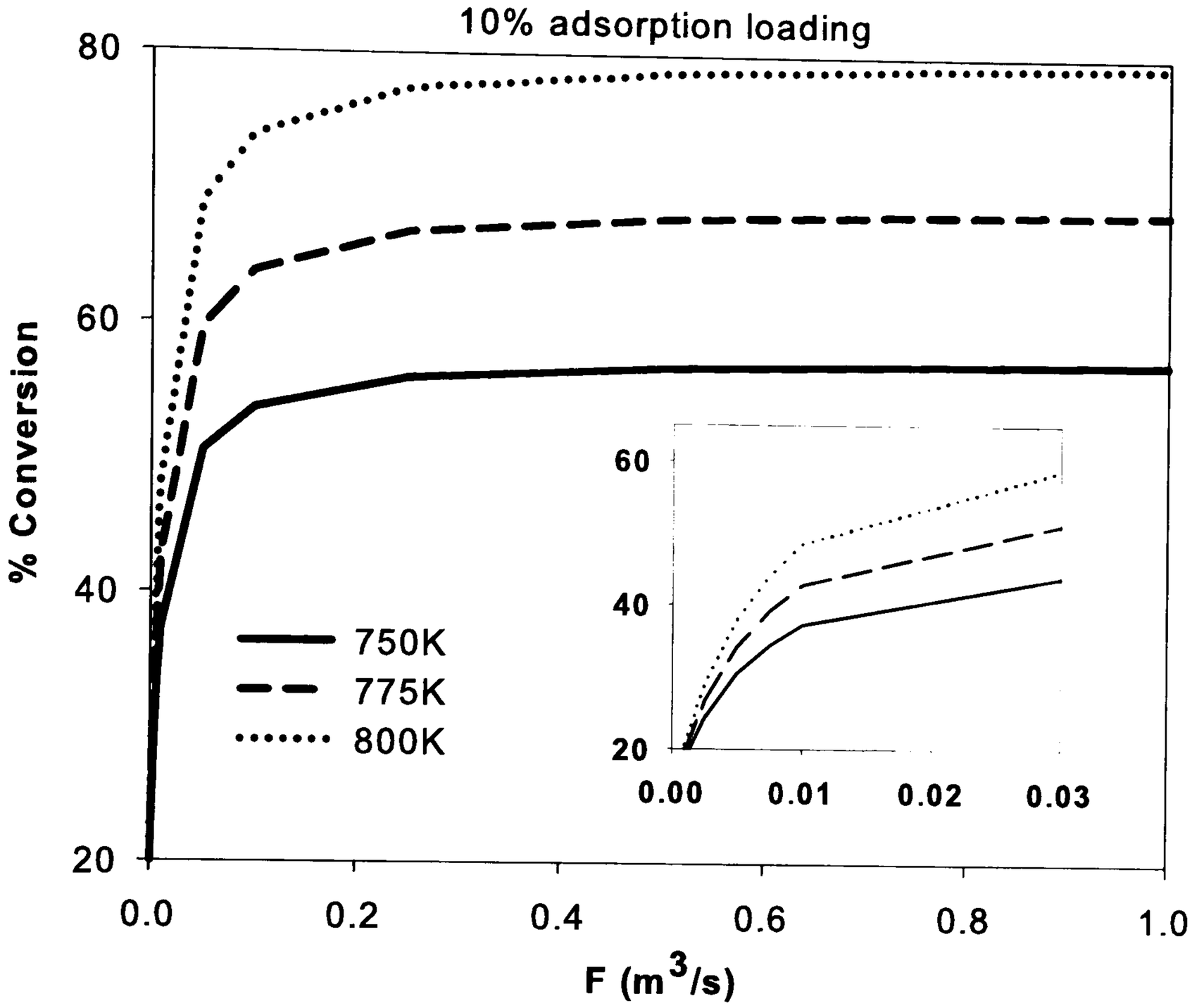



Figure 4.7: $CH_4$ conversion as function of steam flow rate ($F$) at different steam inlet temperatures ($T_{in}$) and 10% adsorbent loading.

steam for regeneration (larger flowrates). Compared with other purge gases (e.g. nitrogen), steam can be easily separated from the purge stream. The amount of purge steam needed for complete desorption per mole of $CO_2$ captured in the reactor must be minimised

Table 4.1: Calculated asymptotic values of methane conversion ($X$), enhancement factor ($E$) and $CO_2$ recovery ($R$) at different values of steam temperature, $T_{in}$.

| | **1% adsorbent loading** | | | **5% adsorbent loading** | | | **10% adsorbent loading** | | |
|---|---|---|---|---|---|---|---|---|---|
| | $X(\%)$ | $E(\%)$ | $R(\%)$ | $X(\%)$ | $E(\%)$ | $R(\%)$ | $X(\%)$ | $E(\%)$ | $R(\%)$ |
| **750K** | 39.2 | 39.0 | 86.7 | 54.1 | 68.6 | 97.2 | 59.1 | 76.2 | 98.2 |
| **775K** | 41.0 | 38.3 | 86.5 | 62.9 | 69.0 | 97.3 | 68.5 | 74.8 | 98.3 |
| **800K** | 42.5 | 31.0 | 86.3 | 72.2 | 67.0 | 97.4 | 79.4 | 70.7 | 98.5 |

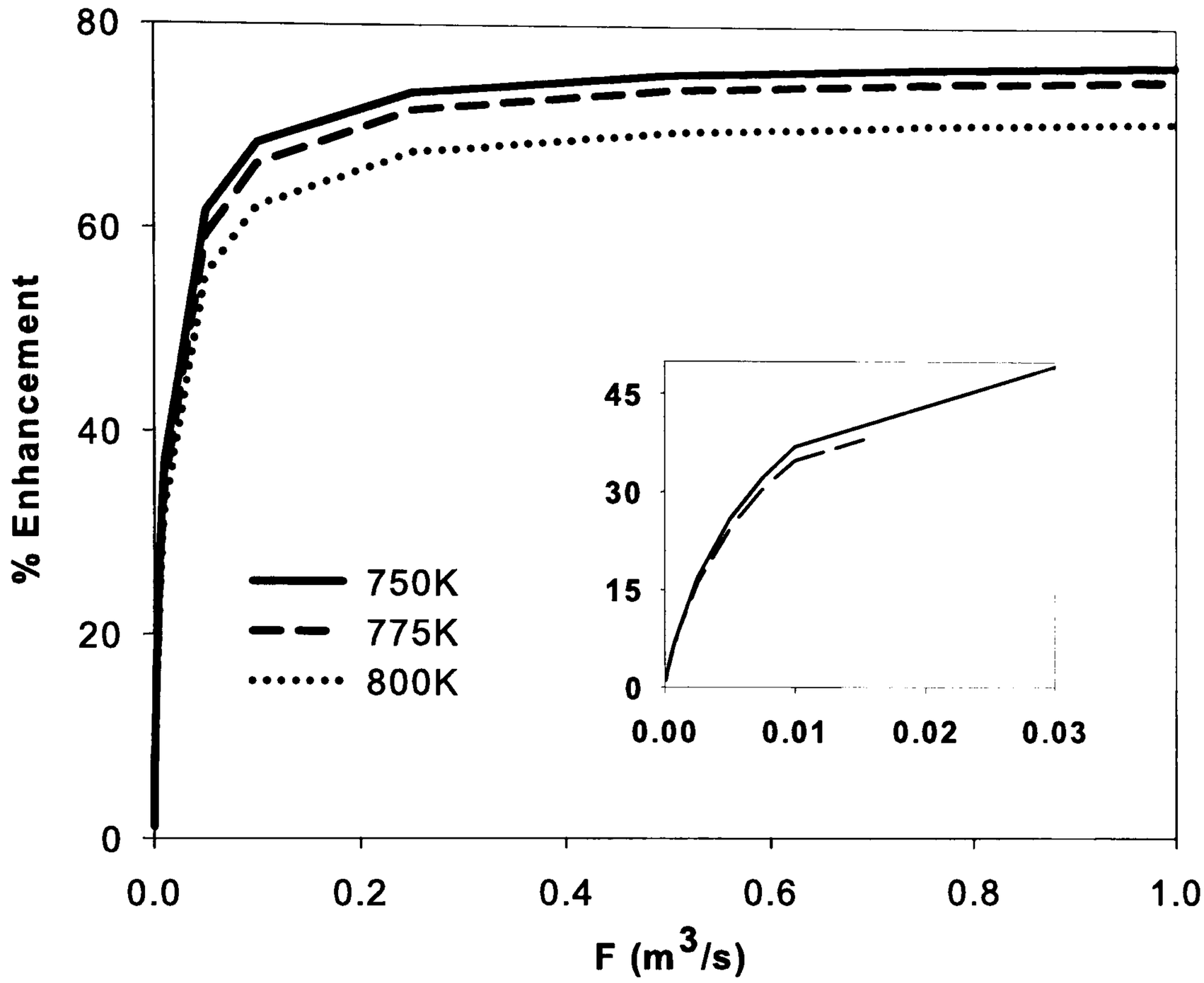



Figure 4.8: Enhancement factor as function of steam flow rate ($F$) at different steam inlet temperatures ($T_{in}$) and 10% adsorbent loading.

in order to obtain an acceptable system efficiency. The configuration of the regeneration unit and its operation mode are of great importance for the viability of the overall process.

It is evident that the reaction and the regeneration stages of the process are closely coupled for this particular study. The mode of desorption and the operation of the desorber are critical for the performance of the adsorptive reactor and vice versa. An issue of great significance at the process level is the energy integration between the reaction and regeneration stages. In the subsequent chapter, process optimisation studies are presented, attempting to address these key issues, although the detailed design of the desorber unit is not included in the optimisation problem, since the design proposed in this work (*i.e.*, well–mixed fluidised bed type of arrangement) is clearly limited. A different set–up, such as a multi–stage fluidised bed configuration or the use of indirect heating, may be more

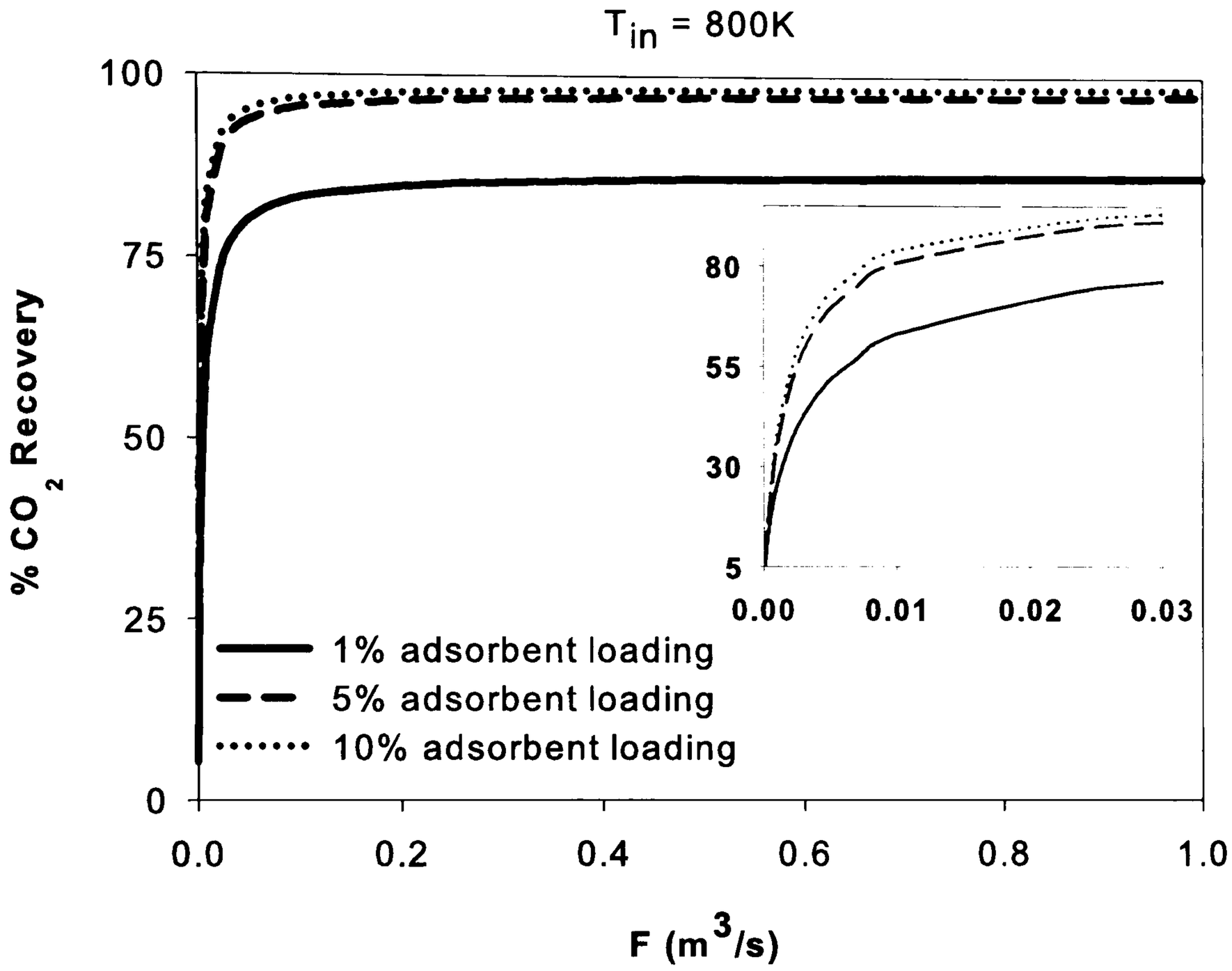



Figure 4.9: $CO_2$ recovery as a function of steam flow rate ($F$) at different adsorbent loadings.

advantageous.

Note that the analysis presented in this work is based on a scenario in which the flowing adsorbent medium is the only means of supplying additional heat for the endothermic SMR process. Alternative process configurations could also be investigated, e.g. the use of structured reactor arrangements in which some channels are used for heat supply purposes, and others for reactant processing or the use of a reaction–only section followed by an adsorptive reactor.

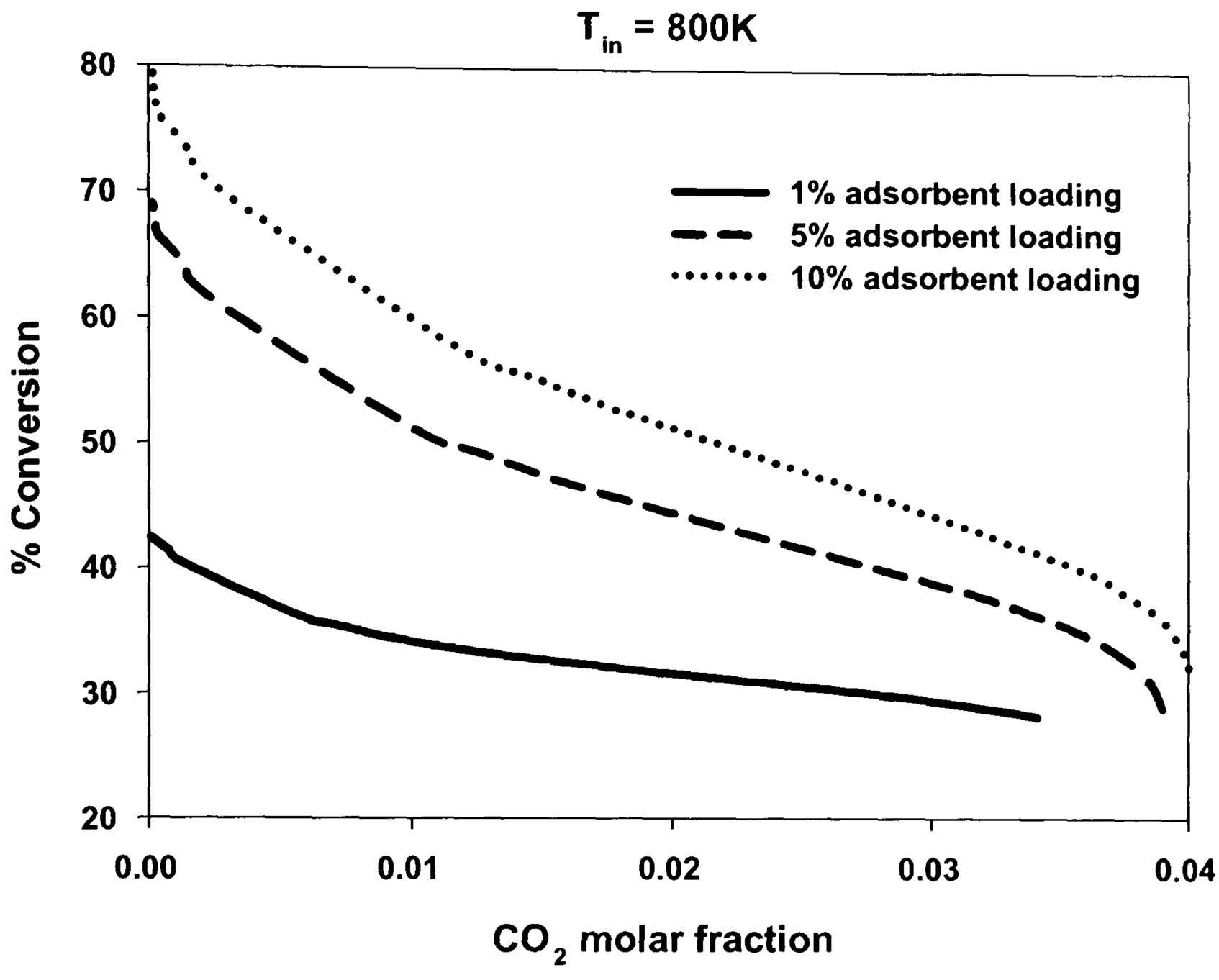



Figure 4.10: $CH_4$ conversion as a function of $CO_2$ molar fraction at different adsorbent loadings.

## 4.2 Effect of adsorbent characteristics

In this section, attention is given to the influence of the $CO_2$ adsorption kinetics and capacity – *i.e.*, the parameters $k_{LDF}$ in Eq. 3.36 and $m_{CO_2}$ in Eq. 3.34, respectively – on the process performance for fixed values of all other operating parameters as given in Table 3.3. The adsorbent temperature at the reactor inlet is set at 750K and the loading at 2 % (v/v) for this specific analysis. It should be noted that the adsorbent loading is defined as the volumetric ratio of the adsorbent in the 2–phase gas–solid mixture ($\varphi = 0.02$).

Based on the kinetics and capacity of $CO_2$ adsorption, adsorbents can broadly fall into four categories, *i.e.*, fast kinetics–high capacity, fast kinetics–low capacity etc. Obviously, adsorbents with high capacity and fast kinetics are considered ideal. On the other hand,

adsorbents with low capacity and slow kinetics are clearly inappropriate. Usually, the available adsorbent materials, suitable for $CO_2$ adsorption at high temperatures, lie in the other two classes, *i.e.*, there is a trade-off between high capacity for $CO_2$ and the adsorption/desorption kinetics. Typical examples of adsorbents having relatively fast kinetics but lower capacity are hydrotalcites (Ding and Alpay, 2000a), whereas lithium zirconate-based adsorbents (Ochoa-Fernández et al., 2005) would generally offer comparably higher capacity, but relatively slow kinetics (due to chemisorption). The objective is, therefore, to carry out a further parametric study of the sorption-enhanced SMR process, focusing on the effect of the two aforementioned adsorbent characteristics on the methane conversion enhancement and the $CO_2$ recovery in order to ascertain which class of available adsorbent materials is more suitable for the process and what the theoretical limits of the sorption-enhanced process are.

### 4.2.1 Effect of adsorbent capacity

The conversion enhancement factor as function of the adsorbent capacity at several values of the LDF coefficient is plotted in Fig. 4.11, and the $CO_2$ recovery for the same parameter values in Fig. 4.12. In all cases, emphasis is given to the performance of the reactor by assuming that fresh adsorbent is fed. Several trends are immediately noticeable: both conversion enhancement and $CO_2$ recovery are strongly non-linear functions of the adsorbent capacity. Higher $CO_2$ capacity favours both conversion and recovery; however, the $CO_2$ recovery as function of adsorbent capacity tends to an asymptotic value relatively soon (around $m_{CO_2} \approx 0.7$ mol kg$^{-1}$ for $k_{LDF} > 0.25$ s$^{-1}$) while the conversion enhancement continues to increase with increasing sorption capacity even beyond the parameter range investigated.

This can be explained by considering the adsorbent-phase concentration of $CO_2$ at the reactor exit in comparison with the one at equilibrium, *i.e.*, $q$ and $q^*$ respectively. As shown in Fig. 4.13, the values of $q$ at the reactor outlet were found to lie quite close to the adsorption isotherm in the cases of fast kinetics. Calculations additionally indicated that they are comparable in these cases. Therefore, the *absolute* amount of $CO_2$ that is

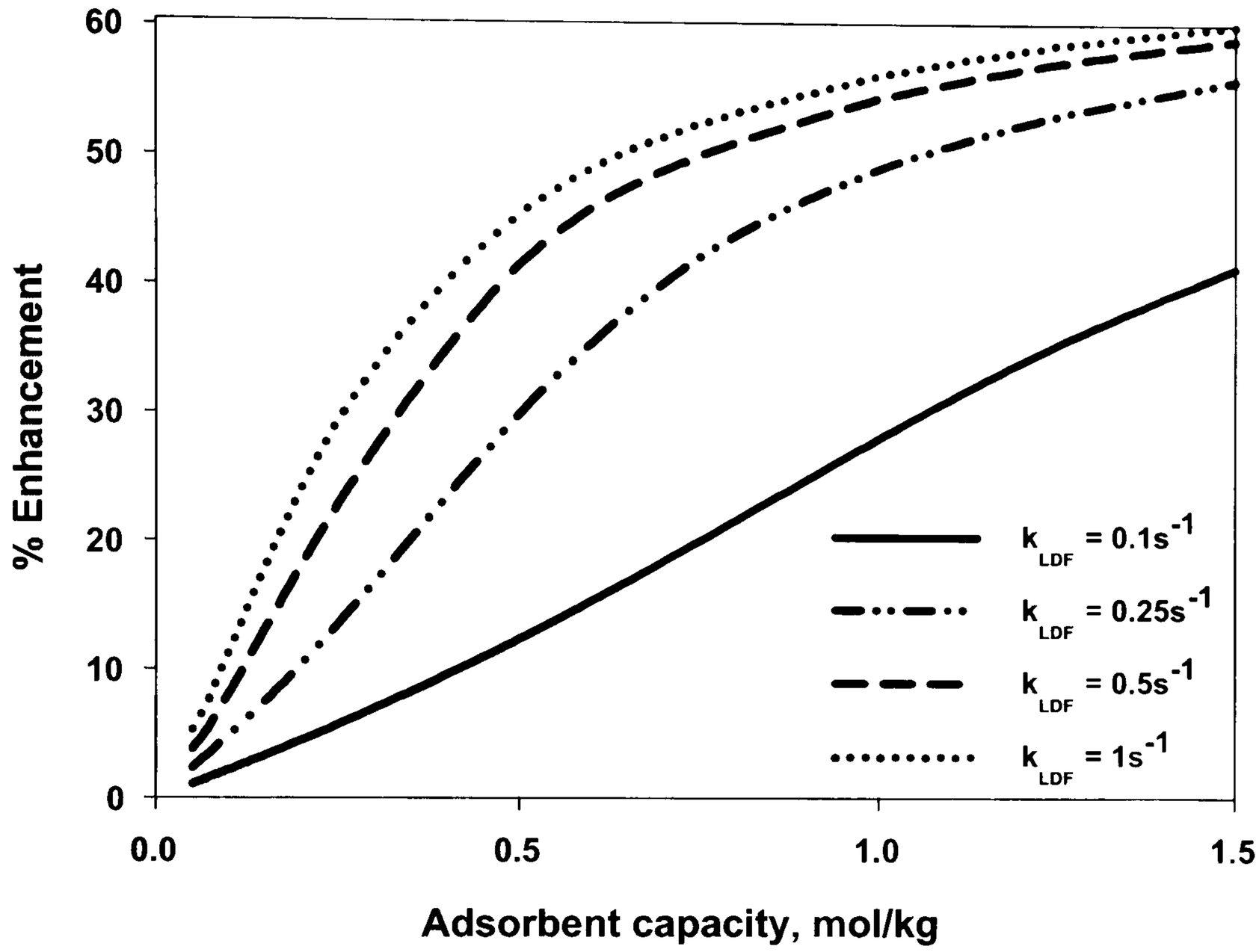



Figure 4.11: Conversion enhancement factor as function of adsorbent capacity $m_{CO_2}$ for several values of the linear driving force coefficient $k_{LDF}$.

removed is similar; however, the higher the capacity, the lower the corresponding $CO_2$ partial pressure, as shown in Fig. 4.13 and hence the higher the conversion.

### 4.2.2 Effect of sorption kinetics

With regard to the sorption kinetics, it can be seen in both Fig. 4.11 and Fig. 4.12 that above approximately $k_{LDF} \approx 0.25$ s$^{-1}$ neither the conversion nor $CO_2$ recovery appear to improve for higher capacities. This trend can be seen even better when conversion enhancement and recovery are plotted as function of $k_{LDF}$ for several values of the sorption capacity, as shown in Fig. 4.14 and Fig. 4.15, respectively. It is evident that both conversion enhancement and $CO_2$ recovery reach a plateau as function of $k_{LDF}$ in all four $m_{CO_2}$ cases, *i.e.*, increasing the sorption kinetics beyond a certain limit does not improve neither

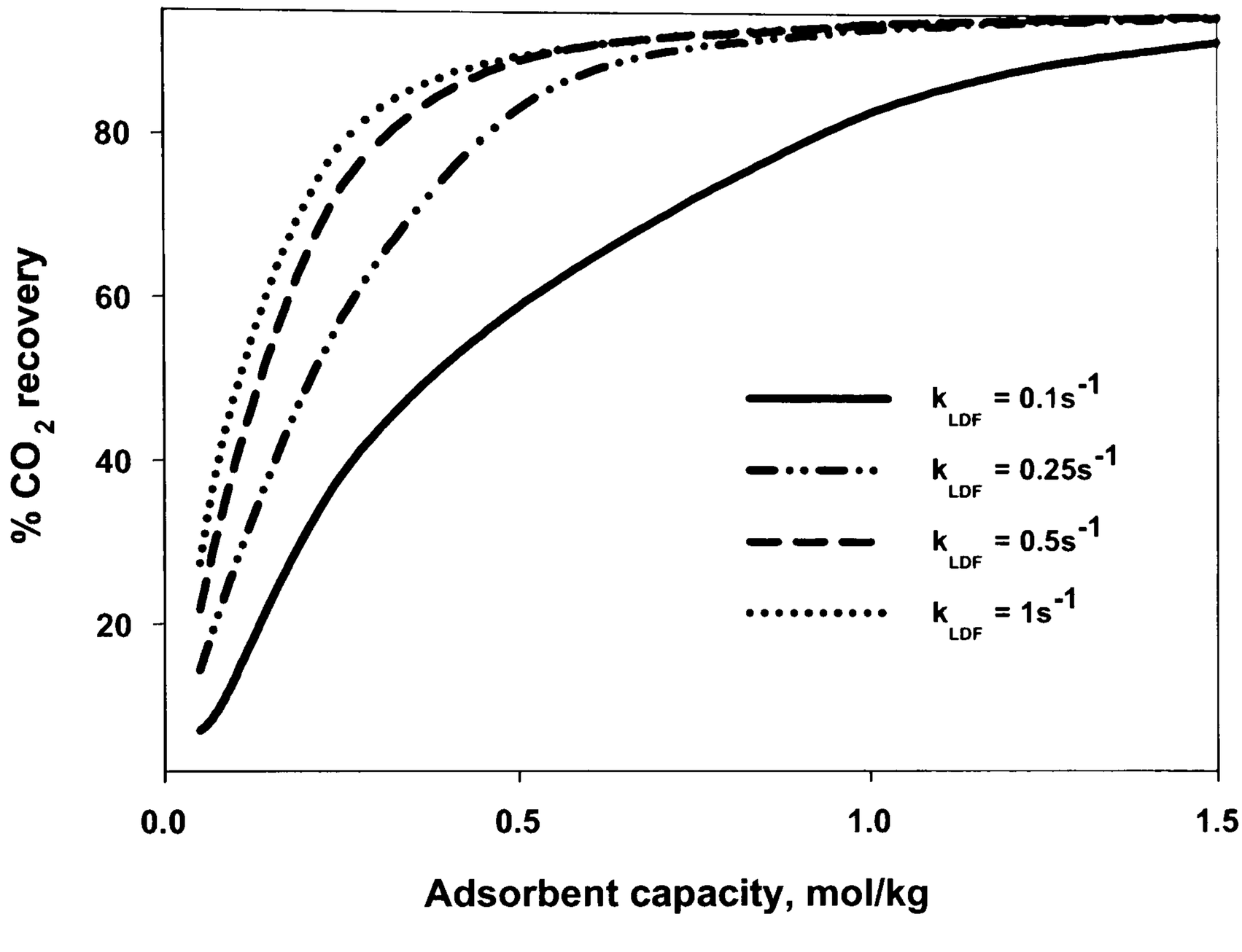



Figure 4.12: $CO_2$ recovery as function of adsorbent capacity $m_{CO_2}$ for several values of the linear driving force coefficient $k_{LDF}$.

conversion nor $CO_2$ recovery. This behaviour can be understood by considering the time-scales of $CO_2$ production by the reaction and $CO_2$ sequestration by adsorption. In order to achieve the desired effect in a sorption-enhanced reaction process, it is important to match the rates of $CO_2$ production and $CO_2$ sequestration; however, increasing the $CO_2$ sequestration kinetics beyond the rate of $CO_2$ production does not bring any additional benefits, as is seen in Figs. 4.14–4.15. When the adsorbent regeneration step is also considered, however, faster adsorption/desorption kinetics is still an advantage because it allows a shorter residence time in the desorber.

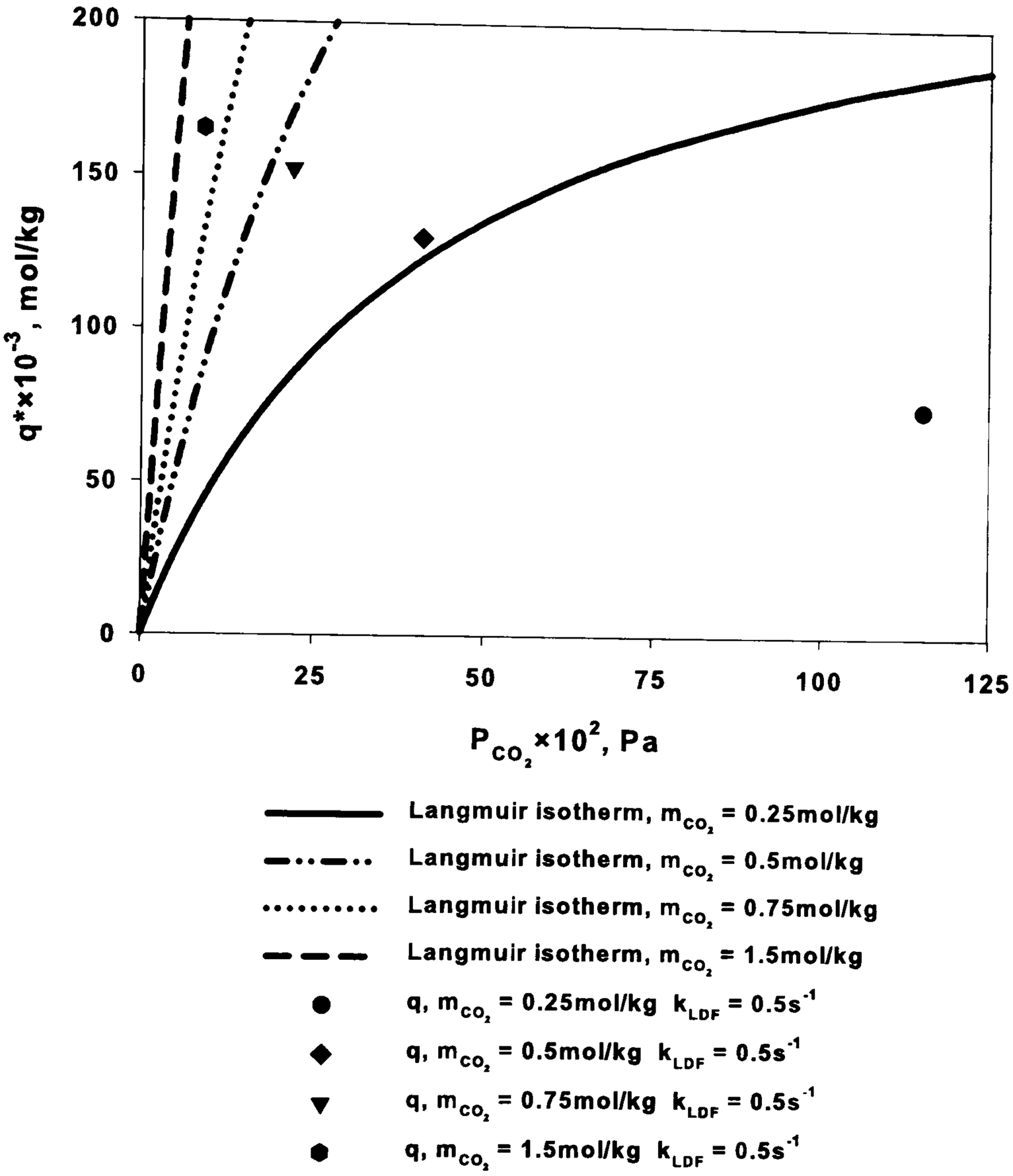



Figure 4.13: Langmuir isotherms and corresponding values of $q$ at the reactor exit.

### 4.2.3 Effect of regeneration conditions

Let us now consider the full process as shown in Fig. 3.1, *i.e.*, including adsorbent regeneration. It is important to understand that if the adsorbent regeneration in the desorber is not complete in a single pass – which would always be the case in reality unless the residence time is extremely large – $CO_2$ can accumulate on the adsorbent particles so that at steady state not the entire sorption capacity is utilised but the amount adsorbed cycles between two points on the adsorption isotherm that may be close to each other despite

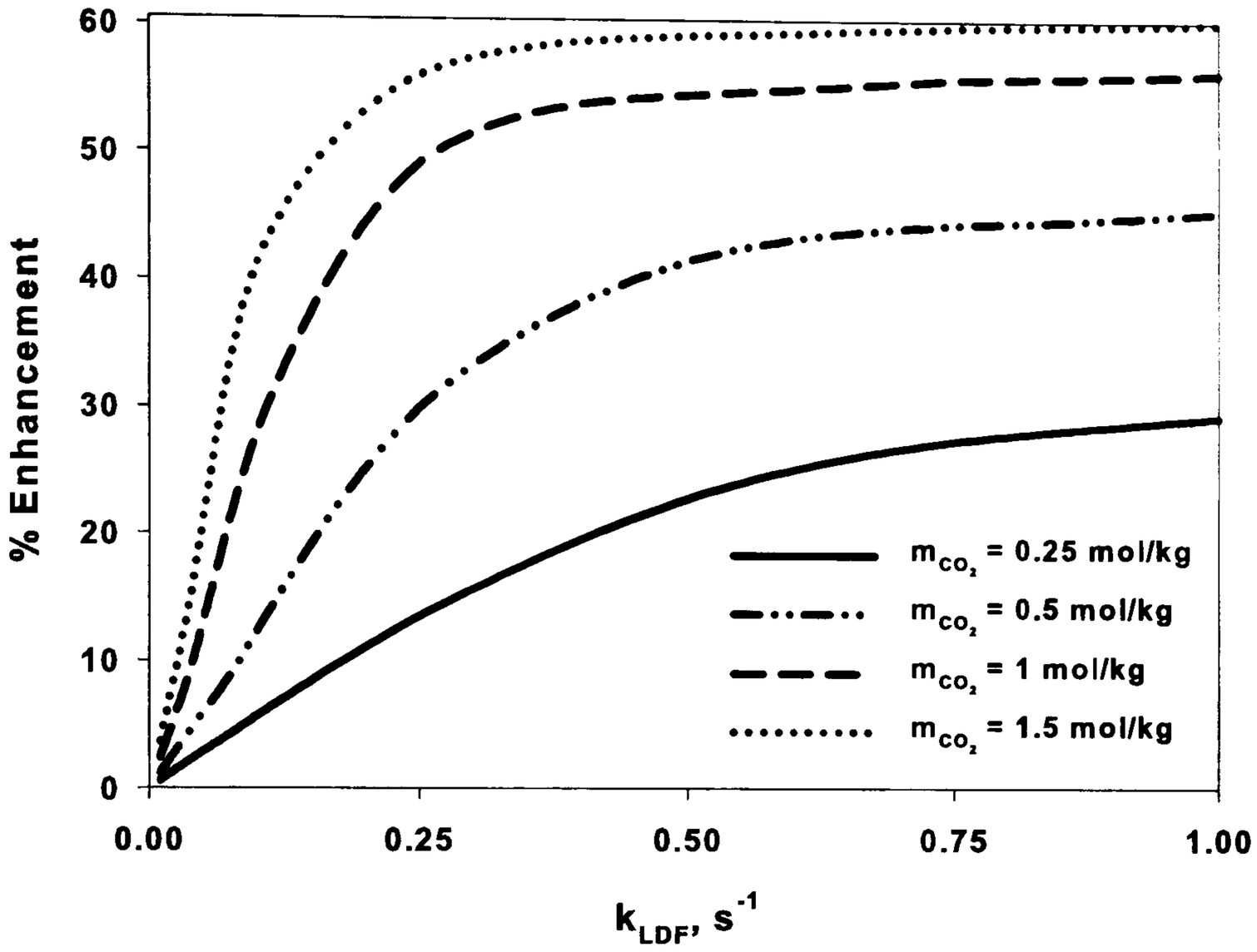



Figure 4.14: Conversion enhancement factor as function of linear driving force coefficient $k_{LDF}$ for several values of adsorbent capacity $m_{CO_2}$.

high overall $CO_2$ adsorption capacity.

The conversion enhancement and $CO_2$ recovery as function of the purge stream flowrate in the desorber are plotted in Fig. 4.16 and Fig. 4.17, respectively, for a combination of two values of adsorbent capacity and kinetics chosen in order to cover the four limiting cases, previously discussed. It is worth noting that, while adsorbent with higher capacity is always superior in terms of conversion enhancement when fresh adsorbent is fed into the reactor (Fig. 4.11), when regeneration is considered as well, comparable performance is obtained for both high capacity–slower kinetics, and lower capacity–fast kinetics combinations. The reason is that in a steady–state operation with adsorbent recycle and regeneration, high adsorbent capacity on its own is not a sufficient condition for high conversion as it is the case when fresh adsorbent is fed. Here, high adsorbent capacity must be accompanied by fast adsorption/desorption kinetics in order to fully realise its

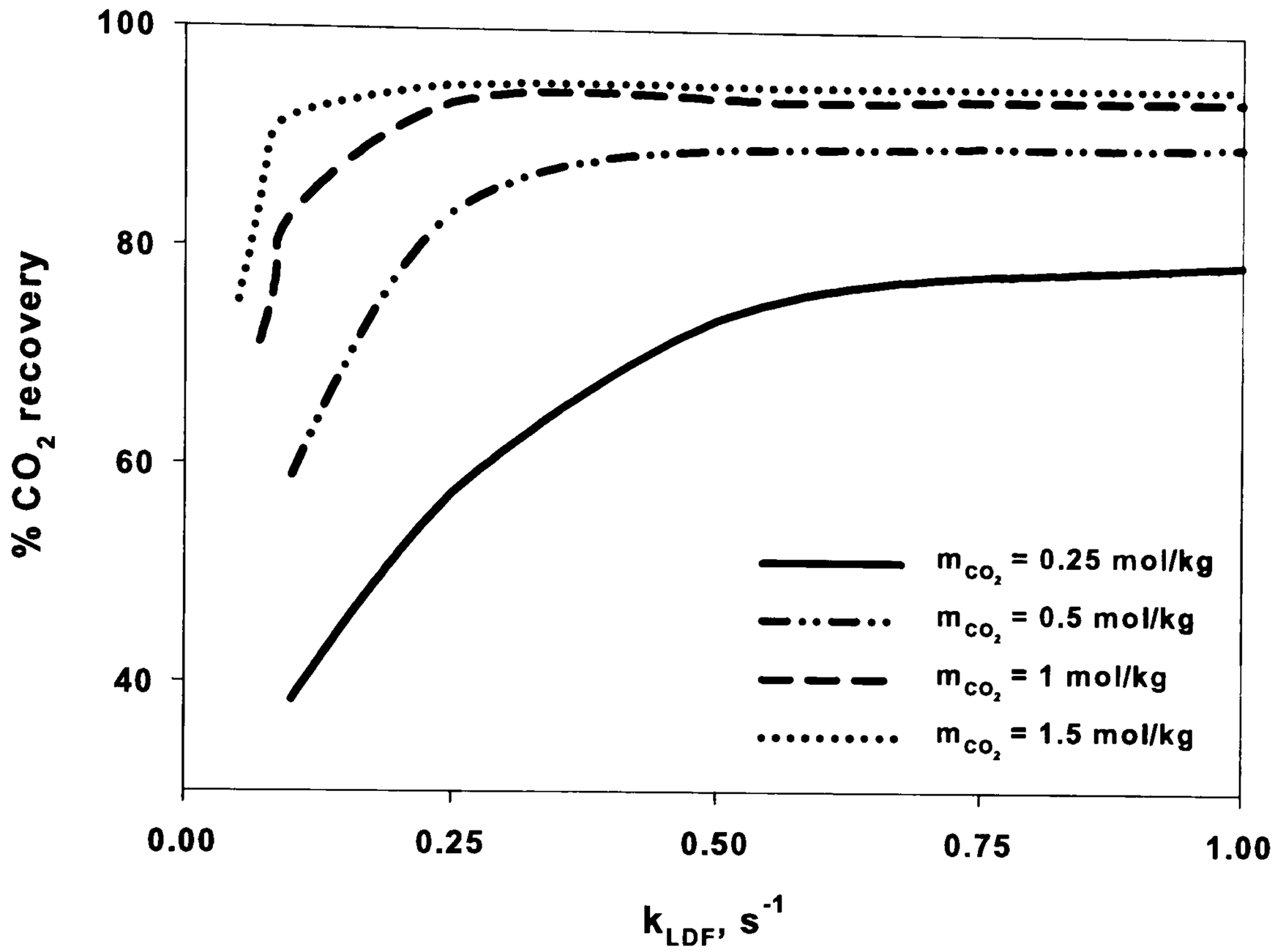



Figure 4.15: $CO_2$ recovery as function of linear driving force coefficient $k_{LDF}$ for several values of adsorbent capacity $m_{CO_2}$.

potential, *i.e.*, desorb the $CO_2$ accumulated on the adsorbent particle in the reactor. This is exemplified by the significantly higher conversion as well as $CO_2$ recovery values achievable for the ideal combination of high capacity ($m_{CO_2} = 1.5$ mol kg$^{-1}$) and fast kinetics ($k_{LDF} = 0.75$ s$^{-1}$). The reason for the high conversion enhancement achieved in this case is that the high adsorbent capacity is indeed fully utilised, thanks to the fast kinetics (nearly complete regeneration).

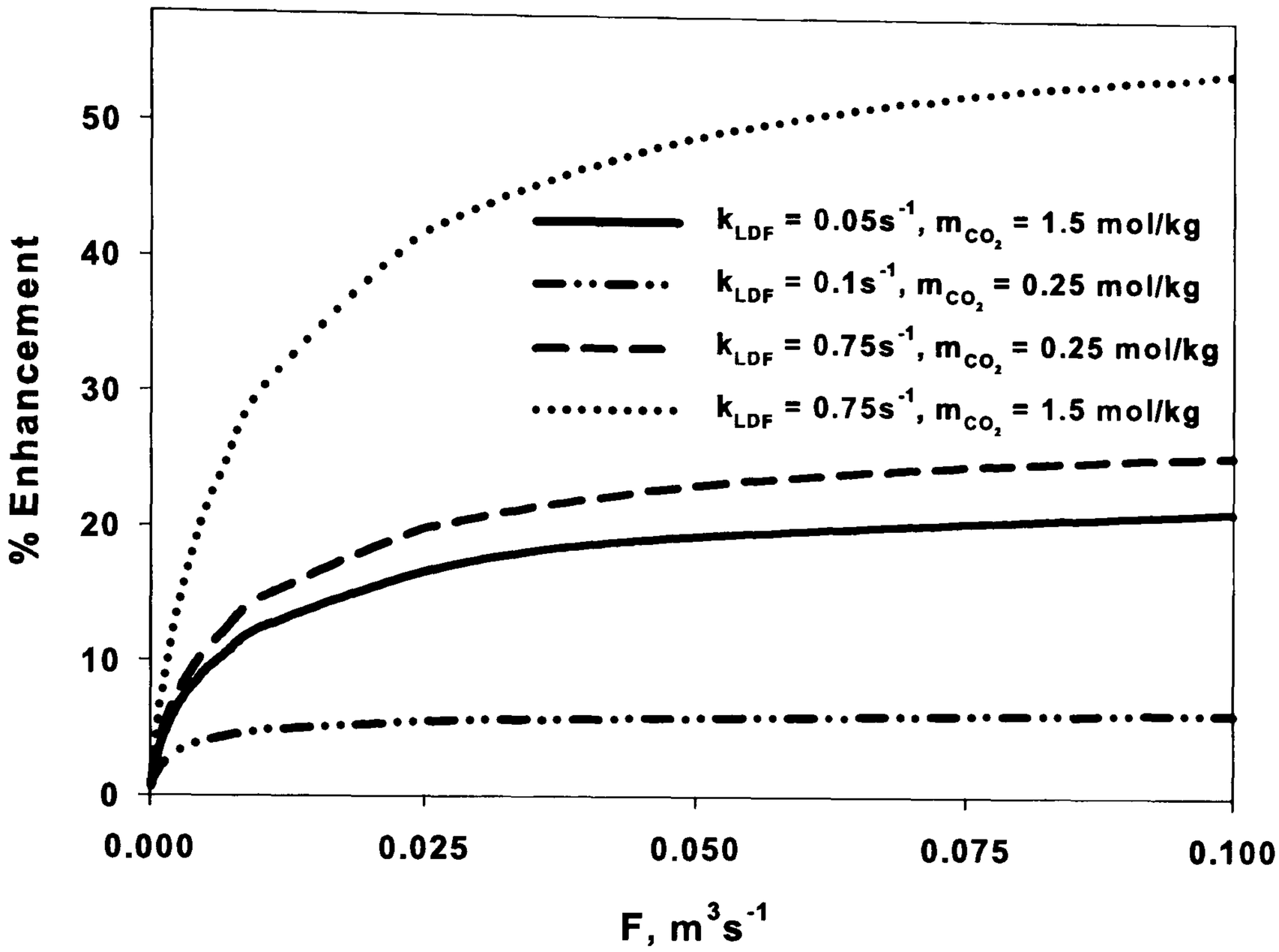



Figure 4.16: Conversion enhancement factor as function of the purge steam flowrate in the desorber.

## 4.3 Concluding remarks

The results presented in this chapter reveal interesting features of the proposed continuous SE–SMR process. The key findings can be summarised, as follows:

1. The feasibility of the proposed reactor concept is demonstrated by predicting a definite degree of $CH_4$ conversion enhancement (up to 75% compared to the conventional operation under same conditions) at moderate temperatures (750K).

2. Important design and operating parameters are identified, namely the adsorbent loading and temperature, denoting the two–fold contribution of the adsorbent, *i.e.*, separation as well as extra heat for the endothermic reaction. This gives rise to an interesting optimisation problem comprising the reaction versus separation trade off.

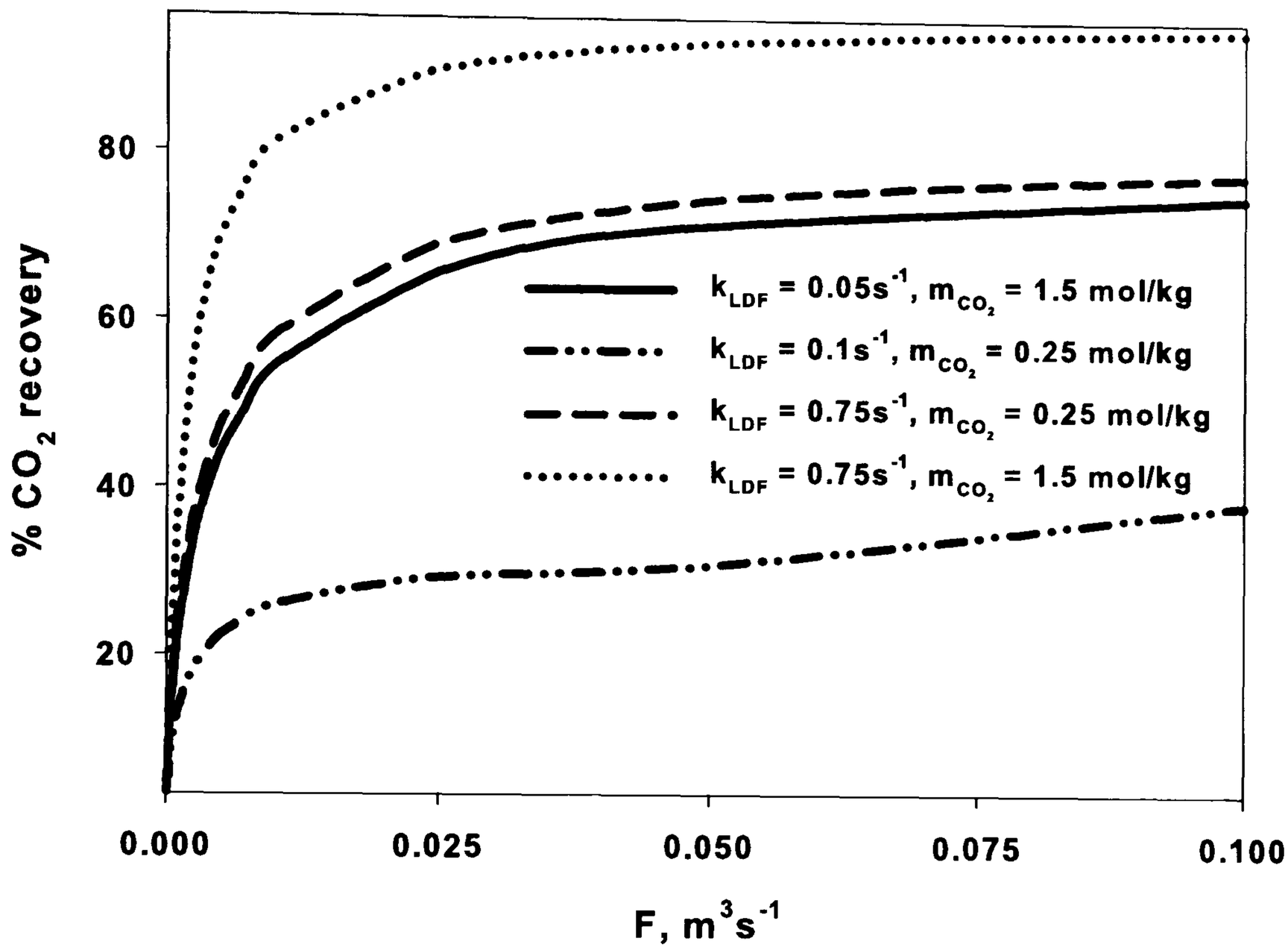



Figure 4.17: $CO_2$ recovery as function of the purge steam flowrate in the desorber.

3. The interaction between the reaction and regeneration stages of the process is of great significance. The scope and directions for further process improvement are underlined and alternative process configurations are discussed (see Chapter 6).

4. Adsorbent characteristics are critical for process design. High–capacity adsorbents with fast adsorption/desorption kinetics (e.g. $m_{CO_2} = 1.5$ mol $kg^{-1}$, $k_{LDF} = 0.75$ $s^{-1}$) could extensively exploit the potential of the proposed process.

More specifically, ~70% and ~80% methane conversions were calculated for 5% and 10% adsorbent loading, respectively, at 800K. Although these results depict a ~70% conversion enhancement, they come at the expense of low molar fraction of the recovered $CO_2$, which is ~97–98% of the total amount produced. The parametric studies form a platform upon which the process optimisation is carried out, as presented in the following chapter of this thesis.

# Chapter 5

# Optimisation studies

As shown in Chapter 4, the performance of the proposed sorption–enhanced reaction process is affected by a number of highly interacting design and operating parameters. In this chapter, a formal model–based optimisation approach is developed to determine an optimally configured and operated adsorptive reactor. The hybrid nature of the process necessitates the special consideration of various performance criteria that reflect the synergetic effect of combined reaction and adsorption, e.g. methane conversion and $H_2$ product purity. The energy requirement of the process is also touched upon by means of the reactor efficiency.

Based on the model presented in chapter 3, optimisation is performed using gOPT, the optimisation tool of gPROMS (Process Systems Enterprise Ltd.). This optimiser converts the optimisation problem to a non–linear programming (NLP) problem using a control vector parametrisation (CVP) technique with a successive quadratic programming (SQP) algorithm, as implemented in the SRQPD code. The solution tolerance for the optimisation is 0.001. In other words, convergence is deemed to occur when a linear combination of the gradients of the Lagrangian function on one hand, and the violation of the constraints on the other, drops below this tolerance. Scaling is applied to the optimisation decision variables according to the ranges of their values. As a result, the scaled variables vary between -1 and 1.

Since the underlying mathematical model is a steady–state one, a so–called "**point**" optimisation is performed. From a mathematical point of view, this is equivalent to solving a purely algebraic problem in which a generally nonlinear objective function is maximised or minimised subject to generally nonlinear constraints by manipulating a set of optimisation decision variables that may be either continuous or discrete. For the non–convex problem described in this work, optimality is dependent on the starting point (*i.e.*, initial guess) and global optimality cannot be guaranteed.

## 5.1 Optimisation problem formulation

The optimisation approach seeks to determine the optimal values of important design and operating parameters as identified by the parametric studies presented in chapter 4. Ideally, all the process performance measures (see chapter 3) should be simultaneously treated as the objectives of the optimisation problem. To tackle this limitation, a single performance objective is optimised whereas some of the remaining performance criteria are treated as constrained variables.

The general form of the mathematical non–linear programming problem considered in this work is as follows:

$$\underline{Maximise} \quad \textbf{Performance objective} \tag{5.1}$$

(5.2)

$$\underline{subject\ to}$$

**Decision variables :**

$$\Omega^{lower} \leq \Omega^{initial} \leq \Omega^{upper} \tag{5.3}$$

**Performance measures :**

$$\Pi \geq \text{set point} \tag{5.4}$$

The process performance indices incorporated in the optimisation problem are:

- The hydrogen yield, $Y_{H_2}$
- The methane conversion, $X(\%)$
- The carbon dioxide recovery, $R(\%)$
- The hydrogen product purity, $H_2(\%)$
- The reactor efficiency, $\Upsilon(\%)$

The choice of their set points is based on literature data (Xiu et al., 2002a; Johnsen et al., 2006b; Ryden, 2006), depicting a "high–standard" process performance.

The set of optimisation decision variables include the following model parameters:

- The reactor length, $L$
- The temperature of the gas at the reactor inlet, $T_f$
- The superficial gas velocity, $u_g$
- The voidage of the reactor, $\varepsilon$
- The temperature difference $T_{ads} - T_f$ at the reactor inlet, $\vartheta$
- The adsorbent loading, $\varphi$

The lower and upper values of the aforementioned model parameters are given below:

$$0.1 \text{ m} \leq L \leq 1 \text{ m} \tag{5.5}$$

$$700 \text{ K} \leq T_f \leq 823 \text{ K} \tag{5.6}$$

$$0.5 \text{ m s}^{-1} \leq u_g \leq 2 \text{ m s}^{-1} \tag{5.7}$$

$$0.2 \leq \varepsilon \leq 0.75 \tag{5.8}$$

$$0 \text{ K} \leq \vartheta \leq 300 \text{ K} \tag{5.9}$$

$$0.01 \leq \varphi \leq 0.1 \tag{5.10}$$

As previously mentioned, the optimisation procedure cannot in principle guarantee the global optimal solution, since the optimal results may be affected by the initial guesses and bounds of the constrained parameters. With this in mind, a systematic approach was adopted to direct the optimisation towards improved process performance in comparison with the "base case" presented in the previous chapter. Firstly, the objective was to maximise the hydrogen yield, $Y_{H_2}$, while maintaining a "high–standard" performance in terms of the other four indices. The optimisation was performed repeatedly with various distinct sets of initial guesses. The best solution obtained was considered (assumed) the global optimum. The corresponding values of the decision variables were then used as initial guesses for the other optimisation problems. However, even in these cases several optimisation tests were performed resulting in insignificant discrepancies. Again the best solution was assumed the global optimum. The optimisation results presented below can reduce experimental effort by providing useful insights into the key factors affecting the optimal process performance.

## 5.2 Optimisation results

The results of the optimisation scenarios that were considered are given below. Table 5.1 summarises the optimal values of the decision variables for all the cases under investigation.

### Maximise hydrogen yield

The optimisation problem is described by the formulation below:

$$\max \quad Y_{H_2} \quad s.t. \quad X,\ R,\ H_2,\ \geq 95\% \ ,\ 70\% \leq \Upsilon \leq 85\%$$

The optimal value of the hydrogen yield is 4 moles $H_2$ per mole $CH_4$ fed. The optimal

results for the constrained performance indices are:

$$X = 99.5\%$$

$$R = 98.8\%$$

$$H_2 = 99.5\%$$

$$\Upsilon = 79.9\%$$

Regarding the statistics of the SRQPD optimiser, the total computational time for the optimisation was 10 s on a Pentium IV machine with dual 1 GHz CPU. The number of the NLP iterations and the line search steps were both 14.

**Maximise conversion**

The problem formulation is the following:

$$\max \quad X \quad s.t. \quad R,\ H_2,\ \geq 95\% \ ,\ 70\% \leq \Upsilon \leq 85\%$$

The maximum methane conversion is equal to 99.8%. As for the other performance measures, their optimal results are given below:

$$R = 98.0\%$$

$$H_2 = 99.4\%$$

$$\Upsilon = 79.7\%$$

The total CPU time was 35 s. 14 NLP iterations and 20 line search steps needed for the optimisation.

**Maximise $CO_2$ recovery**

The optimisation problem is formulated as follows:

$$\max \quad \%R \quad s.t. \quad X,\ H_2,\ \geq 95\% \ ,\ 70\% \leq \Upsilon \leq 85\%$$

The optimal value of $CO_2$ recovery was found equal to 99.5%. The other optimal indices were calculated as follows:

$$X = 97.1\%$$

$$H_2 = 98.9\%$$

$$\Upsilon = 79.5\%$$

As for the statistics of the optimiser, the total CPU time was 5 s. the number of the optimisation iterations was equal to 13, and the number of NLP line search steps 14.

**Maximise hydrogen purity**

The optimisation formulation is:

$$\max \quad H_2 \quad s.t. \quad X,\ R,\ \geq 95\%\ ,\ 70\% \leq \Upsilon \leq 85\%$$

The results showed that the maximum obtainable product purity is 99.7%. The corresponding optimal values of the constrained variables are:

$$X = 98.9\%$$

$$R = 99.3\%$$

$$\Upsilon = 79.8\%$$

The total CPU time for the optimisation was 23 s, the number of iterations and line search step 22 and 62, respectively.

**Maximise reactor efficiency**

The problem formulation is presented below:

$$\max \quad \Upsilon \quad s.t. \quad X,\ R,\ H_2 \geq 95\%$$

The optimal reactor efficiency was estimated equal to 84.8%. In this case, the constrained

performance measure are:

$$X = 99.0\%$$

$$R = 99.0\%$$

$$H_2 = 99.5\%$$

The total CPU time for the optimisation was 8 s. The number of iterations was equal to 31 and the number of line search steps 42.

Table 5.1: Summary of optimisation results

| Optimisation scenarios | | | | | |
|---|---|---|---|---|---|
| Maximise: | $Y_{H_2}$ | X (%) | R (%) | $H_2$ (%) | $\Upsilon$ (%) |
| Optimal decision variables | | | | | |
| L (m) | 0.73 | 0.7 | 0.81 | 0.72 | 0.96 |
| $T_f$ (K) | 832 | 808 | 797 | 800 | 794 |
| $u_g$ (m $s^{-1}$) | 0.83 | 0.51 | 0.5 | 0.69 | 0.91 |
| $\varepsilon$ | 0.27 | 0.37 | 0.64 | 0.44 | 0.31 |
| $\vartheta$ (K) | 106 | 161 | 76 | 100 | 108 |
| $\varphi$ | 0.06 | 0.03 | 0.1 | 0.09 | 0.06 |
| Performance indices | | | | | |
| $Y_{H_2}$ | **4** | 3.99 | 3.88 | 3.97 | 3.97 |
| X (%) | 99.5 | **99.8** | 97.1 | 98.9 | 99 |
| R (%) | 98.8 | 98 | **99.5** | 99.3 | 99 |
| $H_2$ (%) | 99.5 | 99.4 | 98.9 | **99.7** | 99.5 |
| $\Upsilon$ (%) | 79.9 | 79.7 | 79.5 | 79.8 | **84.8** |

In all the optimisation scenarios under investigation, the process performance is characterised by the production of high purity hydrogen and acceptable reactor efficiency. However, it should be emphasised that simulation results, using the optimal values of the decision variables from Table 5.1, indicated that the enhancement effect ($E$) is "minimised" in all cases. The calculations revealed conversion enhancement factors ($E$) ranging

between 3% and 19%, as presented in Table 5.2. These results follow the predicted trend shown in Fig. 4.2. This finding clearly shows that the optimal results presented above are obtained at the expense of the reaction enhancement due to $CO_2$ capture, albeit the high separation capacity ($R$) predicted.

Table 5.2: Calculated values of E (%) for each optimisation scenario.

| | Optimisation scenarios | | | | |
|---|---|---|---|---|---|
| Maximise: | $Y_{H_2}$ | X (%) | R (%) | $H_2$ (%) | $\Upsilon$ (%) |
| E(%) | 3.0 | 3.1 | 18.7 | 9.7 | 10.0 |

Therefore, further work is needed towards the exploration of the process trade-offs. For example, appropriate tools may be employed to perform multi–objective optimisation that will generate a set of non–dominating solutions rather than a unique solution. This so called Pareto set of optimal solutions has the property that when one moves from anyone point to another on the set, one objective function improves but the other worsens. Hence, neither solution "dominates" over the other and additional information is needed to choose between them (Rajesh et al., 2000).

## 5.3 Sensitivity analysis

The accuracy of the optimisation results presented above is obviously subject to the same assumptions as the underlying mathematical model. The sensitivity analysis performed sought to examine the validity of the following main assumptions:

- equal gas and adsorbent particle velocities ($u_g^{int} = u_{ads}^{int}$)
- heat transfer coefficient between the gas phase and the adsorbent particle, $k_{h,ads}$ equal to $k_h$

Furthermore, as discussed in Chapter 3, the calculation of mass and heat transfer coefficients, $k_m$ and $k_h$, respectively, is a source of uncertainty, as is the value of the thermal

conductivity, $\lambda$. Simulations were therefore carried out to evaluate the sensitivity of the process performance to variation in the aforementioned model parameters.

More specifically, the model was simulated using the optimal values of the decision variables presented in the last column of Table 5.1, which represent the scenario of maximising the reactor efficiency, $\Upsilon$. The values of the adsorbent particle velocity ($u_{ads}^{int}$), the gas–adsorbent heat transfer coefficient ($k_{h,ads}$), the mass ($k_m$) and heat ($k_h$) transfer coefficients, and the thermal conductivity ($\lambda$) were varied as shown in Table 5.3, as part of a local, one–at–a–time sensitivity analysis.

Table 5.3: Sensitivity analysis results

| | Performance indices | | | | |
|---|---|---|---|---|---|
| | X(%) | E(%) | R(%) | $H_2$(%) | $\Upsilon$(%) |
| $u_{ads}^{int} = 0.9u_g^{int}$ | 98.89 | 10.51 | 98.89 | 99.39 | 84.61 |
| $u_{ads}^{int} = 0.8u_g^{int}$ | 98.70 | 11.12 | 98.73 | 99.30 | 84.43 |
| $u_{ads}^{int} = 0.7u_g^{int}$ | 98.44 | 11.90 | 98.50 | 99.17 | 84.15 |
| $k_{h,ads} = 2k_h$ | 99.08 | 10.04 | 99.03 | 99.48 | 84.86 |
| $k_{h,ads} = 0.5k_h$ | 98.91 | 10.03 | 98.99 | 99.42 | 84.54 |
| $k_m + 10\%$ | 99.04 | 10.06 | 99.02 | 99.47 | 84.77 |
| $k_m - 10\%$ | 99.00 | 10.02 | 99.01 | 99.45 | 84.73 |
| $k_h + 10\%$ | 99.07 | 10.07 | 99.03 | 99.48 | 84.78 |
| $k_h - 10\%$ | 98.97 | 10.02 | 99.01 | 99.44 | 84.71 |
| $\lambda + 20\%$ | 99.03 | 10.05 | 99.02 | 99.47 | 84.77 |
| $\lambda - 20\%$ | 99.02 | 10.04 | 99.01 | 99.46 | 84.74 |

The results summarised in Table 5.3 indicate that no significant discrepancies in the performance indices arise due to the variations introduced. Only when some slip velocity is considered, does the enhancement factor, $E$, increase by up to 19%. Nevertheless, the overall process performance seems to be unaffected in all cases under investigation. A more rigorous sensitivity analysis method – global sensitivity analysis – can however be employed to quantify the effect of parameter interactions on the system behaviour. This

would take into account the possibility of more than one sources of variation acting on the system simultaneously. It should be noted that the aforementioned findings may be due to the present mathematical formulation of the process model. As a result, further model development involving a more detailed description of the underlying phenomena is necessary in order to compare the two different modelling approaches. Thence, safer conclusions on the sensitivity of the process performance can be drawn (see §6.3).

## 5.4 Concluding remarks

The results of the process optimisation have been presented in this chapter. Based on a detailed mathematical model, a non–linear optimisation approach was employed (i.e. gOPT) to identify promising design options and operating alternatives for a number of different performance objectives. The findings indicated that high methane conversions can be achieved resulting in the production of high–purity hydrogen, whilst the maximum efficiency of the monolithic adsorptive reactor was found equal to 84.8%. A local sensitivity analysis on five model parameters revealed no significant alterations in the optimal overall performance of the process. Optimisation studies should be extended to a detailed investigation of the process operating trade–offs by means of multi–objective optimisation techniques. Overall, the optimisation results presented here can guide experimental work towards an optimally configured and operated adsorptive reactor system.

# Chapter 6

# Concluding remarks and future directions

## 6.1 Summary of results

A novel concept for non–periodic adsorption–enhanced SMR has been presented in this thesis. Mathematical models were developed, comprising differential mass and energy balances in the monolithic reactor and the adsorbent regeneration unit. The reactor model was spatially 1–D, pseudo–homogeneous, *i.e.*, explicitly accounting for the catalyst, gaseous, and adsorbent phase. A well–mixed fluidised–bed type of model was adopted for the desorber.

Parametric studies were carried out, initially focusing on two areas: the identification of important operating parameters of the adsorptive reactor and the fundamental analysis of the overall process performance. The feasibility of this novel concept was demonstrated by showing a significant degree of conversion enhancement (up to 75%) at moderate temperatures (750K). The associated key features of this process were highlighted, *i.e.*, adsorbent loading and reactor inlet temperature. The adsorbent loading determines the separation capacity available in the reactor. The adsorbent inlet temperature is a means of providing the heat for the endothermic reaction. This gives rise to an optimisation problem, which is based on the underlying trade-off between the two objectives of reaction and separa-

tion. The interaction between the reaction and the regeneration stages of the process is a significant characteristic of the process. The operation of the regeneration unit is linked with the performance of the adsorptive reactor.

It should also be noted that this analysis was based on a scenario in which the only means of providing heat for the endothermic SMR process is the flowing adsorbent medium. Alternative process schemes and designs may also be examined and compared. For example, the use of pre–reactor in order to approach equilibrium conversion before adsorption enhanced reaction or the use of monolith channel arrangements in which some channels are used for reactant processing and others for heat supply purposes.

The effect of adsorbent properties – the $CO_2$ sorption capacity and adsorption/desorption kinetics – on the performance of the process was additionally investigated. The main conclusions of the parametric studies can be summarised as follows: when a fully regenerated adsorbent is fed to the adsorptive reactor, higher $CO_2$ sorption capacity always leads to higher methane conversion; increasing the sorption kinetics however, only improves conversion (as well as $CO_2$ recovery) up to a point where the rate of $CO_2$ adsorption in the reactor matches that of its production by reaction.

However, when the full cycle of sorption–enhanced reaction followed by desorption and recycle of the adsorbent particles was considered, the adsorption/desorption kinetics played a more important role as it determines to what extent the $CO_2$ capacity of the adsorbent will be utilised. In the case of slow sorption kinetics, $CO_2$ will accumulate on the adsorbent due to incomplete regeneration, which was the case in this parametric study, and only a smaller proportion of the full capacity will be utilised. The results of the study presented in this work highlight the need for adsorbent particle engineering rather than just synthesis of novel materials with large capacity regardless of kinetics, and show that the sorption enhanced steam methane reforming process still has a significant potential for improvement if adsorbents merging both high capacity and fast kinetics are developed.

Model–based optimisation was performed, revealing the optimal values of key design and

operating parameters (see Table 5.1). Without incorporating the detailed design of the regeneration unit, optimisation studies underlined the process feasibility in terms of the reactor efficiency (~85%). Further work is necessary though towards the determination of the optimal process configuration by fully capturing the associated design and operating trade–offs.

## 6.2 Main conclusions

A number of conclusions can be drawn from the above findings:

1. Under identical operating conditions, the enhancement of $CH_4$ conversion to $H_2$ can be increased by up to 75% for currently available adsorbent materials e.g. hydrotalcites, and even further for next–generation adsorbents.

2. An optimum reactor inlet adsorbent temperature exists that maximises conversion; this optimum temperature is the result of a trade–off between the requirements on heat supply for the endothermic reaction and the $CO_2$ adsorption equilibrium which is favoured at lower temperatures.

3. The conditions and mode of adsorbent regeneration are key to the overall feasibility of the process. While complete adsorbent regeneration is ideal from the reactor point of view, this can only be achieved at the expense of unfeasibly large residence times in the regenerator. The $CO_2$ effluent stream would then be very dilute, which is unfavourable from the sequestration point of view.

4. The adsorbent capacity and $CO_2$ adsorption/desorption kinetics are important factors determining the ultimate success of the process proposed in this work. A parametric study on the effect of these two parameters shows that achieving high $CO_2$ capacity is generally not as crucial as achieving fast adsorption, and particularly desorption kinetics, because only a small proportion of the overall capacity is actually used in the adsorption/desorption cycle.

5. Optimisation studies indicate the potentiality of the novel process ($CH_4$ conversion, $CO_2$ removal and $H_2$ purity in the range of 99.5% combined with good reactor

efficiency) and also reveal interesting features for its further development.

The research output also highlights the scope and directions for further process improvement. In particular, the de–coupling of heat supply to the reactor by the adsorbent particles and through external heating would enable further conversion enhancement, as well as possible distributed feed of the adsorbent particles flow, *i.e.*, a pre–reactor (equilibrium conversion section) followed by a SE–reaction section. The adsorbent regeneration step can also be further improved by using a multi–stage fluidised bed rather than a well-mixed fluidised bed arrangement.

## 6.3 Recommendations for future work

Based on the results and conclusions of this thesis the following suggestions can be made for future research directions. In the first instance, model advancements could be made to: (i) accommodate the change in number of moles in the adsorptive reaction, (ii) incorporate the carbon–formatting reactions into the reaction kinetics model, investigating the effect of the SMR catalyst deactivation on the system, (iii) account for possible competitive adsorption of $H_2O$ under the process conditions by applying a suitable adsorption isotherm, (iv) consider capacity loss during adsorbent regeneration, (v) represent adsorbent particles attrition, *i.e.*, changes in $\varrho_{ads}$ and $d_p$, (vi) describe the diffusion transport by using the Maxwell–Stefan theory. Attention could also be put on the effect of the adsorption heat (see Table 2.4) on the process performance in conjunction with various design aspects and trade–offs (additional heat for reaction vs. higher temperatures in the regeneration). From an engineering point of view, variations in the adsorbent loading (due to solids handling) could be addressed. Most importantly, a multi–dimensional model for the monolithic adsorptive reactor could be developed to depict in more detail the transport processes and the complex nature of the 2–phase gas–solid flow. Its simulation results will provide a safe measure of the accuracy of the results presented in this work.

Thenceforth, appropriate mathematical models of the potential configurations of both the reaction regeneration stages of the process should be developed. Regarding the "reaction zone", the use of monolith channels for heat transfer purposes as well as the introduction

of a reaction–only section followed by a sorption–enhanced section could be considered. Additional regeneration unit designs would include multi–stage fluidised–bed configuration and use of indirect heating in both well–mixed and multi–stage types of operation. The incorporation of binary variables (selection or not of a particular configuration) in the mathematical model, capturing a general process superstructure, can address the synthesis problem of integrated flowsheets. A systems–modelling approach can therefore be adopted to identify the optimal process scheme in terms of energy utilisation.

Consequently, a research programme can be put forward that will set out to integrate process modelling and optimisation with product design into a single framework by means of multiscale modelling and simulation. This methodology will enable the development of catalyst-adsorbent systems for improved or novel processes, especially in the critical field of hydrogen production from fossil fuels.

Catalytic reactors, such as packed beds or monoliths, consist of many physically separated scales with complex nonlinear interactions between the processes occurring at each scale. Scale separation in a packed bed reactor and typical modelling tools applicable to each scale are shown in Fig. 6.1. The main spatial (and temporal) scales present in the system are the reactor, the catalyst particle, the pore scale and the molecular scale. The distinctive orders of magnitude of these four length scales are: reactor 1 m; catalyst particle 1 cm ($10^{-2}$ m); pore 1 $\mu$m ($10^{-6}$ m); molecular level 1 Å ($10^{-9}$ m). In addition, the corresponding time scales vary broadly; the residence time in the reactor ranges from 1 to 1000 s, the intraparticle diffusion time is approximately 1 s and that inside the pores in the order of $10^{-5}$ s. The temporal scale related to the molecular phenomena, such as adsorption, is usually less than a microsecond. Due to the strong coupling between reaction and transport at micro– and mesoscales and the macroscopic behaviour at the reactor level, the physics at the small scales significantly influence the overall process performance (Chakraborty and Balakotaiah, 2005). It is therefore evident that traditional modelling approaches have limited predictive capability when applied to such systems as they fall short of capturing these interactions and their implications on process design and operation.

Multifunctional reactors combine in a single unit, chemical reaction, physical separation, and energy integration in order to enhance overall performance. However, such hybrid process adds a further degree of complication to process design and optimisation, necessitating the implementation of multiscale analysis in order to express the synergetic effect of the unit's combined functionalities.

Multiscale analysis has been recently identified as a promising mathematical and computational tool that could enable efficient design and optimisation of complex systems. Within the context of chemical engineering, multiscale modelling facilitates the extension of conventional modelling capabilities to new application areas and the attainment of higher levels of detail and accuracy (Ingram et al., 2004). More specifically, new opportunities have been presented for innovation in catalyst, reactor and process technologies (Raimondeau and Vlachos, 2002).

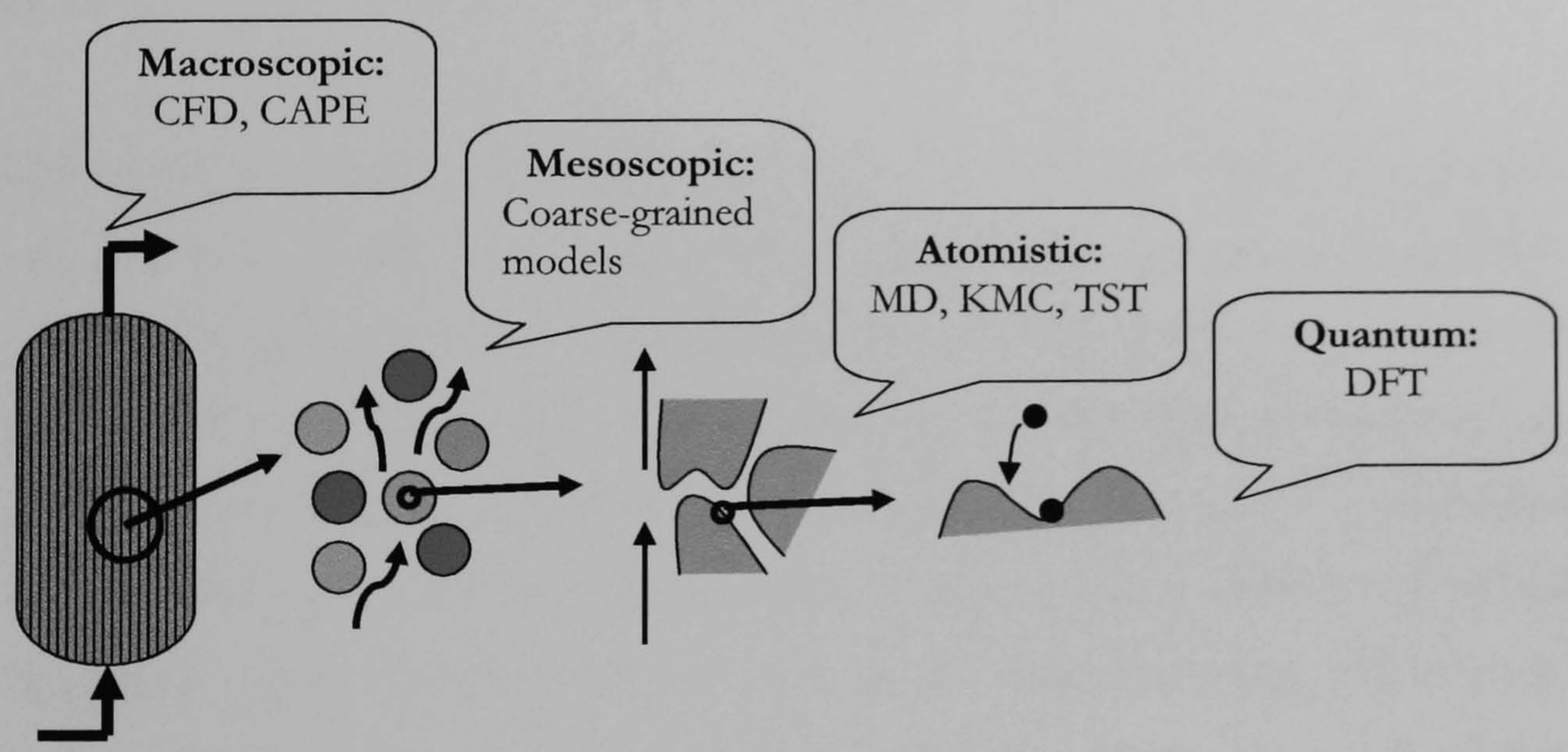



Figure 6.1: Scale separation in a packed bed reactor with main scales and typical modelling tools: L and t are the corresponding length and time scales in m and s respectively. CAPE: computer-aided process engineering; CFD: computational fluid dynamics; DFT: density function theory; KMC: kinetic Monte Carlo; MD: molecular dynamics; TST: transition state theory.

A multiscale model is a composite mathematical formulation comprising at least two sub-models that describe phenomena at different scales. This implies modelling between two or more scales, starting from the quantum level and moving to the atomistic level, then to coarse-grained models at the mesoscale, and finally to the continuum regime. The general idea involves the pass of information from a smaller (finer) scale to a model at a larger (coarser) scale, by leaving out degrees of freedom while moving from finer to coarser scales. The most common goal of multiscale modelling is the prediction of the macroscopic behaviour of a process from first principles (bottom-up approach) (Vlachos, 2005). However, future perspectives in chemical engineering, such as process intensification (Charpentier, 2005), require high–fidelity design of a system in order to accurately predict and control phenomena even at the molecular level (top-down approach). This "reverse" flow of information also gives rise to product-driven engineering, which has recently attracted considerable attention and research effort (Charpentier, 2005; Costa et al., 2006). It is believed that multiscale modelling and simulation can effectively address many features of the last two objectives, which have so far remained obscure (Vlachos, 2005).

The aim of the proposed research is to couple the current modelling work on adsorptive reactors, based on continuum conservation equations and continuum constitutive relations, with molecular and quantum mechanics theory. The complex interaction between adsorption and reaction and the potential operating configurations preclude any intuitive reactor design optimisation. As a result, it is essential to understand the underlying chemistry for the improved design and optimisation of such complex systems. This modelling paradigm imposes new challenges and presents opportunities for further exploitation, since it is strategically positioned at the interface of chemical engineering with chemistry.

Overall, future research is proposed to focus on:

- The development of multiscale modelling concepts for the design and optimisation of novel or improved approaches to hydrogen production
- The synergism of reaction and process engineering principles
- New approaches to integrated process and catalyst design

- Model–based design of multifunctional catalysts

### Hierarchical multiscale modelling of adsorptive reactors

A modernistic, hybrid approach can be adopted, in which each scale is modelled by employing different modelling approaches and tools (see Lerou and Ng, 1996; Charpentier and McKenna, 2004; Vlachos et al., 2006). The overall concept is to develop reliable models hierarchically to ensure minimum computational expense. The complex interaction between adsorption and reaction can exhibit a wide spectrum of time and length scales depending on the process configuration and mode of operation. Hence, it is not essential to simulate all phenomena at all scales with the highest accuracy in order to predict macroscopic properties such as conversion and selectivity. Instead, it can be realised that merely a number of reactions, species, phenomena and some scales are in fact necessary for accurate prediction of macroscopic behaviour. As a consequence, a systematic framework is required to select which scales to study in detail and then decide what type of model is suitable for each one.

The proposed approach of hierarchical multiscale modelling is to start with the simplest possible, still precise model at each scale and then identify the important scales and model parameters at each scale (Vlachos et al., 2006). Model accuracy can be assessed by comparison with process data and the model of the important scale as well as the associated active model parameters can be improved by using a higher–level theory. This process continues iteratively until the key scales and parameters do not change and convergence is achieved. However, the resulting models are often quite complex and model reduction is needed to obtain computationally tractable and physically meaningful formulations. Mathematical tools, such as computational singular perturbation (Shvartsman and Kevrekidis, 1998), scaling analysis (Jahn et al., 1997) and identification of rate determining step (Mhadeshwar and Vlachos, 2005) can be used for model reduction at various scales.

The application of the aforementioned methodology can be extended to enhance the existing model of the adsorption-enhanced hydrogen production process presented in this work. As an initial case study, the extensively studied water–gas shift reaction on Pt catalyst could be considered (Mhadeshwar et al., 2003; Mhadeshwar and Vlachos, 2004,

2005). The modelling work would then concentrate on the more intricate steam reforming of methane on Ni catalyst (Xu and Froment, 1989a,b).

### Adsorptive reactor design optimisation

Subsequently, the work can address the general problem of combined reaction and separation, as well as possible energy integration and network synthesis (Kauchali et al., 2004) in order to optimise overall process performance. The developed multiscale models would be used to determine an optimally configured and operated adsorptive–reactor process. A method for computationally efficient optimisation of the process with multiscale objectives would be required. Appropriate model reduction techniques can be utilised to overcome the computational burdens associated with such large optimisation problems (Christofides and Armaou, 2006; Vlachos et al., 2006). The most cost–effective process scheme in terms of minimum energy utilisation could then be identified subject to operability and production constraints as well as new constraints arising at the microscale. The work could also progress towards the incorporation of dynamic behaviour and uncertainty considerations in the multiscale optimisation problem formulation and solution, since such complex chemical systems may give rise to stochastic phenomena and, thus, operating trade–offs.

### Integrated process and catalyst design

Interacting phenomena (reaction combined with adsorption) in such complex catalytic reactors often occur at such large time and length scales that lie outside the span of molecular models. On the other hand, continuum constitutive equations may be deficient in describing them because of their averaged forms. To tackle problems associated with this intermediate, elusive regime (usually referred to as mesoscale) a strong coupling between the scales is required. The flow of information should therefore be bi–directional, thus presenting challenges since the development of robust and efficient methods for their solution is still at early stages (Raimondeau and Vlachos, 2002).

The proposed multiscale framework can accommodate these challenges and would subsequently enable the integration of process engineering with catalyst and/or adsorbent

design. In particular, the work should address the issue of catalyst and adsorbent suitability for adsorptive reaction systems of specific conversion, selectivity or separation requirements. This would involve coupling of models between scales linking atomistic scale information of materials with global reactor performance criteria. Parametric optimisation can then be applied to yield the catalyst and adsorbent properties that can produce the required macroscopic behaviour. In the long term, such an advance can shape the foundation for a generic tool for the selection of catalysts/adsorbents for novel, intensified process applications.

**Model–based design of multifunctional catalysts**

The developed framework can be employed for the design of novel catalysts with integrated structured functionalities. In such intensified processes, the multi-functionality occurs at the particle level and is usually introduced by combining catalytic properties with an engineered catalyst function (Dautzenberg and Mukherjee, 2001). In the first instance, the potential of multifunctional catalysts with integrated adsorption sites should be evaluated (Grünewald and Agar, 2004). Computational methods need to be developed to obtain the most favourable catalyst structure (formulation) in terms of enhanced process performance. More specifically, the composition of the catalyst would be treated as a manipulated variable which can be optimised by linking information across the scales. The work can then move towards the conceptual design of novel reactors for process intensification. Such a theoretical analysis will be useful in guiding future experimental work in this field, since it can reduce in size the parametric space associated with so complex reaction systems.

Overall, the aim of the proposed research is the development of a hierarchical, multiscale, computational framework that will enable the rational design of multifunctional catalysts for use in novel intensified processes, e.g. multifunctional catalytic reactors. Such a modelling approach will inherently incorporate both process design/optimisation and product design. The area of fuel processing for hydrogen production can initially be used to explore the potential of this multiscale approach. Attention would be given to "compact" processes that combine in a single unit chemical reaction, physical separation and/or energy

integration in order to enhance overall performance. This framework can then be used as a tool for multiscale analysis of other fluid–surface interacting systems such as biocatalysed reactions. In conclusion, the work aims to contribute towards the coupling of mesoscopic and macroscopic scales in reaction engineering applications, while utilising system–level tools such as parameter estimation, sensitivity analysis and model–based optimisation.

# List of publications

### Journal Papers

1. Koumpouras, G.C., Alpay, E., Stepanek, F., 2007. Mathematical modelling of a low–temperature hydrogen production process with in situ $CO_2$ capture. Chemical Engineering Science 62, 2833–2841.

2. Koumpouras, G.C., Stepanek, F., Alpay, E., Lapkin, A., Ding, Y., 2007. The effect of adsorbent characteristics on the performance of a continuous sorption–enhanced steam methane reforming process. Chemical Engineering Science 62, 5632-5637.

### Conference papers

1. Koumpouras, G.C., Stepanek, F., Alpay, E., Lapkin, A., Ding, Y., 2006. The effect of adsorbent characteristics on the performance of a continuous sorption-enhanced steam methane reforming process. In: Proceedings of 19th International Symposium on Chemical Reaction Engineering, Potsdam/Berlin, Germany.

2. Koumpouras, G.C., Alpay, E., 2005. A structured reactor approach to sorption-enhanced hydrogen production. In: Proceedings of 7th World Congress of Chemical Engineering, Glasgow, Scotland.

3. Lapkin, A., Iwan, A., Wen, D., Koumpouras, G.C., Stepanek, F., Alpay, E., Ding, Y., 2005. An alternative technology for low temperature hydrogen production. In: Proceedings of International Hydrogen Energy Congress, Istanbul, Turkey.

## List of abstracts

1. Koumpouras, G.C., Alpay, E., Stepanek, F., 2006. A novel concept in adsorption-enhanced hydrogen production. Annual Meeting of the AIChE, San Francisco, CA. U.S.A. (oral presentation).

2. Koumpouras, G.C., Alpay, E., Stepanek, F., 2005. Theoretical studies on sorption-enhanced hydrogen production. Annual Meeting of the AIChE, Cincinnati, OH. U.S.A. (oral presentation).

# References


Abanades, J. C., Rubin, E. S., Anthony, E. J., 2004. Sorbent cost and performance in $CO_2$ capture systems. Industrial and Engineering Chemistry Research 43, 3462–3466.

Adris, A. M., Pruden, B. B., Lim, C. J., Grace, J. R., 1996. On the reported attempts to radically improve the performance of the steam reforming reactor. Canadian Journal of Chemical Engineering 74, 177–186.

Alpay, E., Chatsiriwech, D., Kershenbaum, L. S., Hull, C. P., Kirkby, N. F., 1994a. Combined reaction and separation in pressure swing processes. Chemical Engineering Science 49, 5845–5864.

Alpay, E., Kenney, C. N., Scott, D. M., 1994b. Adsorbent particle size effects in the separation of air by rapid pressure swing adsorption. Chemical Engineering Science 49, 3059–3075.

Armor, J. N., 1999. The multiple roles for catalysis in the production of $H_2$. Applied Catalysis A: General 176, 159–176.

Balakotaiah, V., West, D. H., 2002. Shape normalization and analysis of the mass transfer controlled regime in catalytic monoliths. Chemical Engineering Science 57, 1269–1286.

Bennett, C. J., Kolaczkowski, S. T., Thomas, W. J., 1991. Determination of heterogeneous reaction kinetics and reaction rates under mass transfer controlled conditions for a monolith reactor. Process Safety and Environmental Protection: Trans IChemE, Part B 69, 209–220.

Bhattacharya, M., Harold, M. P., Balakotaiah, V., 2004. Shape normalization for catalytic monoliths. Chemical Engineering Science 59, 3737–3766.

Bhaumik, S., Maiumdar, S., Sircar, K. K.. 1996. Hollow–fiber membrane passed rapid pressure swing adsorption. AIChE Journal 42, 409–421.

Bjorklund, M. C., Carr, R. W., 1995. The simulated countercurrent moving bed chromatographic reactor: a catalytic and separative reactor. Catalysis Today 25, 159–168.

Brandani, F., Rouse, A., Brandani, S., Ruthven, D. M., 2004. Adsorption kinetics and dynamic behavior of a carbon monolith. Adsorption 10, 99–109.

Carter, J. W., 1975. On the regeneration of fixed adsorber beds. AIChE Journal 21, 380–382.

Carvill, B. T., Hufton, J. R., Anand, M., Sircar, S., 1996. Sorption enhanced reaction process. AIChE Journal 42, 2765–2772.

Chakraborty, S., Balakotaiah, V., 2005. Spatially averaged multi–scale models for chemical reactors. Advances in Chemical Engineering 30, 205–297.

Chang, D., Min, J., Moon, K., Park, Y. K., Jeon, J. K., Ihm, S. K., 2004. Robust numerical simulation of pressure swing adsorption process with strong adsorbate $CO_2$. Chemical Engineering Science 59, 2715–2725.

Charpentier, J.-C., 2005. Four main objectives for the future of chemical and process engineering mainly concerned by the science and technologies of new materials production. Chemical Engineering Journal 107, 3–17.

Charpentier, J. C., McKenna, T. F., 2004. Managing complex systems: some trends for the future of chemical and process engineering. Chemical Engineering Science 59, 1617–1640.

Chatsiriwech, D., Alpay, E., Kershenbaum, L. S., Hull, C. P., Kirkby, N. F., 1994. Enhancement of catalytic reaction by pressure swing adsorption. Catalysis Today 20, 351–366.

Cheng, Y. S., Alpay, E., Kershenbaum, L. S., 1998. Simulation and optimisation of a rapid pressure swing reactor. Computers & Chemical Engineering 22, S45–S52.

Choi, H., Ham, S. W., Nam, J. S., Kim, Y. G., 1996. Honeycomb reactor wash coated with mordenite type zeolite catalysts for the reduction of $NO_x$ by $NH_3$. Industrial & Engineering Chemistry Research 35, 106–112.

Choong, T. S. Y., Scott, D. M., 1998. The linear driving force model for cyclic adsorption and desorption: the effect of external fluid-film mass transfer. Chemical Engineering Science 53, 847–851.

Christofides, P. D., Armaou, A., 2006. Control and optimization of multiscale process systems. Computers & Chemical Engineering 60, 1670–1686.

Costa, R., Moggridge, G. D., Saraiva, P. M., 2006. Chemical product engineering: An emerging paradigm within chemical engineering. AIChE Journal 52, 1976–1986.

Crittenden, B. D., Guan, J., Ng, W. N., Thomas, W. J., 1994. Dynamics of pressurization and depressurization during pressure swing adsorption. Chemical Engineering Science 49, 2657–2669.

Cussler, E. L., 1997. Diffusion: mass transfer in fluid systems. Cambridge University Press, Cambridge.

Cybulski, A., Moulijn, J. A., 1998. The present and the future of structured catalysts–An overview, in A. Cybulski and J. A. Moulijn (eds), Structured catalysts and reactors. Marcel Dekker Inc., New York, pp 1–14.

Dautzenberg, F. M., Mukherjee, M., 2001. Process intensification using multifunctional reactors. Chemical Engineering Science 56, 251–267.

Davis, M. M., LeVan, M. D., 1987. Equilibrium theory for complete adiabatic adsorption cycles. AIChE Journal 33, 470–479.

Davis, M. M., LeVan, M. D., 1989. Experiments on optimization of thermal swing adsorption. Industrial & Engineering Chemistry Research 28, 778–785.

de Montgureuil, G. P., Domine, D., 1964. Process for separating a binary gaseous mixture by adsorption. US Patent 3,155,468 to Air Liquide.

Ding, Y., 2006. Personal communication.

Ding, Y., Alpay, E., 2000a. Equilibria and kinetics of $CO_2$ adsorption on hydrotalcite adsorbent. Chemical Engineering Science 55, 3461–3474.

Ding, Y., Alpay, E., 2000b. Adsorption–enhanced steam–methane reforming. Chemical Engineering Science 55, 3929–3940.

Ding, Y., Wang, Z., Ghadiri, M., Wen, D., 2005. Vertical upward flow of gas solid two phase mixtures through monolith channels. Powder Technology 153, 51–58.

Ding, Y., Wang, Z., Wen, D., Ghadiri, M., Fan, X., Parker, D., 2006. Solids behaviour in a dilute gas–solid two–phase mixture flowing through monolith channels. Chemical Engineering Science 61, 1561–1570.

Do, D. D., 1998. Adsorption analysis: equilibria and kinetics. Imperial College Press, London.

Farooq, S., Ruthven, D. M., 1990. A comparison of linear driving force and pore diffusion models for a pressure swing adsorption bulk separation process. Chemical Engineering Science 45, 107–115.

Geus, J. W., van Giezen, J. C., 1999. Monoliths in catalytic oxidation. Catalysis Today 47, 169–180.

Glueckauf, E., Coates, J. I., 1947. Theory of chromatography. Part IV. The influence of incomplete equilibrium on the front boundary of chromatograms and on the effectiveness of separation. Journal of the Chemical Society, 1315–1321.

Gomes, V. G., Yee, K. W. K., 2002. Pressure swing adsorption for carbon dioxide sequestration from exhaust gases. Separation and Purification Technology 28, 161–171.

Groppi, G., Belloli, A., Tronconi, E., Forzatti, P., 1995a. Analysis of multidimensional models of monolith catalysts for hybrid combustors. AIChE Journal 41, 2250–2260.

Groppi, G., Belloli, A., Tronconi, E., Forzatti, P., 1995b. A comparison of lumped and distributed models of monolith catalytic combustors. Chemical Engineering Science 50, 2705–2715.

Grünewald, M., Agar, D. W., 2004. Enhanced catalyst performance using integrated structured functionalities. Chemical Engineering Science 59, 5519–5526.

Hayes, R. E., Kolaczkowski, S. T., 1994. Mass and heat transfer effects in catalytic monolith reactors. Chemical Engineering Science 49, 3587–3599.

Hayes, R. E., Kolaczkowski, S. T., 1999. A study of Nusselt and Sherwood numbers in a monolith reactor. Catalysis Today 47, 295–303.

Hayes, R. E., Kolaczkowski, S. T., Thomas, W. J., 1992. Finite-element model for a catalytic monolith reactor. Computers & Chemical Engineering 16, 645–657.

Heck, R. H., Wei, J., Katzer, J. R., 1976. Mathematical modeling of monolithic catalysts. AIChE Journal 22, 477–484.

Heck, R. M., Gulati, S., Farrauto, R. J., 2001. The application of monoliths for gas catalytic reactions. Chemical Engineering Journal 82, 149–156.

Hoebink, J. H. B. J., Marin, G. D., 1998. Modelling of monolithic reactors for automotive exhaust gas treatment, in A. Cybulski and J. A. Moulijn (eds), Structured catalysts and reactors. Marcel Dekker Inc., New York, pp 209–237.

Holder, R., Bollig, M., Anderson, D. R., Hochmuth, J. K., 2006. Adiscussion on transport phenomena and three–way kinetics of monolithic converters. Chemical Engineering Science 61, 8010–8027.

Huang, C. C., Hwu, T. L., Hsia, Y. S., 1993. Recovery of acetone vapor by a thermal swing adsorber with activated carbon. J. Chem. Engng Japan 26, 21–27.

Hufton, J. R., Mayorga, S., Sircar, S., 1999. Sorption–enhanced reaction process for hydrogen production. AIChE Journal 45, 248–256.

Hutson, N. D., Speakman, S. A., Payzant, E. A., 2004. Structural effects on the high temperature adsorption of $CO_2$ on a synthetic hydrotalcite. Chemistry of Materials 45, 4135–4143.

Hwang, K. S., Choi, D. K., Gong, S. Y., Cho, S. Y., 1997. Adsorption and thermal regeneration of methylene chloride vapor on an activated carbon bed. Chemical Engineering Science 52, 1111–1123.

Ingram, G. D., Cameron, I. T., Hangos, K. M., 2004. Classification and analysis of integrating frameworks in multiscale modelling. Chemical Engineering Science 59, 2171–2187.

Jahn, R., Snita, D., Kubicek, M., Marek, M., 1997. 3–D modeling of monolith reactors. Catalysis Today 38, 39–46.

Jiang, L., Fox, V. G., Biegler, L. T., 2004. Simulation and optimal design of multiple bed pressure swing adsorption systems. AIChE Journal 50, 2904–2917.

Joensen, F., Rostrup-Nielsen, J. R., 2002. Conversion of hydrocarbons and alcohols for fuel cells. Journal of Power Sources 105, 195–201.

Johnsen, K., Grace, J. R., 2007. High–temperature attrition of sorbents and a catalyst for sorption–enhanced steam methane reforming in a fluidized bed environment. Powder Technology 173, 200–202.

Johnsen, K., Grace, J. R., Elnashaie, S. S. E. H., Kolbeinsen, L., Eriksen, D., 2006b. Modeling of sorption–enhanced steam reforming in a dual fluidized bubbling bed reactor. Industrial & Engineering Chemistry: Process Design and Development 45, 4133–4144.

Johnsen, K., Ryu, H. J., Grace, J. R., Lim, C. J., 2006a. Sorption–enhanced steam reforming of methane in a fluidized bed reactor with dolomite as $CO_2$–acceptor. Chemical Engineering Science 61, 1195–1202.

Jones, R. L., Keller, G. E., 1981. Pressure swing parametric pumping: a new adsorption process. J. Sep. Proc. Tech. 2, 17–23.

Jones, R. L., Keller, G. E., Wells, R. C., 1980. Rapid pressure swing adsorption process with high enrichment factor. US Patent 4,194,892 to Union Carbide Corporation.

Kauchali, S., Hausberger, B., Hildebrandt, D., Glasser, D., Biegler, L. T., 2004. Automating reactor network synthesis: finding a candidate attainable region for the water gas shift (WGS) reaction. Computers & Chemical Engineering 28, 149–160.

Keiski, R. L., Salmi, T., Niemisto, P., Ainassaari, J., Pohjola, V. J., 1996. Stationary and transient kinetics of the high temperature water–gas shift reaction. Applied Catalysis A 137, 349–370.

Kirchner, T., Eigenberger, G., 1996. Optimization of the cold–start behaviour of automotive catalysts using an electrically heated pre–catalyst. Chemical Engineering Science 51, 2409–2418.

Kirchner, T., Eigenberger, G., 1997. On the dynamic behavior of automotive catalysts. Catalysis Today 38, 3–12.

Koci, P., Kubicek, M., Marek, M., 2004. Modeling of three–way catalyst monolith converters with microkinetics and diffusion in the washcoat. Industrial & Engineering Chemistry: Process Design and Development 43, 4503–4510.

Kolaczkowski, S. T., 1995. Catalytic stationary gas turbine combustors: A review of the challenges faced to clear the next set of hurdles. Chemical Engineering Research and Design: Trans IChemE, Part A 73, 168–190.

Kolaczkowski, S. T., 1999. Modelling catalytic combustion in monolith reactors challenges faced. Catalysis Toady 47, 209–218.

Kolaczkowski, S. T., Serbetcioglou, S., 1996. Development of combustion catalysts for monolith reactors: a consideration of transport limitations. Catalysis Toady 138, 199 214.

Kopaygorodsky, E. M., Guliants, V. V., Krantz, W. B., 2004. Predictive dynamic model of single–stage ultra–rapid pressure swing adsorption. AIChE Journal 50, 953–962.

Krishna, R., 2002. Reactive separations: more ways to skin a cat. Chemical Engineering Science 57, 1491–1504.

Kumar, R., Dissinger, G. R., 1986. Nonequilibrium, nonisothermal desorption of single adsorbate by purge. Industrial & Engineering Chemistry: Process Design and Development 25, 456–464.

Kurdyumov, S. S., Brun-Tsekhovoi, A. R., Rozental, A. L., 1996. Steam conversion of methane in the presence of a carbon dioxide acceptor. Petroleum Chemistry 36, 139–143.

Lee, S., Aris, R., 1977. On the effects of radiative heat transfer in monoliths. Chemical Engineering Science 32, 827–837.

Lerou, J. J., Ng, K. M., 1996. Chemical reaction engineering: A multiscale approach to a multiobjective task. Chemical Engineering Science 51, 1595–1614.

Leung, D., Hayes, R. E., Kolaczkowski, S. T., 1996. Diffusion limitation effects in the washcoat of a catalytic monolith reactor. The Canadian Journal of Chemical Engineering 74, 94–103.

LeVan, M. D., Croft, D. T., 1995. Determination of periodic states of pressure swing adsorption cycles. Gas Separation & Purification 9, 13–16.

Lode, F., Houmard, M., Migliorini, C., Mazzotti, M., Morbidelli, M., 2001. Continuous reactive chromatography. Chemical Engineering Science 56, 269–291.

Lu, H., Reddy, E. P., Smirniotis, P. G., 2006. Calcium oxide based sorbents for capture of carbon dioxide at high temperatures. Industrial & Engineering Chemistry Research 45, 3944–3949.

Lu, Z. P., Loureiro, M. D., LeVan, M. D., Rodrigues, A. E., 1993. Pressure swing adsorption processes: intraparticle diffusion/convection models. Industrial & Engineering Chemistry Research 32, 2740–2751.

Martin, P. D., Swanton, S. W., 1997. Improved efficiency of adsorption processes. Applied Thermal Engineering 17, 869–877.

Mhadeshwar, A. B., Vlachos, D. G., 2004. Microkinetic modeling for water–promoted CO oxidation, water–gas shift, and preferential oxidation of CO on Pt. Journal of Physical Chemistry B 108, 15246–15258.

Mhadeshwar, A. B., Vlachos, D. G., 2005. Is the water–gas shift reaction on Pt simple?: Computer–aided microkinetic model reduction, lumped rate expression, and rate determining step. Catalysis Today 105, 162–172.

Mhadeshwar, A. B., Wang, H., Vlachos, D. G., 2003. Thermodynamic consistency in microkinetic development of surface reaction mechanisms. Journal of Physical Chemistry B 107, 12721–12733.

Nakhjavan, A., Bjrnbom, P., Zwinkels, M. F. M., Jaras, S. G., 1995. Numerical analysis of the transient performance of high–temperature monolith catalytic combustors: Effect of catalyst porosity. Chemical Engineering Science 50, 2255–2262.

Nilchan, S., Pantelides, C. C., 1998. On the optimisation of periodic adsorption processes. Adsorption 4, 113–147.

Ochoa-Fernández, E., Haugen, G., Zhao, T., Rønning, M., Børresen, B., Rytter, E., Rønnekleiv, M., Chen, D., 2007. Process design simulation of $H_2$ production by sorption enhanced steam methane reforming: evaluation of potential $CO_2$ acceptors. Green Chemistry 9, 654–662.

Ochoa-Fernández, E., Rusten, H. K., Jakobsen, H. A., Rønning, M., Holmen, A., Chen, D., 2005. Sorption enhanced hydrogen production by steam methane reforming using $Li_2ZrO_3$ as sorbent: Sorption kinetics and reactor simulation. Catalysis Today 106, 41–46.

Ortiz, A. L., Harrison, D. P., 2001. Hydrogen production using sorption–enhanced reaction. Industrial & Engineering Chemistry Research 40, 5102–5109.

Papadias, D., Edsberg, L., Bjrnbom, P., 2000. Simplified method of effectiveness factor calculations for irregular geometries of washcoats: A general case in a 3D concentration field. Catalysis Today 60, 11–20.

Posada, A., Manousiouthakis, V., 2005. Heat and power integration of methane reforming based hydrogen production. Industrial & Engineering Chemistry: Process Design and Development 44, 9113–9119.

Prasad, P., Elnashaie, S. S. E. H., 2004. Novel circulating fluidized–bed membrane reformer using carbon dioxide sequestration. Industrial & Engineering Chemistry Research 43, 494–501.

Raimondeau, S., Vlachos, D. G., 2002. Recent developments on multiscale, hierarchical modeling of chemical reactors. Chemical Engineering Journal 90, 3–23.

Rajasree, R., Kumar, V. R., Kulkarni, B. D., 2006. Performance enhancement of steam methane reforming using tubular packed–bed microreactors and dilution by adsorbent. Energy & Fuels 20, 463–472.

Rajesh, J. K., Gupta, S. K., Rangaiah, G. P., Ray, A. K., 2000. Multiobjective optimization of steam reformer performance using genetic algorithm. Industrial & Engineering Chemistry Research 39, 706–717.

Rase, H. F., 1977. Chemical reactor design for process plants Vol.2, Case studies and design data. Wiley, New York, pp. 44–60.

Readman, J. E., Blom, R., 2005. The use of *in situ* X–ray diffraction in the investigation of dolomite as a potential reversible high–temperature $CO_2$ sorbent. Physical Chemistry Chemical Physics 7, 1214–1219.

Reid, R. C., Prausnitz, J. M., Poling, B. E., 1987. The properties of gases and liquids. McGraw-Hill, London.

Reijers, H. T. J., Valster-Schiermeier, S. E. A., Cobden, P. D., van den Brink, R. W., 2006. Hydrotalcite as $CO_2$ sorbent for sorption–enhanced steam reforming of methane. Industrial & Engineering Chemistry Research 45, 2522–2530.

Ritter, J. A., Yang, R. T., 1991. Pressure swing adsorption: experimental and theoretical study on air purification and vapor recovery. Industrial & Engineering Chemistry Research 30, 1023–1032.

Roduit, R., Baiker, A., Baldyga, J., Wokaun, A., 1998. 3D modeling of SCR of $NO_x$ by $NH_3$ on vanadia honeycomb catalysts. AIChE Journal 44, 2731–2744.

Rouse, A. J., 2004. Fast cycle low pressure drop systems for the separation of $CO_2$. PhD dissertation, University of London, London.

Ruthven, D. M., 1984. Principles of adsorption and adsorption processes. John Wiley & Sons, New York.

Ruthven, D. M., 2000. Past progress and future challenges in adsorption research. Industrial & Engineering Chemistry Research 39, 2127-2131.

Ruthven, D. M., Farooq, S., Knaebel, K. S., 1994. Pressure swing adsorption. VCH Publishers, New York.

Ruthven, D. M., Thaeron, C., 1996. Performance of a parallel passage adsorbent contactor. Gas Separation & Purification 10, 63–73.

Ruthven, D. M., Thaeron, C., 1997. Performance of a parallel passage adsorbent contactor. Separation & Purification Technology 12, 43–60.

Ryden, M., 2006. Hydrogen production with carbon dioxide capture by reforming of natural gas using chemical–looping technologies. PhD dissertation, Chalmers University of Technology, Göteborg.

Santos, A., Bahamonde, A., Schmid, M., Avila, P., García-Ochoa, F., 1998. Mass transfer influences on the design of selective catalytic reduction (SCR) monolithic reactors. Chemical Engineering and Processing 37, 117–124.

Scholz, W. H., 1993. Processes for industrial production of hydrogen and associated environmental effects. Gas Separation & Purification 7, 131–139.

Schork, J. M., Fair, J. R., 1988. Parametric analysis of thermal regeneration of adsorption beds. Industrial & Engineering Chemistry Research 27, 457–469.

Seader, J. D., Henley, E. J., 2006. Separation process principles. John Wiley & Sons, New York.

Serbezov, A., Sotirchos, S. V., 2001. On the formulation of linear driving force approximations for adsorption and desorption of multicomponent gaseous mixtures in sorbent particles. Separation and Purification Technology 24, 343–367.

Shvartsman, S. Y., Kevrekidis, I. G., 1998. Nonlinear model reduction for control of distributed systems: A computer–assisted study. AIChE Journal 44, 1579-1595.

Sincule, J., Hlavacek, V., 1978. Heat and mass transfer in monolithic honeycomb catalysts III: Radiation model. Chemical Engineering Science 33, 839-845.

Sircar, S., Hufton, J. R., 2000a. Why does the linear driving force model for adsorption kinetics work? Adsorption 6, 137–147.

Sircar, S., Hufton, J. R., 2000b. Intraparticle adsorbate concentration profile for linear driving force model. AIChE Journal 46, 659–660.

Skarstrom, C. W., 1960. Method and apparatus for fractionating gaseous mixtures by adsorption. US Patent 2,994,627 to Exxon Research and Engineering.

Smith, O. J., Westerberg, A. W., 1990. Mixed–integer programming for pressure swing adsorption cycle scheduling. Chemical Engineering Science 45, 2833–2842.

Stankiewicz, A., 2003. Reactive separations for process intensification: an industrial perspective. Chemical Engineering and Processing 42, 137–144.

Stitt, E. H., 2004. Multifunctional reactors? Up to a point Lord Copper. Chemical Engineering Research and Design: Trans IChemE, Part A 82(A2), 129–139.

Stutz, M. J., Poulikakos, D., 2005. Effects of microreactor wall heat conduction on the reforming process of methane. Chemical Engineering Science 60, 6983–6997.

Suzuki, M., Suzuki, T., Sakoda, A., Izumi, J., 1996. Piston–driven ultra rapid pressure swing adsorption. Adsorption 2, 111–119.

Tomasic, V., Gomzi, Z., 2004. Experimental and theoretical study of NO decomposition in a catalytic monolith reactor. Chemical Engineering and Processing 43, 765–774.

Tomasic, V., Zrncevic, S., Gomzi, Z., 2004. Direct decomposition of NO in a monolith reactor: comparison of mathematical models. Catalysis Today 90, 77–83.

Tronconi, E., Forzatti, P., Gomez-Martin, J. P., Malloggi, S., 1992. Selective catalytic removal of $NO_x$: a mathematical model for design of catalyst and reactor. Chemical Engineering Science 47, 2401–2406.

Turnock, P. H., Kadlec, R. H., 1971. Separation of nitrogen and methane via periodic adsorption. AIChE Journal 17, 335–342.

Twigg, M. V., 1996. Catalyst Handbook. Manson, London.

van Noorden, T. L., Lunel, S. M. V., Bliek, A., 2003. Optimization of cyclically operated reactors and separators. Chemical Engineering Science 58, 4115–4127.

Vaporciyan, G. G., Kadlec, R. H., 1989. Periodic separating reactors: Experiments and theory. AIChE Journal 35, 831–841.

Viecco, G. A., Caram, H. S., 2006. Comparison between simulated moving bed and reverse flow chromatographic reactors for equilibrium limited reactions. Chemical Engineering Science 61, 6869–6879.

Vlachos, D. G., 2005. A review of multiscale analysis: Examples from systems biology, materials engineering, and other fluid–surface interacting systems. Advances in Chemical Engineering 30, 1–61.

Vlachos, D. G., Mhadeshwar, A. B., Kaisare, N. S., 2006. Hierarchical multiscale model-based design of experiments, catalysts, and reactors for fuel processing. Computers & Chemical Engineering 30, 1712–1724.

Waldron, W. E., Hufton, J. R., Sircar, S., 2001. Production of hydrogen by cyclic sorption enhanced reaction process. AIChE Journal 47, 1477–1479.

Waldron, W. E., Sircar, S., 2000. Parametric study of a pressure swing adsorption process. Adsorption 6, 179–188.

Wang, Y.-N., Rodrigues, A. E., 2005. Hydrogen production from steam methane reforming coupled with in situ $CO_2$ capture: Conceptual parametric study. Fuel 84, 1778–1789.

Wanker, R., Raupenstrauch, H., Staudinger, G., 2000. A fully distributed model for the simulation of a catalytic combustor. Chemical Engineering Science 55, 4709–4718.

Westerterp, K. R., Kuczynski, M., 1987. A model for a countercurrent gas–solid-solid trickle flow reactor for equilibrium reactions. The methanol synthesis. Chemical Engineering Science 42, 1871–1885.

Williams, J. L., 2001. Monolithic structures, materials, properties and uses. Catalysis Today 69, 3–9.

Xiong, R., Ida, J., Lin, Y. S., 2003. Kinetics of carbon dioxide sorption on potassium doped lithium zirconate. Chemical Engineering Science 58, 4377–4385.

Xiu, G. H., Li, P., Rodrigues, A. E., 2002b. Sorption-enhanced reaction process with reactive regeneration. Chemical Engineering Science 57, 3893–3908.

Xiu, G. H., Li, P., Rodrigues, A. E., 2003b. New generalized strategy for improving sorption–enhanced reaction process. Chemical Engineering Science 58, 3425–3437.

Xiu, G. H., Li, P., Rodrigues, A. E., 2004. Subsection–controlling strategy for improving sorption–enhanced. Chemical Engineering Research and Design: Trans IChemE, Part A 82(A2), 192–202.

Xiu, G. H., Soares, J. L., Li, P., Rodrigues, A. E., 2002a. Simulation of five step one bed sorption–enhanced reaction process. AIChE Journal 48, 2817–2832.

Xiu, G. H., Soares, J. L., Li, P., Rodrigues, A. E., 2003a. Adsorption enhanced steam methane reforming with intraparticle–diffusion limitations. Chemical Engineering Journal 95, 83–93.

Xu, J., Froment, G. F., 1989a. Methane steam reforming, methanation and water gas shift: I. Intrinsic kinetics. AIChE Journal 35, 88–96.

Xu, J., Froment, G. F., 1989b. Methane steam reforming, methanation and water gas shift: II. Diffusional limitations and reactor simulation. AIChE Journal 35, 97–103.

Yang, R. T., 1987. Gas separation by adsorption processes. Butterworths, Boston.

Yang, R. T., Doong, S., 1985. Gas separation by pressure swing adsorption: a pore–diffusion model for bulk separation. AIChE Journal 31, 1829–1841.

Yong, Z., Mata, V., Rodrigues, A. E., 2001a. Adsorption of carbon dioxide onto hydrotalcite–like compounds (HTlcs) at high temperatures. Industrial & Engineering Chemistry Research 40, 204–209.

Yong, Z., Mata, V., Rodrigues, A. E., 2001b. Adsorption of carbon dioxide on chemically modified high surface area carbon–based adsorbents at high temperature. Adsorption 7, 41–50.

Yong, Z., Mata, V., Rodrigues, A. E., 2002. Adsorption of carbon dioxide at high temperature–a review. Separation and Purification Technology 26, 195–205.

Yongsunthon, I., Alpay, E., 1998. Design and optimisation of temperature cycled adsorptive reactors. Computers & Chemical Engineering 22, S733–S736.

Yongsunthon, I., Alpay, E., 1999. Design of periodic adsorptive reactors for the optimal integration of reaction, separation and heat exchange. Chemical Engineering Science 54, 2647–2657.

Young, L. C., Finlayson, B. A., 1976a. Mathematical models of the monolith catalytic converter–I. Development of model and application of orthogonal collocations. AIChE Journal 22, 331–341.

Young, L. C., Finlayson, B. A., 1976b. Mathematical models of the monolith catalytic converter–II. Application to automobile exhaust. AIChE Journal 22, 343–353.

Zygourakis, K., Aris, R., 1983. Multiple oxidation reactions and diffusion in the catalytic layer of monolith reactors. Chemical Engineering Science 38, 733–744.

# Appendices

# Appendix A

# Mass balances derivations

General material balance over a volume element of the monolithic adsorptive reactor:

$$\begin{pmatrix}\text{Flowrate of com-}\\ \text{ponent, i, INTO}\\ \text{elemental volume}\end{pmatrix} - \begin{pmatrix}\text{Flowrate of com-}\\ \text{ponent, i, OUT of}\\ \text{elemental volume}\end{pmatrix} + \begin{pmatrix}\text{Rate of generation}\\ \text{of component, i, in}\\ \text{elemental volume}\end{pmatrix} = 0$$

A schematic diagram of the elemental volume is presented in Fig. A.1.

**Definitions**

Volume of the monolith channel: $V = V_g + V_{ads} + V_c$

Free cross–sectional area: $\varepsilon = (V_g + V_{ads})/V$

Adsorbent loading: $\varphi = V_{ads}/(V_g + V_{ads})$

Adsorbent mass flux: $\dot{m} = \varrho_{ads} u_{ads} A$

Gas–phase density: $c_g = P/RT_g$

Catalyst–gas specific area: $\alpha_c = A_c/V\varepsilon = 2/R_c$

Gas–adsorbent specific area: $\alpha_{ads} = A_{ads}/V_{ads} = 6/d_p$

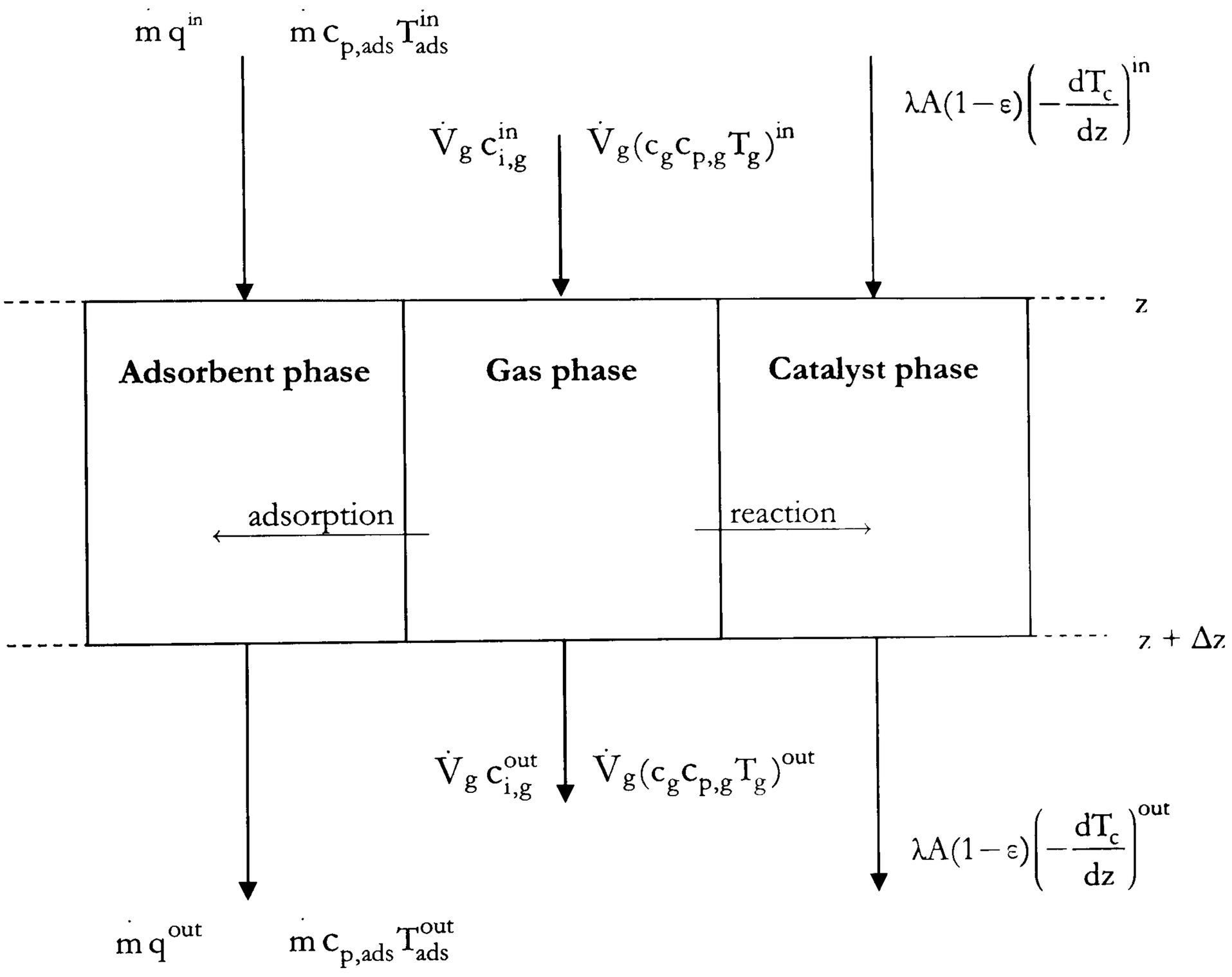



Figure A.1: Schematic representation of the computational domain.

## A.1 Gas phase

$$\dot{V}_g c_{i,g}^{in} - \dot{V}_g c_{i,g}^{out} - k_m \alpha_c A \varepsilon \Delta z (c_{i,g} - c_{i,c}) - m_{ads} r_{ads} = 0$$

$$\div V_g = A\varepsilon(1-\varphi)\Delta z \ , \ \Delta z \to 0$$

$$u_g^{int} \left( -\frac{dc_{i,g}}{dz} \right) - k_m \left( \frac{\alpha_c}{1-\varphi} \right) (c_{i,g} - c_{i,c}) - \varrho_{ads} \left( \frac{\varphi}{1-\varphi} \right) r_{ads} = 0$$

Substituting

$$u_g^{int} = \frac{u_g}{(1-\varphi)\varepsilon}$$

and multiplying by $(1-\varphi)\varepsilon$ results in Eq. 3.1.

## A.2 Catalyst phase

$$k_m \alpha_c A \varepsilon \Delta z (c_{i,g} - c_{i,c}) + \eta m_c r_i = 0$$

$$\div V_c = A(1-\varepsilon)\Delta z$$

$$k_m \alpha_c \left(\frac{\varepsilon}{1-\varepsilon}\right)(c_{i,g} - c_{i,c}) + \eta \varrho_c r_i = 0$$

Note that $\varrho_c = \frac{1}{3}\varrho_s$ where $\varrho_s = 2355.2$ kg m$^{-3}$ (Xu and Froment, 1989b).

## A.3 Adsorbent phase

$$\dot{m}q_{in} - \dot{m}q_{out} - m_{ads}r_{ads} = 0$$

$$\div V_{ads} = A\varepsilon\varphi\Delta z \ , \ \Delta z \to 0$$

$$\left(\frac{u_{ads}}{\varepsilon\varphi}\right)\left(-\frac{dq}{dz}\right) + r_{ads} = 0$$

# Appendix B

# Energy balances derivations

## B.1 Gas phase

$$\dot{V}_g(c_g c_{p,g} T_g)^{in} - \dot{V}_g(c_g c_{p,g} T_g)^{out} + k_h \alpha_c A \varepsilon \Delta z (T_c - T_g) \quad + \\ + \; k_{h,ads} \alpha_{ads} A \varepsilon \varphi \Delta z (T_{ads} - T_g) \quad = \quad 0$$

$$\div \; V_g = A\varepsilon(1-\varphi)\Delta z \;,\; \Delta z \to 0$$

$$\frac{u_g}{\varepsilon(1-\varphi)} \left( -\frac{d}{dz}(c_g c_{p,g} T_g) \right) + k_h \alpha_c \left( \frac{1}{1-\varphi} \right) (T_c - T_g) \quad + \\ + \; k_{h,ads} \alpha_{ads} \left( \frac{\varphi}{1-\varphi} \right) (T_{ads} - T_g) \quad = \quad 0$$

## B.2 Catalyst phase

$$\lambda A(1-\varepsilon)\left(-\frac{dT_c}{dz}\right)^{in} - \lambda A(1-\varepsilon)\left(-\frac{dT_c}{dz}\right)^{out} +$$

$$+ k_h \alpha_c A \varepsilon \Delta z (T_g - T_c) + \sum_{j=I}^{III} \eta m_c (-\Delta H_{R_j}) R_j = 0$$

$$\div V_c = A(1-\varepsilon)\Delta z \ , \ \Delta z \to 0$$

$$\lambda \frac{d^2 T_c}{dz^2} + k_h \alpha_c \frac{\varepsilon}{1-\varepsilon}(T_g - T_c) + \sum_{j=I}^{III} \eta \varrho_c (-\Delta H_{R_j}) R_j = 0$$

## B.3 Adsorbent phase

$$\dot{m}c_{p,ads}T_{ads}^{in} - \dot{m}c_{p,ads}T_{ads}^{out} + k_{h,ads}\alpha_{ads}A\varepsilon\varphi\Delta z(T_g - T_{ads}) \quad +$$

$$+ m_{ads}(-\Delta H_{ads})r_{ads} \quad = \quad 0$$

$$\div V_{ads} = A\varepsilon\varphi\Delta z \ , \ \Delta z \to 0$$

$$\left(\frac{u_{ads}}{\varepsilon\phi}\right)\varrho_{ads}c_{p,ads}\left(-\frac{dT_{ads}}{dz}\right) + k_{h,ads}\alpha_{ads}(T_g - T_{ads}) \quad +$$

$$+ \varrho_{ads}(-\Delta H_{ads})r_{ads} \quad = \quad 0$$

LONDON